Arginine-Rich Ionic Complementary Peptides and Their Drug Delivery Potential

by

Zizhen Wan

A thesis

presented to the University of Waterloo

in fulfillment of the

thesis requirement for the degree of

Master of Applied Science

in

Chemical Engineering

Waterloo, Ontario, Canada, 2013

AUTHOR'S DECLARATION

I hereby declare that I am the sole author of this thesis. This is a true copy of the thesis, including any required final revisions, as accepted by my examiners.

I understand that my thesis may be made electronically available to the public.

Abstract

Ellipticine (EPT), a natural plant polyphenolic compound, has long been known for its significant anticancer and anti-HIV activities. Recent study on its photophysical properties has revealed that ellipticine has three molecular states: protonated, neutral and crystalline. Further *in vitro* cytotoxicity tests indicated that protonated ellipticine exhibited much higher anticancer activity than the other two states. To maximize drug therapeutic effect, a small library of ariginine-rich ionic complementary peptides derived from EAK, including EAR8-II, EAR8-a, ELR8-a, and EAR16-II, were investigated as a potential carrier to deliver prescribed protonated ellipticine for treatment of cancer. Fluorescence study demonstrated that all four peptides were able to solubilize and stabilize protonated ellipticine in aqueous solution at 5:1 mass ratio of peptide-to-ellipticine (0.5: 0.1 mg/mL) even upon 4000 times dilution. Physicochemical characteristics of peptides self-assemblies and peptide-ellipticine complexes such as particle size, surface charge, secondary structure and morphology were determined by dynamic light scattering (DLS), zeta potential, circular dichroism (CD) , atomic force microscopy (AFM) and transmission electron microscopy (TEM), respectively. Then the ellipticine maximum suspension was determined by ellipticine UV-absorption. With the help of the peptides and mechanical stirring overtime, up to 100% ellipticine could be uptaken and stabilized in the solution as protonated ellipticine. *In vitro* cytotoxicity tests indicated that the peptides were demonstrating significant biocompatibility without affecting the survival of two cancer cell lines, human lung carcinoma cell line A549 and breast cancer cell line MCF-7, whereas the complexes with protonated ellipticine were found to show great anticancer activity to the two cancer cell lines. The IC50 values were obtained for

each of four different peptide-ellipticine complexes ranged from 0.36±0.12 to 18.90±0.46 μM. It is worth noting that the IC50 value of EAR16-ellipticine complex to MCF-7 was over 50 times higher than that one to A549, which presented that EAR16-ellipticine complex has a selective targeting activity to A549, with the lowest IC50 value of 0.36±0.12 μM among all four complexes. Such a result indicated that this library of novel arginine-rich ionic complementary peptides had a great potential to encapsulate prescribed protonated ellipticine and exhibited an excellent anticancer activity upon serial dilution in aqueous solution. Overall, the charge distribution and increased hydrophobicity of the short (8 amino acids length) peptides seemed not to affect the complex formation and its therapeutic efficacy *in vitro;* however, the increase in length of the peptides significantly altered the nanostructure of peptides and its complexation with ellipticine, increased the therapeutic efficacy of EAR16-EPT to A549. This work provides essential information for peptide sequence design in the development of self-assembling peptide-based delivery of hydrophobic anticancer drugs.

Acknowledgements

I would like to express my great thanks to my supervisor, professor Pu Chen, who has provided me unlimited support, critical guidance and valuable advisory during my M.A.Sc study at the University of Waterloo. His guidance helped me to overcome difficulties in my research and discover new aspects in nano-bioengineering. He was the most encouraging people in my research to assist me to become an open minded, thoughtful and independent researcher. I am also grateful to the readers of my thesis, Dr. Frank Gu and Dr. Michael Tam for their valuable suggestions.

I am glad to work with all the amazing research members in drug delivery group in University of Waterloo. They were always ready to help me in any part of the project. I am so grateful to receive the fantastic training from PhD candidate Sheng Lu, Parisa Sadatmousavi and previous lab manager Tatiana Sheinin during my project. I learned the most valuable experimental skills from them. Their advice was really helpful for improving the research in all experimental and data analysis aspects. I would like to thank Ali Sheikholeslam and Yond Ding for their kindly assistant in AFM training session, kaveh sarikhani for his great help in the set up and operation of Axisymmetric Drop Shape Analysis-Profile (ADSA-P) technique. And thanks to my colleague Danyang Zhao, who carried out the hemolysis test part during our collaboration. Also, Wen Xu, Ran Pan and Baoling Chen, who gave me advice on cell culture in SiRNA group.

I am so grateful to meet and collaborate with amazing individuals who have contributed to the experiments on my research project. I would like to thank Terence Tang, the Flow Cytometry technician in Biology Department for his help to gather important FACS data. I

would appreciate nice help from Dr. Juewen Liu for UV measurement and his graduate student Biwu Liu. Also, thanks Dale Weber for his valuable trainings for TEM at Biology Department.

Most importantly, I would like to thank my parents for their endless supports. Even though they were far from me in the past two years, but they have always been encouraging me. Special thank to my true love, Kevin Wang, for his enormous encouragement. Without them none of my achievements would be possible.

This thesis is dedicated to all of them.

Table of Contents

List of Figures

List of Tables

Nomenclatures

Acronym	Full name
ADSA-P	Axisymmetric drop shape analysis-profile
AFM	Atomic force microscopy
CAC	Critical aggregation concentration
CCK8	Cell counting kit
CD	Circular dichroism
CMC	Critical micelle concentration
CPT	Camptothecin
DDS	Drug delivery system
DLS	Dynamic light scattering
DMSO	Dimethyl sullfoxide
EDTA	Ethylenediaminetetraacetic acid
EPR	Enhanced permeability retention
EPT	Ellipticine
EtOH	Ethonal
F12	F-12 Kaighn’s modification
FACS	Fluorescence-activated cell sorting
FBS	Fetal bovine serum
ICT	Intramolecular charge transfer
IGF	Insulin-like growth factor
MEM	Minimum Essential Medium Eagle
MTT	3-(4,5-Dimethylthiazol-2-yl)-2,5-diphenyltetrazolium bromide
Mw	Molecular weight
PBS	Phosphate buffer saline
TEM	Transmission electron microscopy
THF	Tetrahydrofuran
UV	Ultraviolet

Chapter 1
Introduction

1.1 Overview

Over the past half century, cancer remains one of the major public health problems in North America[1]. As the second leading cause of death in the world after cardiovascular and cerebrovascular diseases, an average of 21 people was diagnosed with some kind of cancer per every hour of every day, and nine people died from cancer in Canada in 2012[2]. Cancer is a class of diseases sharing one important characteristic: loss of control of the normal cell cycle processes[3,4]. That is, cancer develops from changes that disrupt the normal functions of cell growth and reproduction. These changes often result from inherited mutations or are induced by environmental factors like chemicals, tobacco products, viruses, UV light and X-rays[5]. As a result of these mutations, cancer cells obtain new characteristics such as limitless proliferation potential, decreased cell adhesion, resistance to growth-inhibitory signals, as well as spread and invade other normal tissues.

To date, surgery, radiotherapy and chemotherapy remain the most common therapies in the fight against cancer[6,7]. Even though many advances have been achieved in conventional treatments, these methods are limited by several drawbacks[8], such as lack of selectivity, not just killing cancer cells, but also inhibiting the normal grow process of healthy cells, and cause low white blood cell count, gastrointestinal distress and hair loss. On the other hand, most anti-cancer drugs are very hydrophobic and have poor bioavailability, larger than enough drug doses are demanded, which lead to even higher toxicity to normal cells, along with an increased incidence of multiple drug resistance[9].

Over the past two decades, the field of novel drug delivery system has evolved due to the slow progress in the diagnosis and treatment of severe diseases at the cellular level. Recent interest has been focusing on developing nanoscale delivery carriers capable of controlling the release of encapsulated chemotherapeutic drugs directly into cancer cells and cellular compartments[10, 11, 12]. This new strategy for the practice of medicine provides a more efficient solution to overcome the limitations existed in conventional anticancer therapy as discussed above.

The main considerations when designing nanoscale delivery carriers are to prolong drug circulation time, improve membrane permeation, increase cell targeting capabilities and reduce cytotoxic effects on normal human cells[12, 13]. Up to now, several classes of materials have been developed, including liposomes[14,15], polymeric nanoparticles[16,17], dendrimer[18,19,20], and self-assembly peptides[21,22] incorporating cytotoxic therapeutics; some of them are already on the market and others are under clinical and preclinical research[19].

Self-assembling peptides are of interest for various biomedical applications because of their favorable properties, such as biodegradable, inherent biocompatibility, cell targeting, cell penetration and simplicity in producing a variety of nanostructures[23,24,25]. These peptides can assemble into well-ordered nanostructures by van der waals interaction, hydrogen bonding or hydrophobic interaction, which can withstand high temperatures, extreme pHs, and high concentrations of electrolyte[26]. Moreover, they exhibit good biocompatibility with many cultured mammalian cells and no detectable immune responses can be observed when introduced into animals[27]. As a result, self-assembling peptides are ideal nanomaterials for tissue engineering, regenerative medicine and controlled drug delivery system[28,29]. The

family of EAK16s is probably the most commonly studied class of self-assembling ionic-complementary peptides in drug delivery research. They are discovered from a yeast Z-DNA binding protein by Dr. Wang in the early 1990s[30]. These peptides feature a unique amphiphilic structure consisting of alternating hydrophilic and hydrophobic amino acids in the sequence, where the hydrophilic residues form alternating positive and negative charges, resulting in a complementary ionic structure[22]. It is known these EAK16s are able to form stable β-sheet structure in aqueous solution to provide a protected and stable environment for hydrophobic anticancer drugs ellipticine (EPT) in aqueous solution[21]. *In vitro* studies have also shown that the EAK-EPT complex exhibit anti-cancer activity at killing both MCF-7 and A549 cells.

Ellipticine (5, 11-dimethyl-6H-pyrido [4, 3-b] carbazole), a natural plant alkaloid, has long been known for its significant anticancer and anti-HIV activities[31]. Studies have showed its high efficiency against several types of cancer, including leukemias, melanoma, breast cancer, sarcomas, lung cancer cells and neuroblastomas[31,32]. Although the potential of EPT as an anticancer drug was discovered fifty years ago, its poor aqueous solubility, severe side effects and low bioavailability constituted major obstacles toward its medical deployment[33]. In recent years, several effective drug delivery vehicles have been developed, such as polymer[17,34], micelles[35] and peptides[21,36] to improve clinical applicability of EPT, as well as other hydrophobic drugs[37,38]. Our previous studies have shown that EAKs peptide could be a potential vehicle to encapsulate EPT in three different molecular states: neutral form, EPT crystals and protonated EPT[21]. Meanwhile, it was found that the molecular states of EPT have great effect on the release kinetics of EPT from the peptide-EPT complex to EPC

vesicles. In more recent work, we first proposed that the different molecular states of EPT in the peptide-EPT complex would possess different drug efficacies in therapy[39]. *In vitro* studies indicated that complexes with protonated EPT had much higher toxicity than complexes with crystalline EPT against cancer cells. Studies in living cells also revealed that only protonated EPT can exist in the nucleus[32]. In order to maximize drug therapeutic effects, it is necessary to develop new drug carriers that can deliver a drug with a prescribed molecular state. However, much of research work on EPT delivery system is focused on creating hydrophobic carrier to encapsulate neutral EPT; very few studies have been performed on this special issue.

In the first part of this research, I first elucidated the basic design principles for investigating a small library of model peptides that can self-assemble in aqueous solution to encapsulate particular protonated EPT. The self-assembly capability of these peptides were characterized by Axisymmetric Drop Shape Analysis-Profile (ADSA-P) technique and 1-anilino-8-naphthalene sulfonate (ANS) fluorescence assay. Then I explored the potential of these peptides in drug delivery application, the fluorescence technique was utilized to characterize the molecular state of EPT in the complex to see if the prescribed protonated EPT could be encapsulated in the peptide self-assemblies. In the second part, we studied the effect of peptide length, sequence and hydrophobicity on the formation of peptide-EPT complexes in aqueous solution. The peptide and their complexes with EPT are studied in details for its secondary structures, morphology, particle size distribution and surface charge. The third part of this research was considered for the anticancer activity of the peptide-EPT complexes tested *in vitro* against two cancer cell lines: non-small cell lung cancer cell A549

and breast cancer cell MCF-7. The stability of the complexes after serial dilutions in aqueous solution was further investigated in relation to anticancer activity. The information obtained in this study is aimed at providing appropriate design principles for selecting peptide sequences, to construct advanced functional peptide carriers for anticancer drug delivery.

1.2 Research objectives

The goal of this research is to design a small library of model self-assembling ionic complementary peptides, which can self-assemble in aqueous solution to encapsulate particular protonated EPT and stabilized them for a long time. The specific objectives of this research study are listed as following:

(1) Basic design principals of arginine-rich ionic complementary peptides as drug delivery system.
(2) Study the surface tension properties of peptides and their potential to encapsulate protonated EPT.
(3) Investigate the effect of length, charge distribution and hydrophobicity on the physicochemical properties of peptide assemblies and peptide-EPT complexation.
(4) Evaluate the anticancer activity of peptide-EPT complexes and their dilutions *in vitro*.

1.3 Outline of the thesis

This thesis consists of five chapters as below:

Chapter 1 gives an overview of the thesis, including a brief introduction to cancer statistics, cancer therapy, self-assembling peptides as a potential carrier in drug delivery. The objective of the research is given in this chapter.

Chapter 2 reviews the literature about properties of cancer, traditional cancer therapy, novel drug delivery systems and application of self-assembling ionic-complementary peptides as hydrophobic anticancer drug carrier.

Chapter 3 presents the required material and experimental methods in detail for this research.

Chapter 4 reports the results and discussion based on each research objective.

Chapter 5 presents the conclusion of studies in the thesis and recommendations for future work.

.

Chapter 2
Literature Review

2.1 Cancer and Cancer Therapy

2.1.1 Introduction

Cancer is one of the most serious health problems world-wide and is responsible for approximately 13% of all deaths, according to the World Health Organization[1]. In Canada alone, an estimated 186,400 new cases of cancer (excluding 81,300 non-melanoma skin cancers) and 75,700 deaths from cancer in 2012 was reported by The National Canadian Statistics[2]. Although prognosis is better now, the large variety of cancer types and metastases makes treatment very difficult[40]. Cancer is a disease in which the control of growth is lost in one or more cells, leading to an abnormal tissue mass of cells known as a tumor[41]. In the early stages of tumor growth, cancer cells often resemble the original cells; however, they can lose their appearance and function of their origin at a later stage. The rate of cancerous cells outgrows normally controlled cell populations and form a tumor mass. Studies show that the genetic changes that promote the progressive transformation of healthy cells at many different sites into tumor cells[42]. Tumor formation may result from changes to DNA sequence or structure by internal factors, such as mutations, addition or loss of DNA, or epigenetic changes. While external factors like viruses, bacterial infections, chemicals, or radioactivity can also lead to tumorigenesis[5].

Cancer treatment comprises more than one approach, and the strategy adopted depends on the nature of the cancer and how far it has progressed. Currently, the main treatments are

radiotherapy[7], chemotherapy[6] and surgery. However, other approaches such as photodynamic therapy[43], antibody- and vaccine related approaches[44], and gene therapy are in development.

2.1.2 Properties of Cancer

Cancer cells are abnormal cells in which the processes regulating normal cell cycle are disrupted; therefore, they no longer require special signals to regulate cell growth and division. In terms of cell division, cancer cells differ from normal cells in the following four ways[45].

First, external growth factors are required by normal cells to divide. When synthesis of these growth factors is inhibited by normal cell regulation, the cells stop dividing. While, cancer cells can proliferate without these positive growth factors, so they divide whether or not these factors are present. As a result, cancer cells have become independent cells, not behave as part of normal tissue anymore.

Second, normal cells show contact inhibition; that is, they respond to contact with other cells by ceasing cell division. Since cancer cells have lost this characteristic, they will continue to grow even after they touch other cells, causing a large mass of cells to form. These cancer cells may even penetrate the normal cells cause metastasis.

Third, the ability of normal cells to replicate DNA is about fifty times, and then they die, are replaced in a controlled and orderly manner by new cells. In adult cells, each time the chromosome replicates, the ends (telomeres) shorten, limiting the number of times the cell can divide. However, telomerase is activated in cancer cells, allowing an unlimited number of cell division.

Fourth, normal cells cease to divide and die when there is DNA damage or when cell division is abnormal. Cancer cells continue to divide, even when there is a large amount of damage to DNA or when the cells are abnormal. These progeny cancer cells continue to divide they accumulate even more damaged DNA.

2.1.3 Genetics of Cancer

A small number of genes in the human genome are associated with cancer. Alterations in these genes cause different forms of cancer. These malfunctioning genes can be broadly classified in to three groups, proto-oncogenes, tumor suppressors, and DNA repair genes[46,47,48]. Proto-oncogenes and tumor suppressor genes work as the accelerator and brakes of the cell growth, respectively. Proto-oncogenes accelerate controlled cell growth, while tumor suppressors slow cell growth. The overactivity mutation of proto-oncogenes and underactivity of tumor suppressor genes lead to cells proliferate abnormally and create cancer. The third group includes DNA repair genes, which help prevent mutations that induce cancer.

Oncogenes are the mutated forms of proto-oncogenes that activate producing signaling molecules, resulting in an increased production of factors that stimulate cell growth. For example, *MYC* is a proto-oncogene that codes for a transcription factor. Mutations in *MYC* convert it into an oncogene associated with seventy percent of cancers. *RAS* is another oncogene that normally functions as an “on-off” switch in the signal cascade. Mutations in *RAS* cause the signaling pathway to remain “on”, leading to uncontrolled cell growth. About thirty percent of tumors- including lung, colon, thyroid, and pancreatic carcinomas- have a mutation in *RAS*[46].

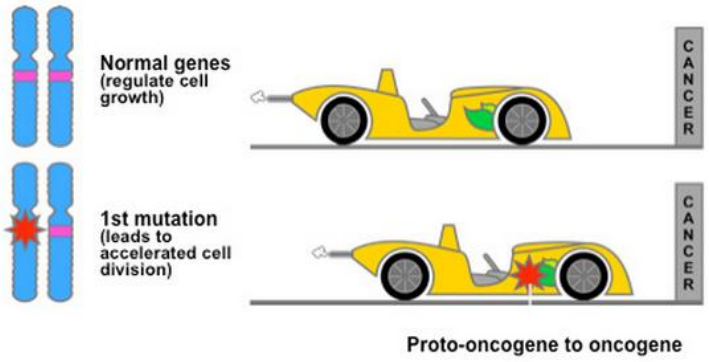

Figure 2.1 Illustration of proto-oncogene to oncogene[46]

Tumor suppressor genes in normal cells serve as braking signals during phase G1 of the cell cycle[48]. When working properly, the proteins made by tumor suppressor genes control the processes of cell growth and cell death, which prevent tumor formation. If a tumor suppressor gene is mutated, the normal brake mechanism will be disabled, leading to tumor formation or growth (cangenom).

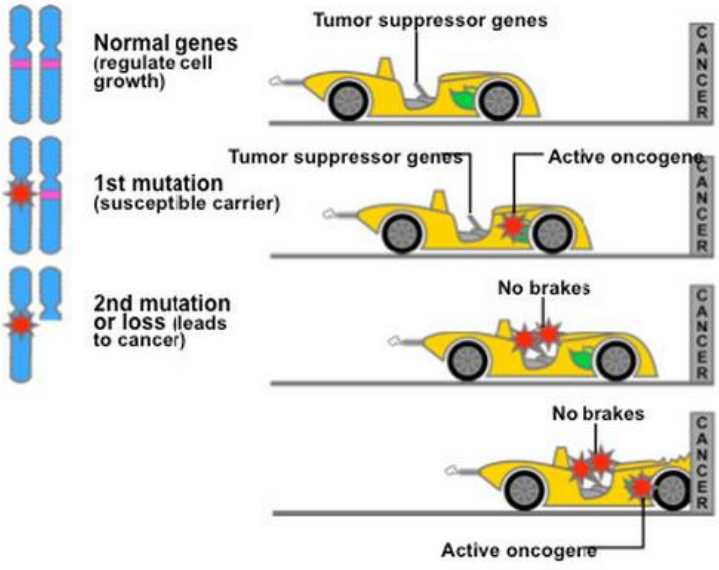

Figure 2.2 Illustration of tumor suppressor genes[46]

During cell division, mistakes may occur. Errors in DNA replication can lead to mutations[49]. If these mutations occur in proto-oncogenes or tumor suppressor genes, DNA repair genes will correct the damage to chromosomes, thereby minimizing mutation in the normal cells. When these genes are mutated or altered, the mistakes that can not be repaired will accumulate and increase the frequency of cancerous changes in the cells.

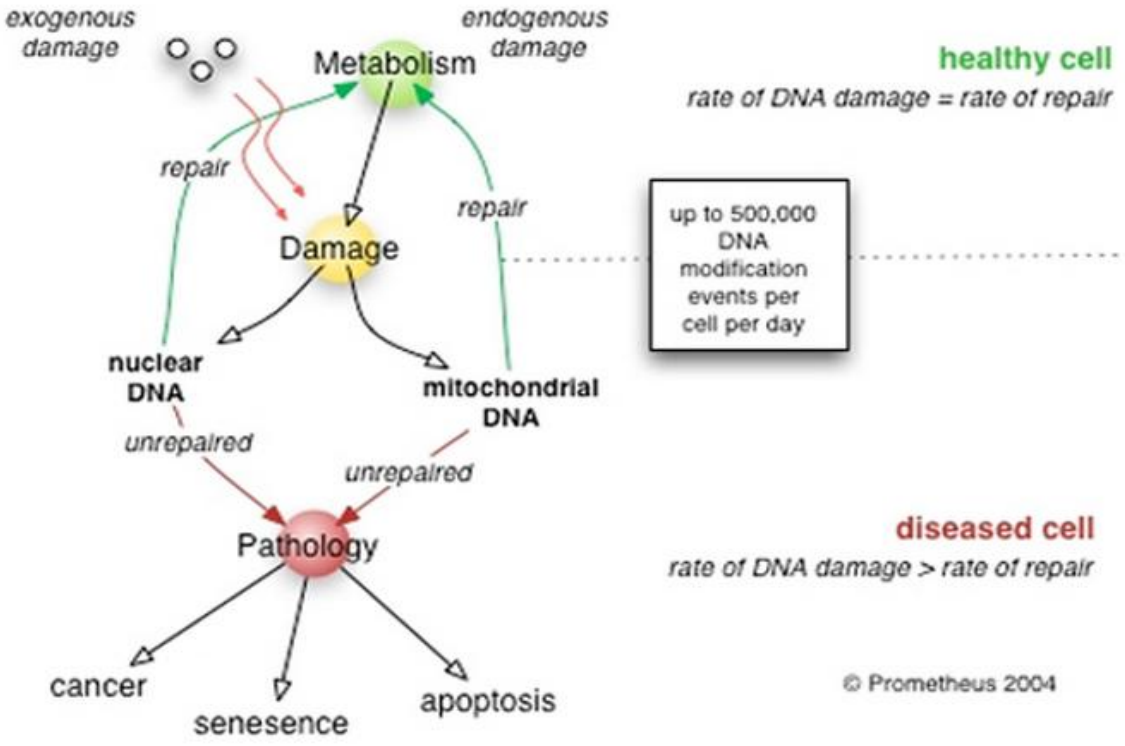

Figure 2.3 Errors in DNA replication[49]

2.1.4 New Treatments for combating cancer

The traditional treatments for combating cancer include surgery, radiation and chemotherapy[6,7]. Among them, surgery is the oldest form of cancer treatment, which is used to remove solid tumors. Even today, surgery is still the first treatment for early stage cancers and benign tumors. However, it is not a good option in many patients with malignant tumors

due to the tumor size, location and presence of metastases. Radiation is considered as a local therapy, which kills cancer cells in a specific localized area of the body with high-energy rays[7]. It damages DNA and stops DNA's replication in the rapidly divided cancer cells. At the same time, radiation also kills some normal cells, but because normal cells are growing more slowly, they are able to repair the radiation damages if radiation treatments are given in a small daily dose. In contrast to local therapy, chemotherapy is systemic therapy, which travels throughout the body[6]. Most of the chemotherapy drugs are toxic compounds to interrupt the synthesis of precursors for DNA replication. While other drugs damage DNA extensively and stop the DNA's replication. However, the side effects of both radiation and chemotherapy are severe, they kills a large amount of normal cells and cause low white blood cell count, gastrointestinal distress and hair loss.

Hormone Therapy

Hormones are important factors that affect normal cell growth. Even though cancer cells have lost part of the normal responses to growth factors, some types of cancer cells still require hormones to grow, such as breast cancer[50] and prostate cancer[51]. Hormone therapy tries to starve the cancer cells of these hormones, make cancer cells grow more slowly or even kill cancer cells. This is usually done with drugs that stop the production of the hormones or interfere with the activity of the hormone. For example, estrogens are the primary female sex hormones, which are required by some breast cancer cells for growth. Blocking the binding site for estrogen is the effective way to slow the growth of these breast cancers. Tamoxifen and Raloxifene[52,53] are the typical examples of this type of drugs. Similarly, some prostate cancer cells require androgen hormone to grow. Selective androgen

receptor modulators are drugs that block the binding of testosterone to these cancer cells, inhibiting their growth and possibly preventing prostate cancer.

Antiangiogenesis therapy

Angiogenesis, the formation of new blood vessels, is a physiological process controlled by chemical signals in the body. These signals can help repair the damaged blood vessels and form the new blood vessels. On the other hand, angiogenesis inhibitor interferes with the formation of new blood vessels. These two effects are balanced so that new blood vessels form only when and where they are needed[54].

Angiogenesis performs a key role in the growth of cancer. Normally small solid tumor (<1-2cm) are not vascularized. To spread, tumors can produce angiogenesis signaling molecules to cause the blood supply to form, or stimulate nearby normal cells to give off chemical angiogenesis signals. The new formation of blood vessels provide growing tumor with oxygen and nutrients, allowing the cancer cells to invade nearby normal tissues, and to move to other areas of the body.

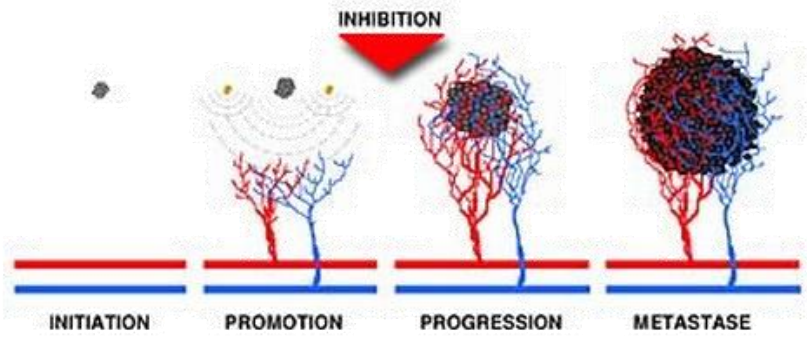

Figure 2.4 Process of angiogenesis formation[54]

In the early 1970s Dr. Judah Folkman[55] first suggested inhibiting new blood vessel formation as a new approach to "starve" cancer cells. In the next few decades, several angiogenesis inhibitors were developed, which interfere with the angiogenic process to inhibit tumor progression and metastatic progression that accompanies with the growth of tumor. Until 2004, Bevacizumab[56], the first commercially angiogenesis inhibitor, was approved by the U.S. food and drug administration (FDA) for certain metastatic cancers. It was shown to slow tumor growth, more important, to extend the lives of patients. After that, other drugs that inhibit angiogenic activity were approved by the FDA, including sorafenib (Nexavar®) for hepatocellular carcinoma and kidney cancer, sunitinib (Sutent®) and everolimus (Afinitor®) for both kidney cancer and neuroendocrine tumors, and pazopanib (Votrient®) for kidney cancer[56].

Chemoimmunotherapy

Immunotherapy has been investigated for over a century as an attractive strategy for cancer treatment[57]. It is treatment that uses the patient's immune system to fight diseases such as cancer. This can be done either through immunization of the patient, in which case the patient's own immune system is stimulated to work harder or smarter to attack cancer cells, or through administration of immune system components such as antibodies, in which case the patient's immune system is recruited to destroy tumor cells by the therapeutic antibodies.

Chemoimmunotherapy strategically integrate immune-based therapy with chemotherapy. Chemotherapy drugs were attached to antibodies that are specific for some cancer cells. The cancer-cell-specific antibody then delivers the drug directly to cancer cells without harming normal cells, reducing the toxic side effects of chemotherapy[58].

2.2 Current Advances in Nanoparticle Delivery Systems for Cancer Therapy

2.2.1 Introduction

Despite many advances in conventional cancer treatments, cancer therapy is still far from optimal because of the severe side effects. Thus, there is an urgent need to develop new and innovative technologies that could enhance the therapeutic efficacy and minimize the side effects. The past decade has witness tremendous advances in the field of nanoparticle delivery systems[10],[12]. Several drug nanocarriers have been developed, including liposomes[14-15], polymeric nanoparticles[15,59] , and dendrimers[19,60].

As with any nanomaterial used in drug delivery, there are a number of important parameters for the successful development and manufacturing of targeted drug delivery vehicles[61]. These parameters include (a) the use of biodegradable and biocompatible materials which can be degraded or metabolized into non-toxic components and cleared quickly; (b) submicron size distribution and surface charge may affect the efficiency and pathway of cellular uptake by influencing the adhesion of the particles and their interactions with cells. (c) capability to increase drug stability and maximize drug action; (d) to increase the drug concentration at desired tumor sites and reduce damage on the normal tissues.

Passive and active cancer targeting are the two strategies on delivering drug-encapsulated nanoparticles to tumor tissue[62,63]. Passive cancer targeting employs the unique properties of the tumor microenvironment, such as leaky tumor vasculature and a dysfunctional lymphatic drainage system. These features provide an enhanced permeability and retention (EPR) effect, which could accumulate nanoparticles in tumor tissues. As a result, the concentration of drug-encapsulated nanoparticles in tumors can be much higher

than those in normal tissue. Abraxane®, albumin-bound paclitaxel nanoparticles for the treatment of metastatic breast cancer, and Doxil®, a poly (ethylene glycol)-coated (PEGylated) liposomal system for doxorubicin (Dox) delivery, are representative examples of nanocarrier-based drugs using EPR effect for treatment of cancer[62]. However, this approach suffers from several limitations. For example, the EPR effect is not feasible in all tumors because the degree of tumor vascularization and porosity of tumor vessels can vary with the tumor type and status. The drug-encapsulated nanoparticles concentration is still insufficient at the tumor site[64]. In active targeting, active targeting ligands are attached to the surface of the nanoparticle for recognizing and binding to specific receptors overexpressed at the surface of cancer cells. Compare to passive targeting, active targeting can deliver drug-encapsulated nanoparticles to uniquely identified sites with minimal undesired harmful toxicity to non-cancerous cells adjacent to the targeted tissue. Currently the major problem in active targeting is ligand-drug conjugate and to enhance the systems by encapsulating the drug in nanoparticles efficiently.

2.2.2 Liposome

As early as 1970s, liposomes had been suggested as drug carriers in cancer chemotherapy by Gregoriadis et al[65]. Since then, the liposome systems as drug carrier are being extensively studied. Liposomes or lipid vesicles are composed of either synthetic or natural phospholipids[11], which contribute to the predominant physical and chemical properties of a liposome, including permeability, charge density and steric hindrance. It appears that different applications require different types of liposomes. There are three major types of liposome based on the particle size, the small unilamellar vesicles (SUV< 0.1μm),

the multi-lamellar vesicles (MLV> 0.1 μm) and the large unilamellar vesicles (LUV >0.1 μm). MLV and LUV are cleared rapidly from the circulation, while SUV remains in circulation system for longer period of time. As a proven candidate for delivery of a wide range of therapeutics, liposomes can encapsulate their payload by several methods, as shown in Figure 2.5.

In the early days, the design of liposome drug delivery system is relatively simple. Water soluble drug and DNA is designated to be encapsulated in their internal aqueous compartment, whereas lipid soluble drug can be embedded within the phospholipids bilayer. Up to now, the strategies are becoming increasingly complex to fulfill the growing requirement for treating several different diseases. A significant advanced liposomal delivery is the surface chemical modification of liposomes with certain polymers, such as poly (ethylene glycol) or other polymers including poly(acrylamide) and poly(N-vinyl pyrrolidine)[66]. This strategy could impart the in vivo long-circulating time to the liposomes. The first approved liposomal formulations of anticancer drugs for human use, Doxil® has achieved the most prolonged circulation to date, with a terminal half-life of 55 hours in humans[67].

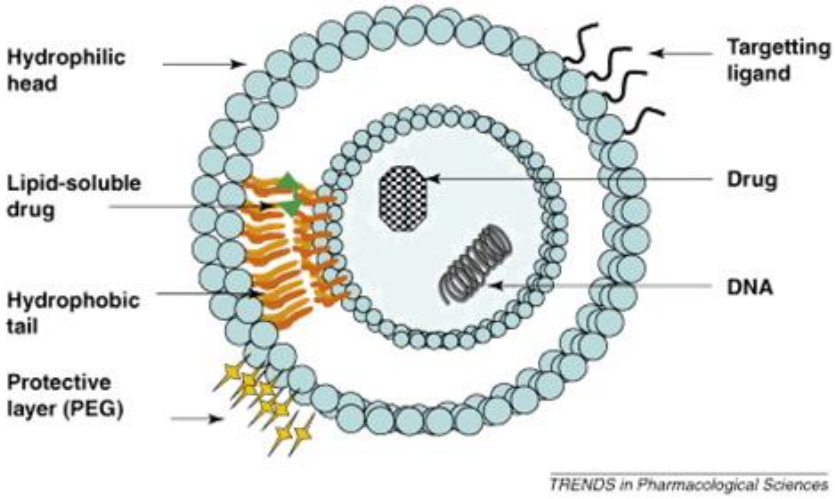

Figure 2.5 Diagram of a bilaminar liposome. The hydrophobic region traps drugs in the central core when the liposomes are prepared. The outer surface can be functionalized with ligands for active targeting or PEGylated[14].

Another significant advance in development of liposome-based drug delivery is incorporation of targeting moieties. By attaching targeting ligands to the liposomes surface, liposomes can search for and attach themselves to the specific receptors on tumor cell surfaces[37]. For example, the folate attached to the outer surface of liposomes is able to conjugate with the folate receptors overexpressed on tumor cell surfaces, which can avoid nonspecific attacks on normal tissue and increase cellular uptake within target cancer cells.

As one of the most successfully drug delivery systems that are currently in clinical use, liposomes-based nanoparticles offered us a wide range of tools for the construction of more complex and multifunctional devices in pharmaceutical application.

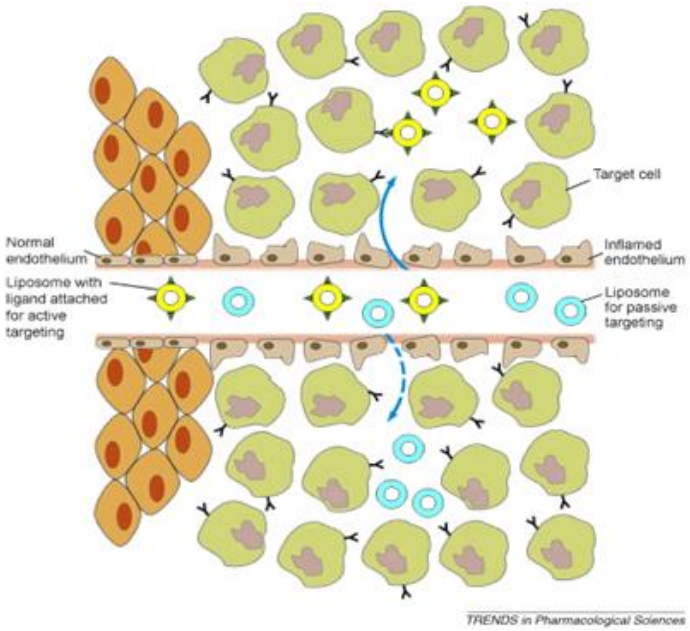

Figure 2.6 Active and passive targeting of cells for drug targeting using liposomes[68].

2.2.3 Polymeric Nanoparticles

Polymeric nanoparticles have been investigated as another attractive delivery system for cancer treatment since liposome due to their favorable physiochemical properties, such as controlled size distribution, relatively high drug carring capacity, and tunable properties[69]. Recently, several polymer-mediated delivery systems, including polymer micelles, polymer-drug conjugates, polymer-drug polyplexes, and hydrogels, have been developed to improve efficacy of drug delivery[70]. These novel polymeric nanoparticles are expected to protect the drug from enzymatic digestion and rapid clearance, as well as providing the potential for controlled release.

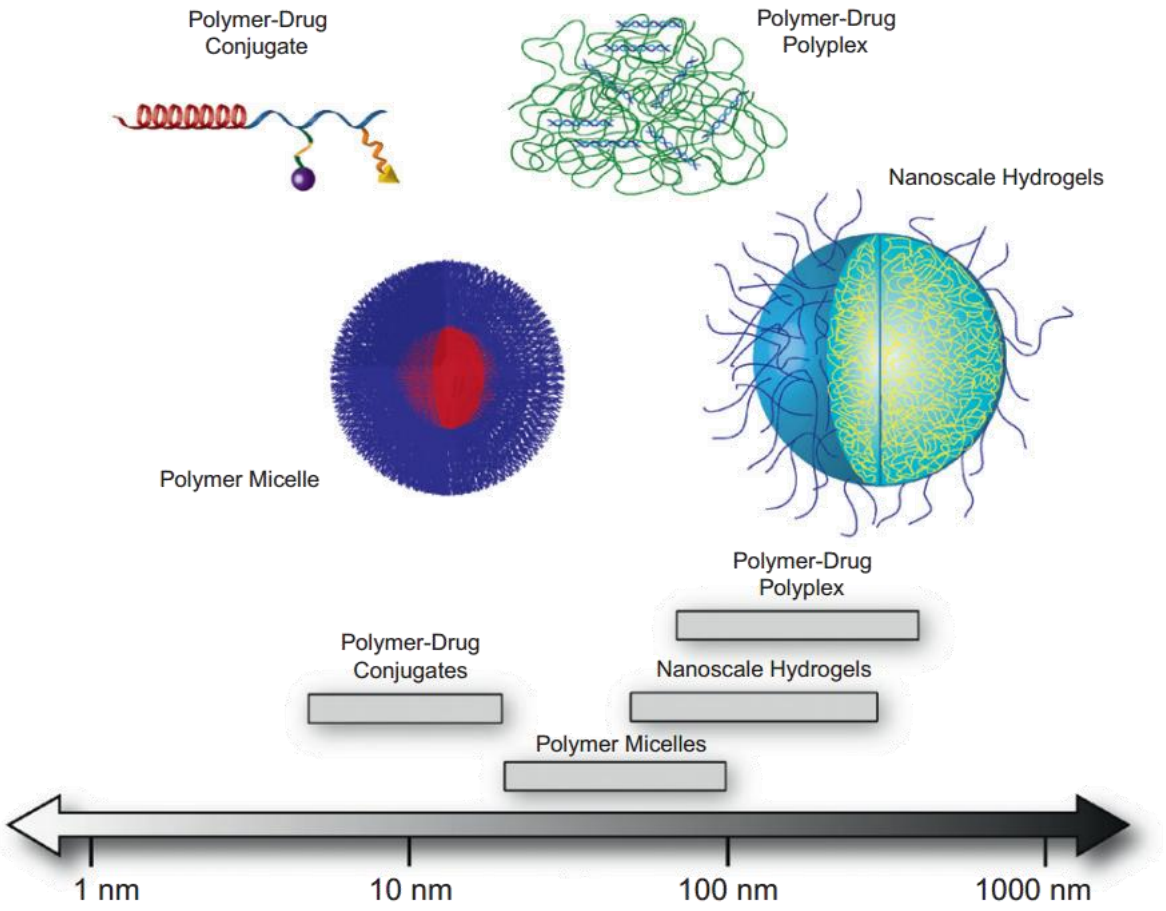

Figure 2.7 Typical length scales of responsive nanoscale drug delivery systems[70].

Polymer Micelles

Most polymer micelles are formed with hydrophobic interior and a hydrophilic corona by amphiphilic block copolymers. Hydrophobic or water-insoluble drugs can be encapsulated in the hydrophobic core like surfactant micelles. Comparing with classic surfactant micelles, the thermodynamic and kinetic stability of polymer micelles is better, which allow them to retain integrity, even after extreme dilution (e.g. intravenous injection) or extended circulation time[40]. Polymeric micelles also have several advantages over other nanosized drug delivery systems. One favorable property of polymer micelles is their moderate size

distribution. The typical micelle size (20-100 nm) is small enough to avoid or minimize rapid uptake by RES while large enough to avoid renal clearance, which allows prolonging the circulation time of these particles in human body[10]. Another favorable property is that physical encapsulation of hydrophobic drugs within polymer micelles won't affect their bioavaibility or deactivate the drug's active site[71].

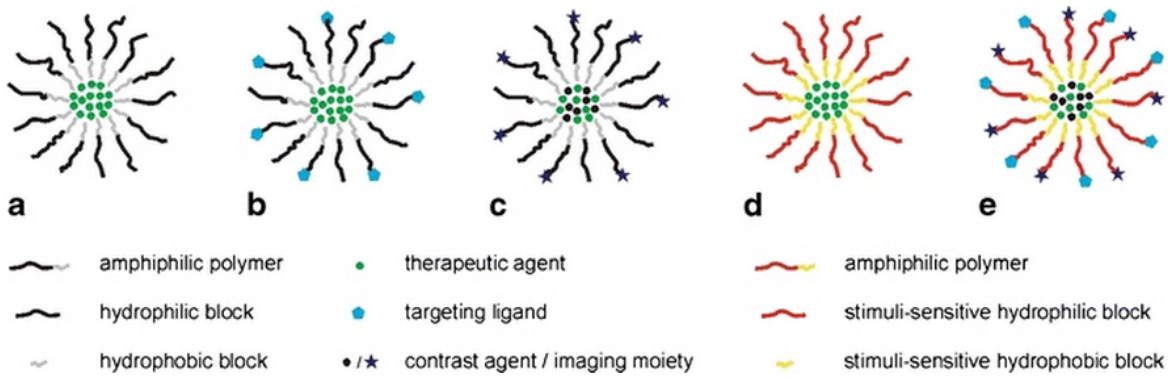

Figure 2.8 Schematic drawing of polymeric micelle (a). Micelle conjugated with a targeting ligand (b). Micelle containing an incorporated contrast agent or chelated imaging moieties (c). Micelle modified for triggered drug release (d). Either the hydrophilic or hydrophobic polymer can be rendered thermo/pH/light/ultrasound-sensitive. Optimized micelle for anticancer therapy, bearing targeting ligands, contrast agents or imaging moieties, therapeutic drugs and polymers suitable for triggered, controlled release (e)[40].

By modifying the structure of single copolymer monomer, different polymer micellar formulations for anticancer therapy can be achieved, as shown in Figure 2.8[40]. Targeting ligands can be attached to the outer surface of micelles which recognize and bind to specific receptors overexpressed in tumor cells. Incorporation or chelation of imaging moieties provides an efficient method for tracking micelles in vivo for biodistribution studies. Moreover, pH-, thermo-, light-, or ultrasound-sensitive block copolymers allow for controlled micelle dissociation and triggered drug release[16].

Table 2.1 Polymeric Micelles in Clinical Trials

Polymeric micelle	Block copolymer	Drug	Diameter	Indication	Clinical phase
NK012	PEG-PGlu(SN-38)	SN-38	20 nm	Breast cancer	II
NK105	PEG-P(aspartate)	Paclitaxel	85 nm	Advanced stomach cancer	II
SP1049C	Pluronic L61 and F127	Doxorubicin	22-27 nm	Adenocarcinoma of oesophagus, gastroesophageal junction and stomach	III
NC-6004	PEG-PGlu(cisplatin)	Cisplatin	30 nm	Solid tumors	I/II
Genexol-PM	PEG-P(D,L-lactide)	Paclitaxel	20-50 nm	Breast cancer	IV
				Pancreatic cancer	II
				Non-small-cell lung cancer in combination with carboplatin	II
				Pancreatic cancer in combination with gemcitabine	I/II
				Ovarian cancer in combination with carboplatin	I/II

Currently, five micellar formulations for cancer therapy have been tested in clinical trials , as shown in Table 2.1, including NK012[72], NK105[73], SP1049C[74], NC-6004[75], and Genexol-PM[76]. Among these five formulations, Genexol-PM has been granted FDA-approval to be used in patients with breast cancer.

Polymer-Drug Conjugates

Synthetic polymer-drug conjugate used for drug delivery was first proposed by Ringsdorf in the mid-1970[77]. In this model, both chemotherapeutic agents and homing moieties are attached to the same polymeric carrier covalently, so that more drug molecules to the tumor site and active targeting could be achieved at the same time. Unlike polymeric

micelles, they do not entrap the drug inside. Since then, polymer-drug conjugates has become one of the fastest growing fields and generated enormous attention[78]. Various architectures of polymers have been developed as drug carriers due to their several advantages, including (1) an enhancement of drug bioavailability in aqueous solution; (2) protection of drug during circulation; (3) a reduction in immunological body response; (4) the ability to provide active or passive targeting of the drug to the site of tumor; (5) the possibility to include several other active components to form an advanced complex drug delivery system[17].

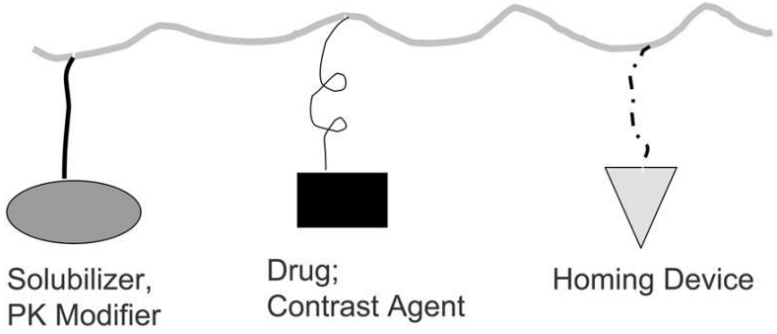

Figure 2.9 Model for targetable polymer-drug conjugates according to Ringsdof[77].

In the past decades, nearly a dozen polymeric conjugates moved into the clinical trial stage[79]. Clinical results collected among these polymer-drug conjugates, poly (L-glutamic acid) (PG)-paclitaxel (PG-TXL) has advanced to Phase III clinic trials, which is positioned as the first-line therapy for metastatic breast cancer and advanced ovatian cancer. Despite progress, further generation of polymer-drug conjugates remain a number of challenges, such as the possibility to modulate rates of degradation, accurate control of polymer weights and molecular weight distributions, and to facilitate noninvasive monitoring of drug delivery efficiency, et al.

Table 2.2 Polymer-drug conjugates in clinical trials[79]

Conjugates	Indication	Status	Company
HPMA-doxorubicin (PK1; FCE28068)	Lung and breast cancers	Phase II as of 2002	Pfizer; Cancer Research Campaign UK
HPMA-doxorubicin-galactosamine (PK2, FCE28069)	Hepatocellular carcinoma	Phase I/II	Pfizer; Cancer Research Campaign UK
HPMA-camptothecin (PNU166148)	Solid tumors	Phase I; discontinued	Pfizer; Cancer Research Campaign UK
HPMA-paclitaxel (PNU166945)	Solid tumors	Phase I; discontinued	Pfizer; Cancer Research Campaign UK
HPMA-platinate (AP5346, ProLindac)	Ovarian, melanoma, and colorectal cancers	Phase I	Access Pharmaceutical
PEG-Camptothecin (Pegamotecan)	Solid tumors	Phase I; discontinued	Enzon
PEG-SN38 (EZN-2208)	Solid tumors	Phase I; initiated as of October 2007	Enzon
Polymeric micelles (NK911)	Pancreatic cancer	Phase II	Nippon Kayaku, Japan
Cyclodextrin-based polymer-CPT (IT-101)	Solid tumors	Phase I	Insert Therapeutics
Carboxymethyldextran-exatecan (DE-310)	Solid tumors	Phase I	Daiichi Pharmaceuticals, Japan
PG-TXL (CT-2103, Xyotax)	Lung, ovarian, colorectal, breast, and esophageal cancers	Phase III	Cell Therapeutics
PG-camptothecin (CT2106)	Colorectal, lung, and ovarian cancers	Phase I	Cell Therapeutics

Polymer-Drug Polyplex

Polymer-drug polyplexes are formed by chain entanglements and hydrophobic interactions between polymers and nucleic acids, low molecular weight drugs, or proteins.

These structures are expected to have increased mechanical stability than polymeric micelles[80].

2.2.4 Dendrimers

Dendrimers represent a novel class of polymeric material that possesses a number of unique physical-chemical properties, including a highly regular branching pattern, a low polydispersity index, and a well-defined number of peripheral groups[11]. Since Tomalia et al and Newkome et al first reported their dendrimer synthesis work in the early 1980s; several novel dendritic scaffolds have been synthesized over the past two decades[81,19, 82]. At the very beginning, studies on dendrimers focused on their syntheses and physical- chemical properties, and its potential application in biological applications was exploited only in the past few years. By comparing the features of dendrimers with those of conventional polymers, dendritic architectures provide several advantages for drug delivery applications[83]. For example, unlike polymeric micelles, dendrimers do not dissociate upon dilution because they are covalent bound, which could provide an efficient way to overcome the problem of sudden release of drug during circulation. In addition, more drug molecules and targeting groups can be attached to the well-defined peripheral groups of dendrimers to increase therapeutic efficacy. Furthermore, the globular shape of dendrimers could affect their biological properties, leading to reproducible pharmacokinetic behavior as opposed to the random coil structure of linear polymers.

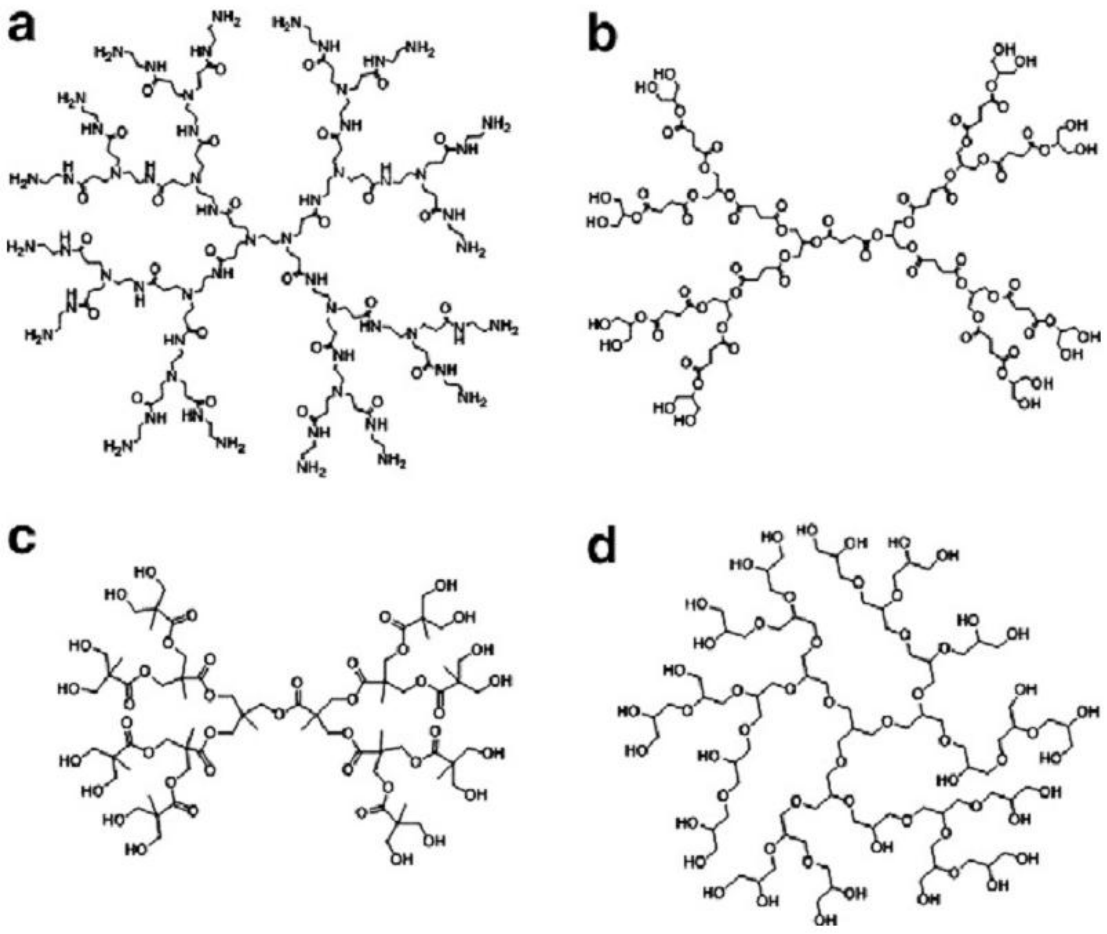

Figure 2.10 Examples of several dendritic scaffolds extensively studied for potential drug delivery applications: (a) PAMAM, (b) poly(glycerol-succinic acid) dendrimer, (c) Boltorn® and, (d) hyperbranched polyglycerol.

Noncovalent encapsulation of drugs

Inspired by the encapsulation mechanisms of liposome and polymeric micelles for drug delivery, initial studies of dendrimers as drug delivery carriers focused on their use as unimolecular micelles or 'ordendritic boxes' to encapsulate drug molecules by noncovalently bonding[84]. For example, hydrophobic drugs and dye molecules were trapped into various dendrimer hydrophobic cores, and DNA was complexed with dendrimers for gene delivery

applications. As mentioned above, an advantage of using dendrimers rather than polymeric micelles is that the micellar structures of dendrimer are maintained at all concentrations. However, this method suffers from shortcomings that it is difficult to breakdown the dendritic scaffolds and to control the release of molecules from the dendrimer core.

A promising novel approach to controlling the release of drugs from the dendrimer includes introduction of pH-sensitive hydrophobic acetal groups on the dendrimer periphery. The Haag group developed a library of intelligent core/shell dendrimer structures based on hyperbranched polyglycerol (PG)[85]. The dendritic nanocarriers were assembled by attaching a PEG shell to the hyperbranched PG core through a pH-labile imine bond which was designed to cleave off at pH 5.0. This dendrimer can be used to encapsulate the anticancer drug doxorubicin and a NIR imaging dye indotricarbocyanine.

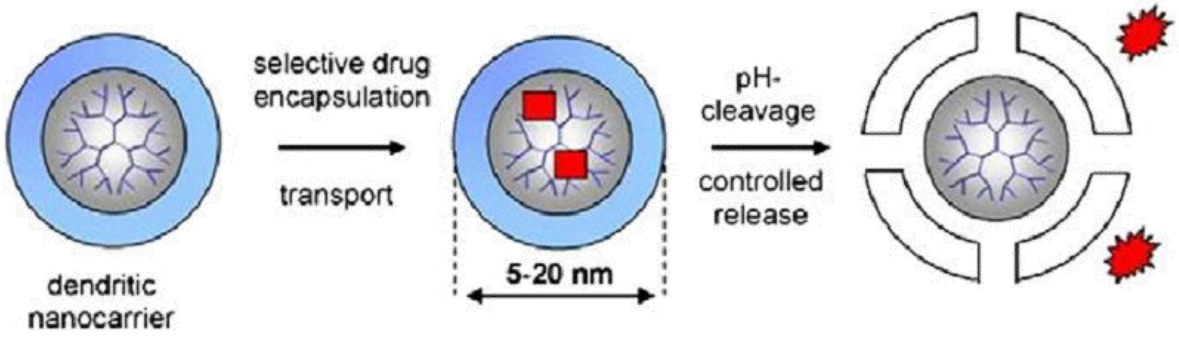

Figure 2.11 Unimolecular dendritic nanocarriers for supramolecular encapsulation of biologically active compounds. Controlled release after triggered shell cleavage (e.g. pHcontrolled)[85].

Covalent dendrimer-drug conjugates

Following Ringsdorf's idea of polymer-drug conjugates, active species and the targeting moiety can be covalent linked to the peripheral end-groups of a dendrimer to create a

multi-functional drug delivery platform. The drug loading can be tuned by altering the dendrimer's generation number, and release of the drug can be controlled by the chemical degradable linkage between the drug and dendrimer[86]. In most cases, the drugs are linked to the periphery groups of dendritic scaffold through an easter or amide bonds. In addition to these two linkage types, hydrazone, carbamate, disulfide, and imine types have also been used. Each of the linkages has their own inherent and differential cleavage mechanisms that separate the drug molecule from the carrier. For instances, easter, carbamates and hydrazone collapse depend on environmental pH, while amides and peptidic sequences need enzymatic hydrolysis for their degradation and release of the drug molecule.

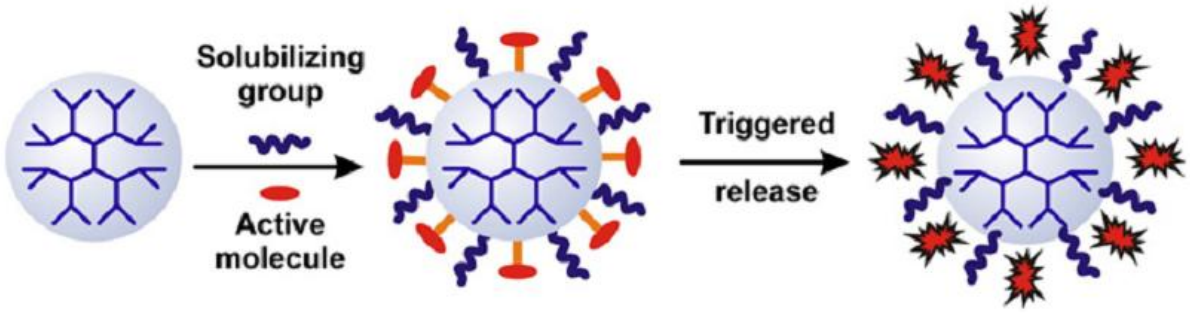

Figure 2.12 Design of a dendritic conjugate by attaching multiple copies of drugs and solubulizing groups to the scaffold. Environment-responsive linker system can facilitate triggered-drug release[86].

Duncan et al. have prepared conjugates of polyamidoamine (PAMAM) dendrimer with cisplatin, an insoluble anticancer drug with nonspecific toxicity[81]. The PAMAM-platinate conjugate showed increased solubility, decreased systemic toxicity (3- to 15- fold) than cisplatin and selective accumulation in solid tumors. In addition, Duncan collaborated with Veronese et al. and first synthesized a novel monodisperse PEG-dendrons[60]. This branched

PEG-based architecture was found to be non-toxic to an endothelial-like cell line at concentrations of 4 mg/mL for over 72h.

Haag group has dedicated their effort on developing novel dendrimer-drug conjucates in the recent years[18]. They synthesized thiolated polyglycerol by coupling PEG-maleimide and DOXO-EMCH onto the scaffold in a one-pot method, thereby yielding polyglycerol-doxorubicin conjugate with a PEG-shell. *In vitro* stability studies indicated that this pH-triggered conjugate could release less than 5% free doxorubicin at pH 7.4, while have a half-life of 3.5 h at pH 4.0. The conjugate also showed excellent antitumor efficacy in the ovarian carcinoma A2780 xenograft model.

Although dendrimer-drug conjugates exhibited substantially positive biological results in current studies, most of the conjugates suffer from a general and serious setback[87]. It is hard to generate homogeneous distribution of ligand-bound dendritic carriers because the number and type of ligand species and synthetic steps varies. Such an inhomogeneous ligand distribution on dendritic surface will hinder their implication for eventual biological and clinical trials.

2.3 Self-Assembling Ionic-Complementary Peptides

2.3.1 Introduction

Molecular self-assembly is a spontaneous and reversible process by which molecules and individual entities into organized structures at multiple length scales. Recently, nanotechnology through molecular self-assembly become tremendously important in various research areas, especially as a fabrication tool. Up to now, it is still the only practical

approach for producing a variety of nanostructures, and conveys a kind of strong power to break conventional top-down fabrication techniques. This ubiquitous but unique free-energy driven process strikes a new episode to create artificial nanoscale scaffold.

In the bio-world, amino acids and short peptides have been considered to be useful building blocks for materials engineering owing to their assortment of functional groups. Over the past decades, extensive research activities have been devoted to the design and fabrication of novel biomimetic nanobiomaterials through peptide self-assembly [23]. Many classes of synthetic peptides have been discovered and explored in various biomedical applications, ranging from drug delivery[88], tissue engineering[89], 3D cell culture[90] to SiRNA and gene delivery. Self-assembling peptides are able to form stable and regularly patterned macroscopic structured aggregates through non-covalent interactions, including ionic bonds, hydrogen bonds, hydrophobic and van der Waals interactions[24]. Even though each of the forces is not strong, the collective interactions can lead to very stable structures and materials.

As early as 1993, Zhang and colleagues has pioneered the studies on a new class of peptide EAK16 originally derived from a left-handed Z-DNA binding protein in yeast[91]. This class of peptides has a specific structure of alternating hydrophilic and hydrophobic amino acid residues, which tend to form β-sheet rich fibers. Such a regular assortment and arrangement of functional residues ensure the peptide monomers assembly into various ordered structures, such as filaments, layers, and nanotubes. They are stable across a broad range of temperature, wide pH ranges in high concentration of denaturing agent urea and guanidium hydrochloride[22]. Besides, they also possessed relatively good biocompatibility

and biodegradability[92]. These nanostructures could act as a basis for fabricating more functional materials with diverse properties, which is believed to have considerable potential for a number of applications in tissue engineering, drug delivery system and scaffold engineering. Since then, many self-assembly ionic complementary peptides have been systematically studied, as listed Table 2.3[93]. These peptides are either derived from the segments of existing proteins or rationally designed to mimic and understand protein secondary structures. As an emerging potential delivery material in biotechnology, a good understanding of the self-assembling process will help us design smarter peptide nanostructures for specific goals. The following sections aim to outline the detailed information of self-assembly ionic complementary peptides, focusing on the factors influencing their nanostructure formation.

Table 2.3 the family of self-assembling ionic-complementary peptide[93]

Name	Charge distribution sequence	Type	Structure
RADA16-I	+−+−+−+−: n-RADARADARADARADA-c	I	β
RGDA16-I	+−+−+−+−: n-RADARGDARADARGDA-c	I	r.c.
RADA8-I	+−+−: n-RADARADA-c	I	r.c.
RAD16-II	++−−++−−: n-RARADADARARADADA-c	II	β
RAD8-II	++−−: n-RARADADA-c	II	r.c.
EAKA16-I	+−+−+−+−: n-AEAKAEAKAEAKAEAK-c	I	β
EAKA8-I	−+−+: n-AEAKAEAK-c	I	r.c.
RAEA16-I	+−+−+−+−: n-RAEARAEARAEARAEA-c	I	β
RAEA8-I	+−+−: n-RAEARAEA-c	I	r.c.
KADA16-I	+−+−+−+−: n-KADAKADAKADAKADA-c	I	β
KADA8-I	+−+−: n-KADAKADA-c	I	r.c.
EAH16-II	−−++−−++: n-AEAEAHAHAEAEAHAH-c	II	β

EAH8-II	−−++: n-AEAEAHAH-c	II	r.c.
EFK16-II	−−++−−++: n-FEFEFKFKFEFEFKFK-c	II	β
EFK12-I	−+−+−+: n-FEFKFEFKFEFK-c	I	β
EFK8-I	−+−+: n-FEFKFEFK-c	I	β
KFE8-I^{T}	+−+−: n-KFEFKFEF-c	I	β
KFE8-I	+−+−: n-FKFEFKFE-c	I	β
KFE12-I	+−+−: n-FKFEFKFEFKFE-c	I	β
KFE16-I	+−+−+−+−: n-FKFEFKFEFKFEFKFE-c	I	β
KIE12-I	+−+−+−: n-IKIEIKIEIKIE-c	I	β
KVE12-I	+−+−+−: n-VKVEVKVEVKVE-c	I	β
KFQ12	+−+−+−: n-FKFQFKFQFKFQ-c	I	β
ELK16-II	−−++−−++: n-LELELKLKLELELKLK-c	II	β
ELK8-II	−−++: n-LELELKLK-c	II	β
EAK16-II	−−++−−++: n-AEAEAKAKAEAEAKAK-c	II	β
EAK12-a	++−−++: n-AKAKAEAEAKAK-c	II	r.c.
EAK12-b	+−−++: n-AKASAEAEAKAK-c	N/A	r.c.
EAK12-c	+−−−++: n-AKAEAEAEAKAK-c	N/A	r.c.
EAK12-d	−−−−++: n-AEAEAEAEAKAK-c	IV/II	α/β
EAK8-II	−−++: n-AEAEAKAK-c	II	r.c.
P18-a	−−−−++++: n-GELELELEQQKLKLKLKG-c	IV	α/β
P18-b	−+−++−+−: n-GELKLELKQQKLELKLEG-c	N/A	α/β
P18-c	−−++−−++: n-GELELKLKQQELELKLKG-c	II	α/β
P18-d	−−−−++++: n-GELEAELEQQKLKAKLKG-c	IV	α/r.c.
P17-a	−+−+−+: n-ETATKAELLAKYEATHK-c	I	α/β
P17-bc	−+−+−+: n-ETATKAELLAKZEATHK-c	I	α/β
P11-I	+−: n-QQRQQQQQEQQ-c	I	α/β
P11-II	+−: n-QQRFQWQFEQQ-c	I	α/β
LEK16	−−++−−++: n-YLEELLKKLEELLKKL-c	II	α

LEK9	+−+−: n-YKLELKLEL-c	I	β
IDR16	−−++−−++: n-YIDDIIRRIDDIIRRI-c	II	α
IDR9	+−+−: n-YRIDIRIDI-c	I	β
P6-c	n-KTVIIT-c	N/A	r.c.
P6-d	n-STVIIT-c	N/A	β
P6-e	+−: n-KTVLIE-c	I	β/r.c.
P6-f	+−: n-KTVIVE-c	I	β/r.c.

β: β-sheet; α: α-helix; r.c.: random coil; N/A: not applicable.

2.3.2 Molecular Structure

Among many self-assembling peptides, the class of ionic complementary peptides is of special interest, because they possess several uncommon important features due to their specific assortment and arrangement of amino acid residues[93,91]. First, one critical important factor is their varieties of charge distribution. The ionic complementary sides have been classified into several modules by their alternating arrangement of negatively and positively charged residues along the peptide backbone. The most widely studied modules of charge distribution are modulus I (− + or + −), modulus II (− − + + or + + − −) and modulus IV (− − − − + + + + or + + + + − − − −). These ordered charge distribution generate unique electrostatic interactions, which promote stable molecular self-assembly besides usual hydrogen bonding and hydrophobic interaction. In addition, the charge orientation can also be tuned in the reverse direction, which can yield entirely different peptides.

A second critical feature is that the new ionic-complementary peptides can be derived by using different amino acids to replace those of the existing peptides with the same charge

distribution[94]. For example, RAD16 can be obtained from EAK16 by replacing the residues glutamic acid (E) and lysine (K), with arginine (R) and aspartic acid (D), respectively. Similarly, the replacement of the hydrophobic residue alanine (A) of EAK16 with phenylalanine (F) or leucine (L) will generate two other ionic-complementary peptides, EFK16 and ELK16, respectively. Their intrinsic properties, secondary structures and biological activities can be changed with the replacement of new amino acids.

A third feature is the specific peptide chain lengths required to exhibit ionic complementarity. The length of self-assembling ionic-complementary peptides depends on the alternating hydrophobic and hydrophilic residues in the peptide sequence (Table 2.1). The minimum number of amino acids required to build modulus I peptides is four, while the creation of modulus II and modulus IV peptides require eight and sixteen amino acids, respectively. Polypeptides such as poly-EAK can be designed by increasing the number of sequence of the short peptides to the desired length.

2.3.3 Peptide Self-Assembly Mechanism and Controlling Factors

A good understanding and precise control of peptide self-assembly is critical to tune the formation of peptide nanostructure, develop peptide-drug complexes, and further control the structure and size of the complex[93]. There are many internal and external factors that can influence peptide self-assembly formation, including (a) amino acid sequence, (b) molecular size, (c) peptide concentration, (d) charge distribution, (e) solution pH, (f) solvent, (g) temperature, (h) surface and its property and (i) mechanical force. The effects of amino acid sequence, charge distribution peptide concentration, and solution pH on peptide nanostructure formation, which are most relevant to this thesis work, are discussed below.

Effect of Amino Acid Sequence

The information for peptide self-assembly is encoded in the amino acid sequence. The type, number and arrangement of amino acids in the sequence are critical to form and tune the secondary structures and self-assembled nanostructures of the peptides. By altering the amino acid sequence, the structural and functional properties of the peptide can be modulated. One classic example is RAD16-II (Ac-RARADADARARADADA-$CONH_2$), which is modified from EAK16-II by replacing R with E and D with K. RAD16-II is similar to EAK16-II, which is highly soluble in water and forms a stable β-sheet structure. Moreover, the β-sheets can self-assemble into even higher macromolecular structures to form hydrogels with greater than 99% water content through self-complementary ionic interactions, hydrophobic interactions and backbone hydrogen bonding between the alanine methyl groups[95].

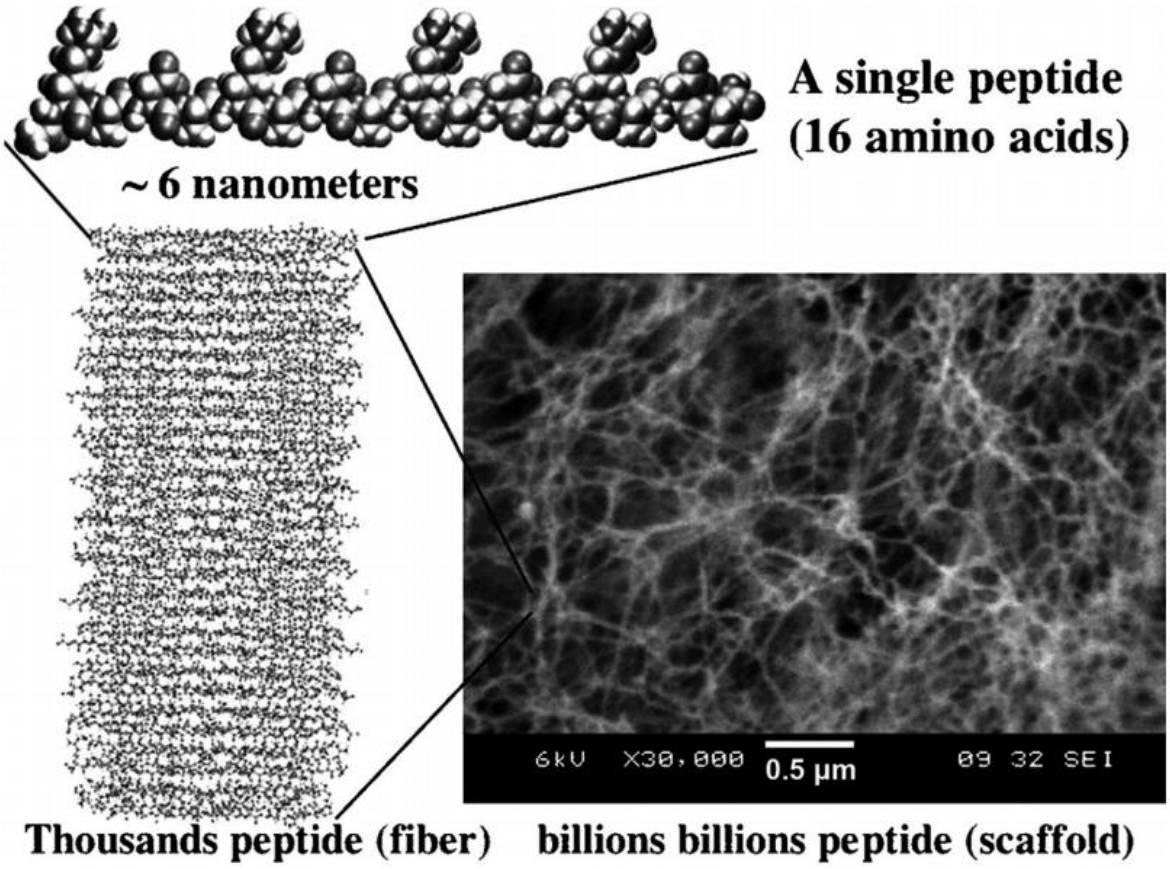

Figure 2.13 Self-assembling peptide RAD16-I nanofiber scaffold hydrogel. Left) Amino acid sequence of RAD16-I and molecular model of a single RAD16-I nanofiber (dimensions are ≈6 nm long, 1.3 nm wide, and 0.8 nm thick); tens and hundred thousands of individual peptides self-assemble into a nanofiber. Right) SEM image of RAD16-I nanofiber scaffold. Scale bar is 0.5 µm or 500 nm[95].

Effect of Charge Distribution

In addition to the type of amino acid, the charge distribution of the peptide sequence has significant impact on its nanostructure formation[22]. For example, Hong has studied the nanostructure formation of self-assembly peptide EAK16s, including EAK16-I, EAK16-II

and EAK16-IV. They have the same amino acid composition (A, E and K), while different sequence and charge distribution. The amino acid sequences of these peptides are AEAKAEAKAEAKAEAK for EAK16-I, AEAEAKAKAEAEAKAK for EAK16-II, and AEAEAEAEAKAKAKAK for EAK16-I, respectively. The first two self-assembly peptides, EAK16-I and EAK16-II form fibrillar assemblies, while EAK16-IV forms globular aggregates at pH 7. Further studies have suggested that both of EAK16-II and EAK16-IV contain β-sheets in their substructures. The β-sheets from EAK16-II further elongate and stack to form linear fibrils, while the assembly of EAK16-IV may bend or fold to form globular aggregates due to the stronger intramolecular electrostatic attractions between the amino acid groups of lysine and the carboxylic acid groups of glutamic acid. The experimental results are supported by Monte Carlo simulations. Therefore, the charge distribution has an effect on secondary structure of peptides and further self-assembly.

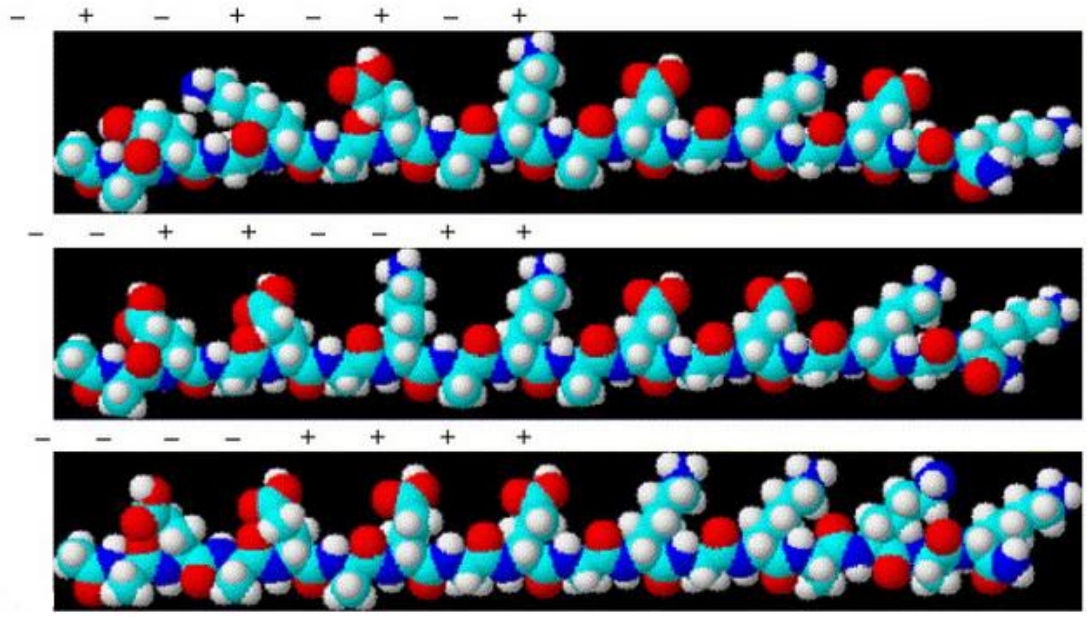

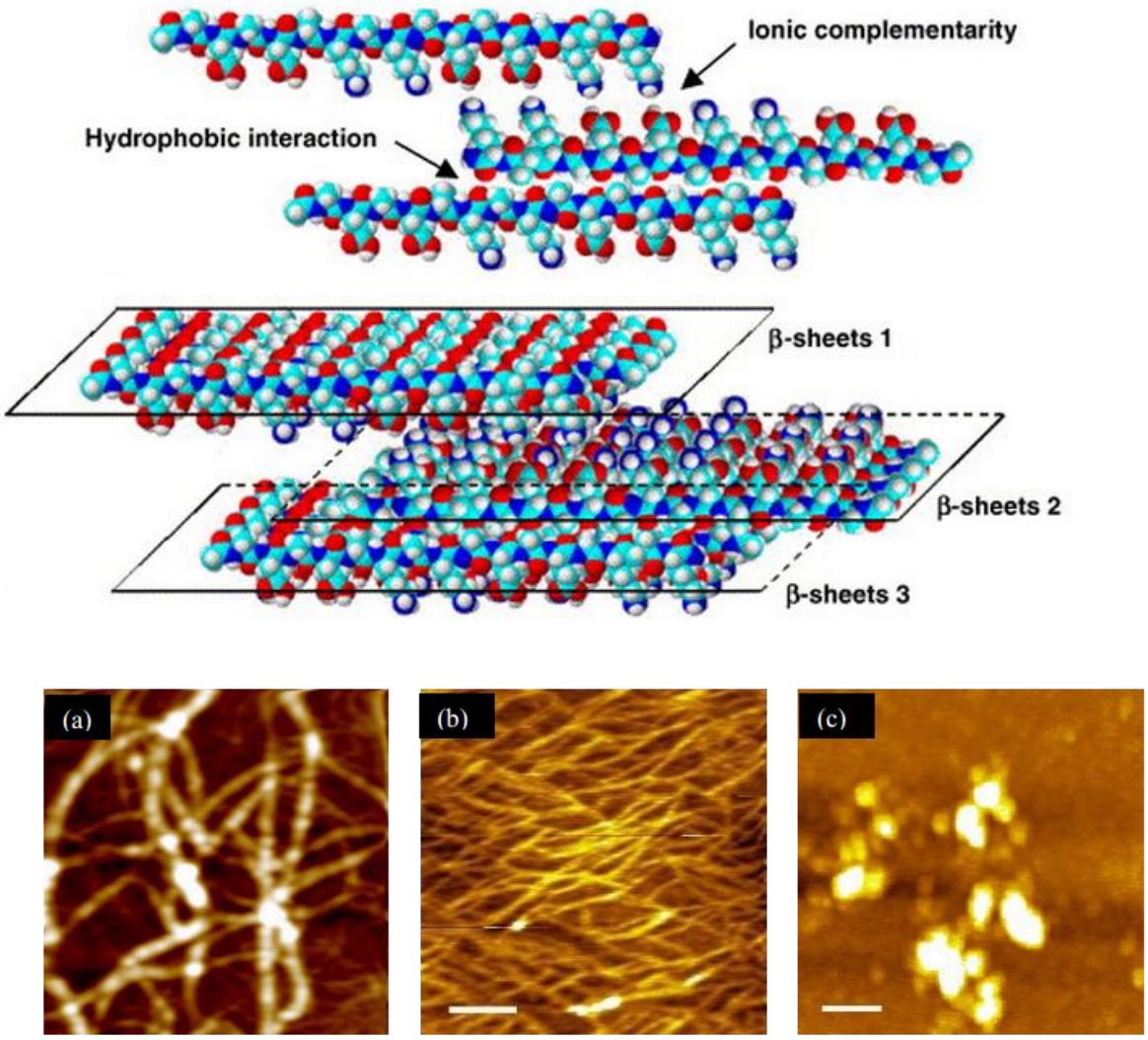

Figure 2.14 (A) Three-dimensional molecular model of EAK16s. The top, middle and bottom schemes represent the EAK16-I, EAK16-II and EAK16-IV structures, respectively. (B) A scheme of EAK16-II self-assembly through hydrophobic interaction and ionic-complementarity. In addition to the hydrogen bonding, hydrophobic and electrostatic interactions help to make stable β-sheets. A proposed model of EAK16-II self-assembly into β -sheet-based aggregates. We proposed that the peptides self-assemble in a fashion of antiparallel to favor the minimum energy state. In fact, some evidence has shown that EAK16-I and -II have a high frequency peak from Fourier-transform infrared (FT-IR) measurements, which implies the antiparallel

β-sheet formation. (C)AFM images of peptide self-assembled nanostructures from (a) EAK16-I, (b) EAK16-II and (c) EAK16-IV[22].

Effect of peptide concentration

Peptide concentration is another critical factor affecting peptide self-assembly and controlling the formation of nanostructure. In colloidal and surface chemistry, surfactant can form micelles above the concentration called the critical micelle concentration (CMC). Similar to surfactants, self-assembly peptide is expected to have a critical aggregation concentration (CAC) that governs the assembly process because of its amphiphilic structure. This CAC has been reported for many amphiphilic peptides and proteins.

Because of the strong molecular interactions among the peptides, it is acceptable that the CAC values of self-assembling ionic-complementary peptides are much smaller than the CMC of most surfactants (around 10^{-3} to 10^{-2}M). Fung et al reported that EAK16-II have a CAC of ~0.1 mg/ml (60 μM) by surface tension measurements[96]. AFM studies of EAK16-II reveal that fiber networks are observed when the peptide concentration is above the CAC, while isolated filaments and globules are formed at concentrations below the CAC. In addition, the peptide concentration is related to fibril size and network density as well. AFM studies also showed that EAK16-I assembly undergo two nanostructure transitions. The first transition from globules to fibril assemblies occurs at the peptide concentration of 0.05 mg/mL (30 μM); the second transition involves dramatic increase in the fibril size as the concentration rises above 0.3 mg/ml (180 μM).

Effect of solution pH

Biological systems are extremely sensitive to pH, which indicates that the solution pH is an important external factor that influences peptide and protein structures[22]. A pH change will have an effect on the ionic state of the charged residues and the net charge of peptides. This will further affect the self-assembly behavior of the peptide and protein folding/aggregation. An attractive class of PA molecules was found to be capable of changing morphology reversibly under the pH range of 6.6-7.4[97]. It consists of three main segments: a charged amino acid sequence, a β-sheet-forming peptide sequence, and a hydrophobic alkyl tail. The peptides would exist as either single molecules or spherical micelles at pH 7.4, and self-assemble into nanofibers upon the acidic environment (pH 6.6). Because the extracellular microenvironment of tumor tissue is slightly acidic (pH 6.6-7.4), this morphological change is ideal for in vivo cancer imaging and drug delivery applications.

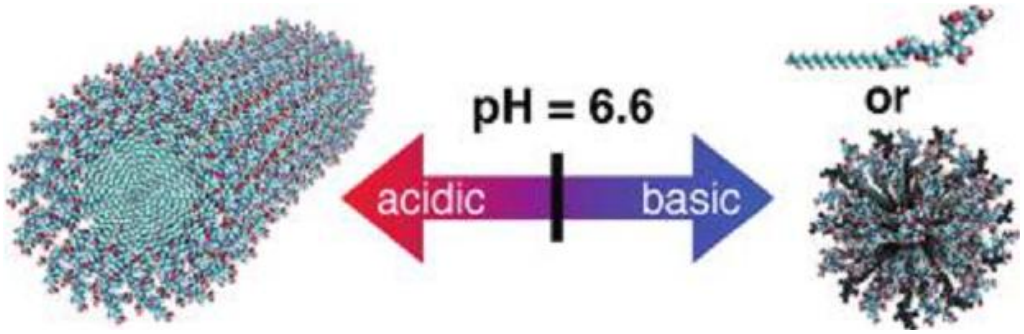

Figure 2.15 Schematic of the target reversible, pH-triggered morpho-logical transition of self-assembling peptide amphiphiles[97].

2.4 Self-Assembling Peptide-Mediated Hydrophobic Drug Delivery

Self-assembling ionic complementary peptides EAK16-II has been extensively studied in our group as a novel and promising biomaterial for constructing drug delivery

carriers[21,98,99]. This unique amphiphilic peptide was utilized first to encapsulate hydrophobic microcrystals of ellipticine or neutral ellipticine through strong hydrophobic interaction. EAK16-II can form β-sheet rich nanofiber networks, which provide a protective microenvironment to stabilize not only microcrystal ellipticine, but also protonated ellipticine by increasing the peptid-to-ellipticine ratio (>5:1 by mass). Further studies showed that protonated EPT had a faster transfer rate than that of crystalline EPT from the peptide-EPT complex to EPC vesicles. *In vivo* studies also indicated that the complexes with protonated ellipticine were more effective at killing cancer cells. However, the stability of EAK16-II-EPT complexes was not very good upon dilution. The cellular toxicity (>60% cell viability) decreased quickly after 16 times dilution of the complexes. If we alter the charge distribution on the peptide sequence (EAK16-II: --++--++ vs. EAK16-IV: ----++++), no obvious difference have been observed both on the complex formation and molecular state of EPT in the complex[98]. On the other hand, EFK16-II, a more hydrophobic residue F replacing A in EAK16-II, stabilized neutral EPT molecules and microcrystalline EPT instead of protonated EPT due to a possible stronger hydrophobic interaction between peptide and EPT. In vitro studies showed that EFK16-II-EPT complexes possessed lower cellular toxicity against cancer cells than EAK16-EPT complexes, but it exhibited good stability upon dilution in water.

2.5 The Anticancer Agent Ellipticine

Natural products have made an enormous contribution to cancer chemotherapy during the past 200 years. Small organic molecules (<3,000 Daltons) derived naturally from plants and microbes have provided a large number of useful anticancer drugs.

Ellipticine (5, 11-dimethyl-6H-pyrido[4, 3-b] carbazole, Figure 2.16), a pyridocarbazole alkaloid first isolated in 1959 from Apocyanaceae plants[31], has long been known for its significant anticancer and anti-HIV activities. The mechanisms of action of Ellipticine and its derivatives arresting cancer cell cycle progression have been extensively studied in the past few years[100]. It happened due to the following actions (1) DNA intercalation, (2) inhibition of topoisomerase Ⅱ, (3) covalent alkylation of macromolecules, and (4) induction of endoplasmic reticulum stress. However, the medical applications of ellipticine were hindered by a few problems. First, its aromatic, planar structure makes ellipticine an extremely hydrophobic agent, with a water solubility of 6.2×10^{-7} M. Such low water solubility limits its clinical application in aqueous solution. Second, severe side effects have been reported in clinical trials, including xerostomia, intravascular hemolysis, and bradycardia[33]. Therefore the novel delivery system is required to minimize the side effects and enhance the therapeutic efficacy.

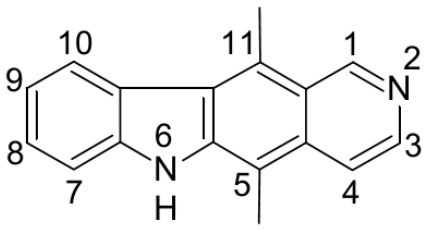

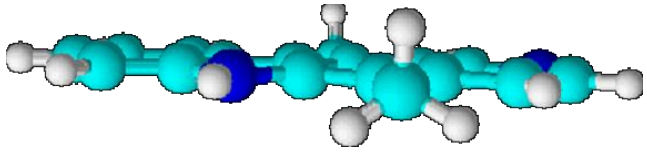

Figure 2.16 (a) Chemical structure of ellipticine; (b) Planar structure of ellipticine. H: white, N: blue, C: canyon.

Fung et al. have investigated the relationship between photophysical properties of ellipticine and the microenvironment of its nanocarrier[101]. It was found that ellipticine has three different molecular states: neutral, crystalline and protonated, with corresponding emission fluorescence peaks at 390-440 nm, 468 nm and 520 nm, respectively. Ellipticine exhibits a large Stokes shift (10000 cm^{-1}) in polar solvent compared to that (8900 cm^{-1}) in non-polar solvents. This dramatic spectra shift is attributed to the different structures adopted by ellipticine in different solvents. Therefore, the change in absorption and emission spectra will make it easy to be monitored either in physicochemical characterization or *in vitro* experiments.

Among these molecular states of EPT, protonated EPT draw our attention because its good anticancer activity[21,39]. In vitro studies indicated that protonated EPT had much higher toxicity than crystalline EPT against both breast and lung cancer cells. Studies in living cells also revealed that only protonated EPT can exist in the nucleus. Although EPT delivery carrier has been extensively studied; the specific delivery carrier can encapsulate prescribe protonated EPT molecules still has not been reported. Therefore, it is necessary to develop new drug carriers that could deliver a drug with a prescribed molecular state and keep good stability upon dilution to maximize drug therapeutic effects.

Chapter 3
Experimental Methods

3.1 Materials

Synthetic peptides EAR8-II, EAR8-a, ELR8-a, EAR16-II were obtained from CanPeptide Inc. (Montreal, Canada), stored at 4℃, and used without further purification. The sequences of peptides are AcN-AEAEARAR-CNH_2 (Mw=913.98g/mol), AcN-AAEEAARR-CNH_2 (Mw=913.98g/mol), AcN-LLEELLRR-CNH_2 (Mw=1082.30g/mol), and AcN-AEAEARARAEAEARAR-CNH_2 (Mw=1782.92g/mol), respectively. A corresponds to alanine (ala), E to glutamic acid (glu), K to lysine (lys), and L to leucine (leu). The N-terminus and C-terminus of the peptide were protected by acetyl and amino groups, respectively. At pH~7, A and L is neutral, while E and R are negatively and positively charged, respectively. Figure 3.1 depicts the molecular structure of four peptides.

The anticancer agent ellipticine (99.8% pure) was from Sigma-Aldrich (Oakville, ON, Canada) and used as received. Tetrahydrofuran (THF, reagent grade 99%) and dimethyl sulfoxide (DMSO, spectral grade 99%) were purchased from Calendon Laboratories Ltd. (Georgetown, ON, Canada) and Sigma-Aldrich (Oakville, ON, Canada), respectively. Cell culture reagents including F-12 Kaighn's modification, minimum essential medium eagle (MEM), fetal bovine serum (FBS) and Trypsin-ETDA were purchased from Invitrogen Canada Inc. (Burlington, ON, Canada). Insulin and Phosphate buffer saline (PBS) was obtained from MP Biomedicals Inc. (Solon, OH, USA). MTT assay and CCK8 kit for cell viability tests were obtained from Sigma-Aldrich (Oakville, ON, Canada) and Dojindo Molecular Technologies, Inc., respectively.

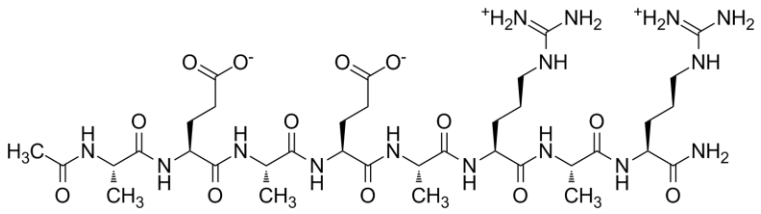

EAR8Ⅱ: n-AEAEARAR-c

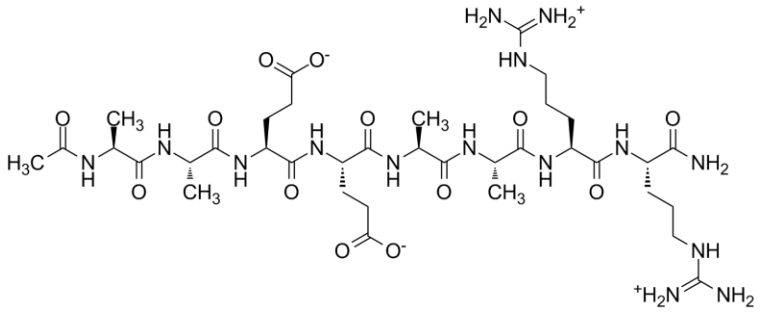

EAR8-a: n-AAEEAARR-c

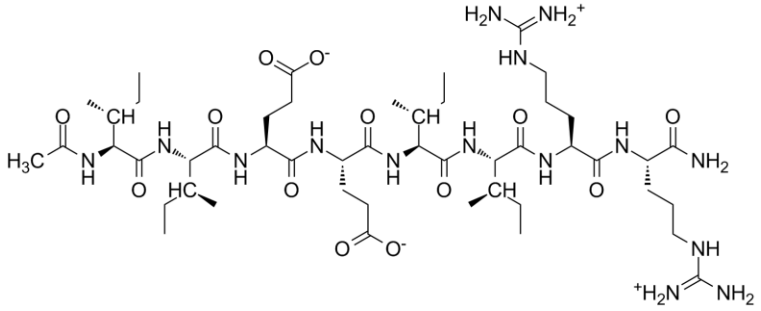

ELR8-a: n-LLEELLRR-c

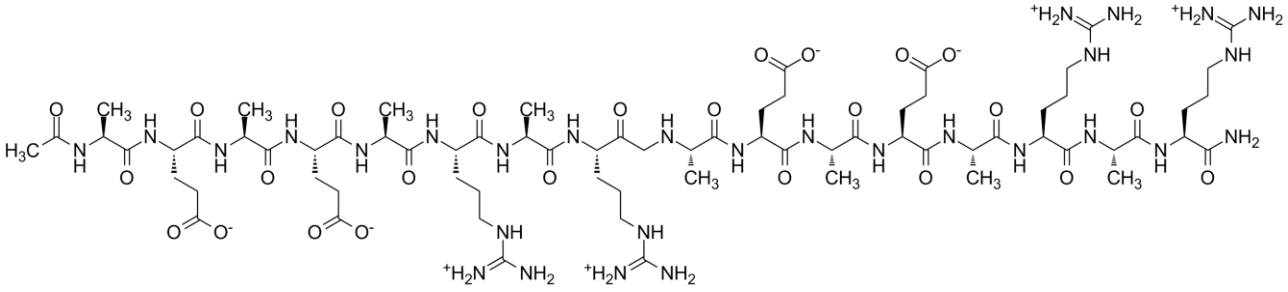

EAR16Ⅱ: n-AEAEARARAEAEARAR-c

Figure 3.1 Molecular structure of EAR8Ⅱ, EAR-a, ELR-a, and EAR16Ⅱ.

3.2 Peptide Solution and Peptide-Ellipticine Complex Preparation

All arginine-rich ionic complimentary peptide solutions (0.05-0.5mg/mL) were prepared in pure water (18.2 M, Milli-Q A10 synthesis) to study their self-assembly behaviors. For the preparation of peptide solutions, certain amounts of lyophilized peptide powder were first dissolved in pure water, followed by sonication for 10 min to dissolve the peptide completely. Their self-assembly properties were studied by Axisymmetric Drop Shape Analysis-Profile (ADSA-P) technique and 1-anilino-8-naphthalene sulfonate (ANS) fluorescence assay. Secondary structure, size distribution and surface charge of peptides were characterized by Circular Dichroism (CD), Dynamic Light Scattering (DLS) and Zeta potential, respectively. The morphology and dimensions of peptide assemblies were examined by Atomic Force Microscopy (AFM) and Transmission Electron Microscopy (TEM).

An appropriate amount of EPT crystals were first dissolved in THF at 0.4 mg/mL; aliquots of EPT-THF solution were then transferred to vials, and dried under gentle air blowing (through a 0.22μm filter) for ~10 min. Fresh peptide solution was then added to the vial, followed by mechanical stirring at 800 rpm for 24 h (as shown in Figure 3.2). An EPT control was prepared in pure water instead of peptide solution at the same EPT concentration, following the same procedure. The physiochemical properties of complexes were determined with same characterization techniques mentioned above. The complexes made of 0.1 mg/mL EPT and 0.5 mg/mL peptide were serially diluted to the lowest concentration of 4000× in pure water to study the colloidal stability and cytotoxicity of peptide-EPT complex upon dilution.

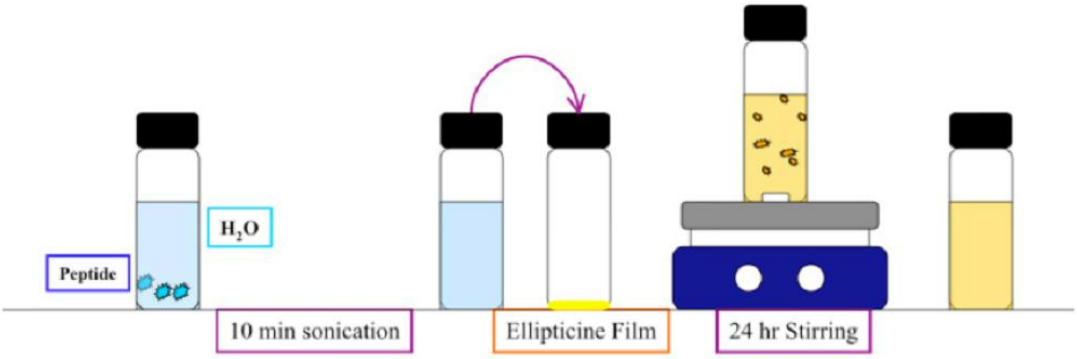

Figure 3.2 The schematic of preparation method of peptide-ellipticine complex

3.3 Surface Tension Measurement

The surface tensions of the peptides at an air-water interface over a period of 2.5 h were done by the Axisymmetric Drop Shape Analysis-Profile (ADSA-P) technique. The experimental setup and operation of ADSA-P were reported in an earlier publication and shown in Figure 3.3[102]. A pendant drop of the peptide solution was extruded at the tip of a vertical Teflon® capillary, which was connected to a motor-driven microsyringe, producing an axisymmetric drop boundary. This was done in a temperature-controlled environmental chamber saturated with water vapor. The entire system was isolated on a vibration-free table. The image of the pendant drop was acquired using an optical microscope and a CCD camera and digitally recorded for 1 h after the pendant drop was formed. Software was used to digitize the image and generate a profile of the pendant drop. A theoretical curve, governed by the Laplace equation of capillarity, was then fitted to the profile, generating the surface tension value as a fitting parameter. The typical standard deviations of all measurements were less than 0.2 mJ/m^2.

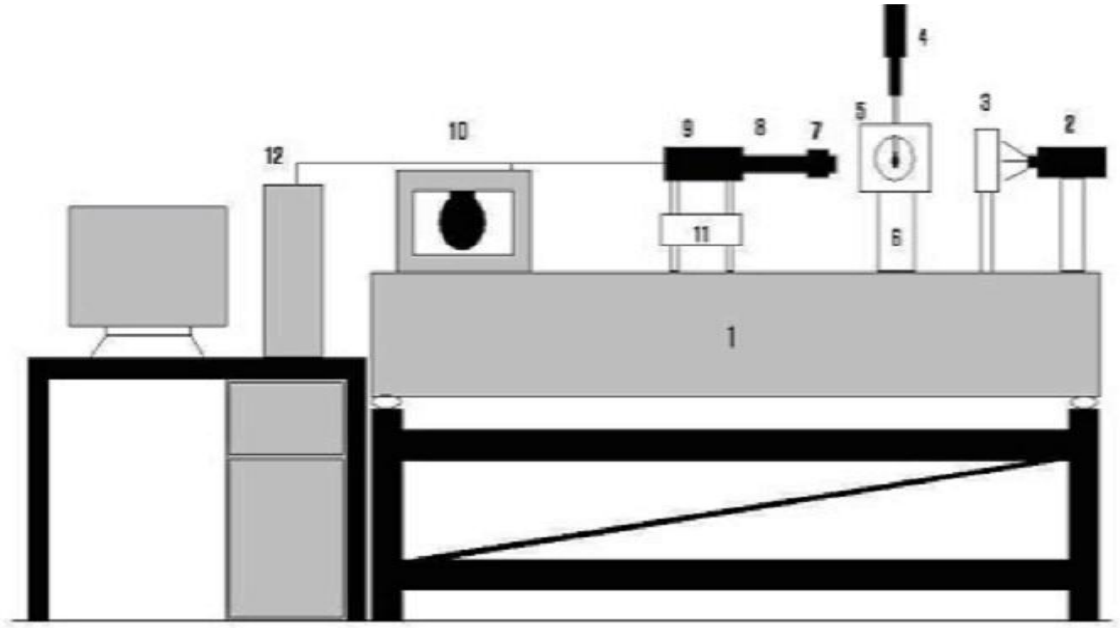

Figure 3.3 Schematic of ADSA-P experimental setup 1-Work Station 2-Light Source 3-Diffuser 4-Syringe 5-Environment Chamber 6-Stage 7-Microscope 8-Lens 9-Camera 10-Monitor 11-Stage 12-Computer

3.4 Fluorescence Spectroscopy

A Photon Technology International Spectrafluorometer (Type QM4-SE, London, Canada) with a continuous xenon lamp as the light source was employed to study the EPT fluorescence in the complex. The excitation and emission slit widths were set at 0.25 mm and 0.5 mm, respectively (0.25 mm corresponds to 1-nm band path). For each sample, 100 μL solutions were transferred into a square quartz cell. All samples were excited at 294 nm and the emission spectra were collected from 320 to 650 nm. A standard sample (2mM ellipticine in ethanol, sealed and degassed) was used in each run to correct the lamp intensity variations. The fluorescence intensity I at 520 nm and standard fluorescence intensity I_s were obtained

by taking the average from 510 to 530 nm and from 424 to 432 nm (peak at 428 nm), respectively.

3.5 1-Anilino-8-Naphthalene Sulfonate (ANS) Fluorescence Assay

The fluorescence of probe ANS has been widely used in molecular self-assembly[103]. ANS solution (10 μM) was prepared in a phosphate buffer (10 mM) at pH 6. The fresh peptide solutions were mixed with equal volume of the ANS solution. A negative control was prepared by mixing ANS solution with pure water in the same way. The mixed solutions (80 μL) were transfer to a quartz microcell and tested on the same spectrafluorometer above. For all concentrations, the fluorescence spectrum was obtained from 400 to 670 nm with the excitation at 360nm. The excitation and emission slit widths were set at 0.5 mm and 1.25 mm, respectively. To correct the lamp fluctuations, the spectra were normalized with light scattering of air at 360 nm.

3.6 Circular Dichroism

Secondary structure of arginine-rich ionic-complementary peptides and the peptide-EPT complexes were obtained on a J-810 Spectropolarimeter (Jasco, USA). A CD spectrum were acquired in the 190-270 nm wavelength range from samples in a 200 μL, 3 mm path length quartz cuvette at 25℃ at 200 nm/min with a response time of 2 s and pitch of 1 nm. All spectra shown were corrected by subtracting the baseline and were expressed as the average of three replicates.

3.7 Dynamic Light Scattering (DLS) and Zeta potential

The hydrodynamic diameter and surface charge of peptide assemblies (0.5 mg/mL) and peptide-EPT complexes (0.5:0.1 mg/mL) were investigated by Dynamic Light Scattering (DLS) and Zeta potential by Laser Doppler Velocimetry (LDV) on a Zetasizer Nano ZS (Malvern Instruments, Worcestershire, U.K.) equipped with a 4 mW He-Ne laser operating at 633 nm. All measurements were performed at a measurement angle of 173° at 25℃. The intensity-based size distribution was obtained with the multimodal algorithm CONTIN, provided in the software package Dispersion Technology Software 5.0 (Malvern Instruments, Worcestershire, U.K.). Three measurements of at least 10 runs per measurement were tested to generate a size distribution plot based on intensity. The size and Zeta-potential were presented as mean value ± standard deviation.

3.8 EPT Maximum Suspension Measurement

The EPT maximum suspension in the peptide-EPT complexes was determined by EPT UV-absorption as published in our previous paper[39]. A calibration curve was obtained from the linear fitting of EPT absorption at a wavelength of 295 nm as a function of EPT concentration (1×10^{-3}-1×10^{-2} mg/mL) prepared in a mixture of 95% DMSO with 5% water. The peptide-EPT complexes solution (0.5:0.1 mg/mL) was diluted in DMSO until within the range of calibration curve. 100 μL of the solution was transferred to a quartz microcell with a 1 cm light path and tested on a UV-vis spectrophotometer (Agilent 8453 UV-vis spectroscopy). The value of EPT maximum suspension was averaged from three measurements, presented as mean value ± standard deviation.

The EPT maximum suspension was defined as the ratio of the mass of the suspended EPT to the mass of the EPT added for complex preparation using the following equation:

$$Maximum\ Suspension\ (MS) = \frac{Amount\ of\ suspended\ EPT}{Amount\ of\ EPT\ added\ for\ complex\ preparation} \times 100\%$$

3.9 Atomic Force Microscopy (AFM)

Dimension Icon^{R} AFM (Bruker Nano Surfaces, Santa Barbara, CA) was employed to study the morphology and dimensions of peptide assemblies and peptide-EPT complexes. The samples were prepared by depositing the peptide/complexes suspensions (50 μL) on a freshly cleaved mica surface for 10-30 min, followed by washing 3 times with 50 μL pure water to remove unattached samples. After drying at room temperature overnight, AFM imaging was performed using PeakForce QNM mode. All images were acquired a silicon nitride tip (type SCANASYST-AIR, Bruker) with a typical tip radius of 2 nm and frequency of 70 kHz. The images with a scan size of 2×2 μm^2 were used.

3.10 Transmission Electron Microscopy Imaging

Transmission electron microscopy was performed with a Philips CM20 electron microscope (Philips Electronics Ltd. Guildford, U.K.) at an accelerating voltage of 200kV. Images were digitalized using a Gatan 679 slow-scan CCD camera and analyzed using DIGTALMICROGRAPH (version 2.1, Gatan Inc. Pleasanton, CA). 10 μL of peptides or peptide-ellipticine complexes solution was incubated on 1 400-mesh carbon-coated Formvar copper grid (Marivac Ltd., St. Laurent, QC) for 15 min. Excess solution was drawn off the

edge of the grid with tissue paper. 10 μL of 2% (w/v) uranyl acetate was used to staine the grid for 10 s. Excess stains were drawn off again, and the grid was air-dried before TEM imaging.

3.11 Cellular Toxicity Tests (MTT and CCK8)

Two cancer cell lines, human lung carcinoma cell line A549 and breast cancer cell line MCF-7, were used for the cellular toxicity tests on the peptide-EPT complexes. A549 and MCF-7 were cultured in F12 containing 10% FBS and MEM containing 10% FBS and 0.1% insulin, respectively. Both of them were grown at 37℃ in a humidified incubator (with 5% CO_2). When the cells were ~95% confluent, they were rinsed once with PBS, followed by trypsinized and suspended in culture medium. After centrifuging at 500 rcp for 5 min, the cell pallets were resuspended in fresh cell culture media at concentrations of 5×10^4 and 1×10^5 cells/mL for A549 and MCF-7, respectively. For each type of cell, the cell suspensions (200 μL) were seeded into each well of a clear, flat bottom, 96-well plate (Costar) and incubated for 24 h. The old media were replaced with fresh culture media (150 μL) followed by an addition of treatments (50 μL) into each well, resulting in a 4-fold dilution of the treatments. The plates were incubated for another 24 h prior to performing the cell viability assay.

MTT assay or CCK-8 assay were used to determine the cell viability after each treatment. The detailed procedure was described in our previous publications[21].

Chapter 4
Results and Discussion

4.1 Basic Design Principals of Arginine-Rich Ionic Complementary Peptides as Protonated EPT Delivery Carrier

An anticancer drug ellipticine (EPT) has long been known for its significant anticancer and anti-HIV activities[31]. However, its poor aqueous solubility, severe side effects and low bioavailability constitutede major obstacles toward its medical deployment[33]. Recently, EPT has drawn renewed attention as new drug delivery technologies have emerged[17, 21, 35, 104]. It was found that EPT has three different molecular states: neutral, crystalline and protonated (Figure 4.1). Among the three molecular states, protonated EPT draws our attention because it has higher anticancer activity than the other two states[21, 39]. Although EPT delivery carrier has been widely studied; the specific delivery carrier could encapsulate prescribe protonated EPT molecules still has not been reported. Therefore, it is necessary to develop a new drug nanocarrier that could deliver protonated EPT and keep good cytotoxicity upon dilution in aqueous solution to maximize drug therapeutic effects.

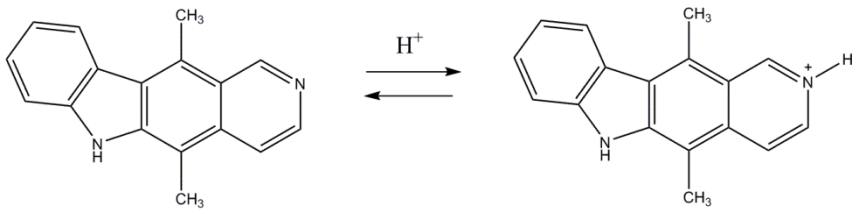

Figure 4.1 Different Forms of Ellipticine

The family of self-assembling peptide EAK16s has been extensively studied in our group as a novel and promising biomaterial for constructing drug delivery carriers. This

unique self-assembling ionic complementary peptide was utilized to encapsulate hydrophobic EPT through strong hydrophobic interaction[21, 105]. By forming β-sheet rich nanofiber networks, EAK16-II could provide a protective microenvironment to stabilize not only microcrystal EPT, but also protonated EPT by increasing the peptide-to-EPT ratio (>5:1 by mass). Further studies showed that protonated EPT had a faster transfer rate than that of crystalline EPT from the peptide-EPT complex to EPC vesicles[21]. *In vitro* cytotoxicity studies also indicated that the complexes with protonated ellipticine were more effective at killing cancer cells. However, the stability of EAK16-II-EPT complexes in relation to its anticancer activity was not very good upon dilution. The cellular toxicity (>60% cell viability) decreased quickly after 16 times dilution of the complexes. In a recent study, a molecular binding model with electrostatic interaction as the primary intermolecular force between the negatively charged glutamic acids in EAK16-II and protonated EPT has been proposed[39]. In this model, we assume that one protonated EPT molecule would bind to only one deprotonated carboxylate of glutamic acid in EAK16-II. There are four glutamic acids in one EAK16 molecule, in theory, could attract four pronated EPT molecules, while the positively charged lysines may render the EAK-EPT complex to be positively charged overall. The EPT loading capacity in EAK demonstrated that each mg of EAK could stabilize about 0.42 mg EPT in slightly acidic environments, which is significantly higher that the usual loading capacity of other carrier systems.

If we altered the charge distribution on the peptide sequence (EAK16-II: --++--++ vs. EAK16-IV: ----++++), no obvious difference have been observed both on the complex formation and molecular state of EPT in the complex[105]. On the other hand, EFK16-II, a

more hydrophobic residue F replacing A in EAK16-II, stabilized neutral EPT molecules and microcrystalline EPT instead of protonated EPT. One possible explanation to this phenomenon is because the benzene ring of phenylalanine may hinder the possibility of its neighbor negatively charged carboxyl group to interacting pyridine-like nitrogen atoms of EPT. *In vitro* studies proved that EFK16-EPT complexes possessed lower cellular toxicity against cancer cells than EAK16-EPT complexes, but it exhibited good stability upon dilution in water due to a possible stronger hydrophobic interaction between peptide and neutral EPT and microcrystalline EPT.

Based on our previous experience, we properly design a series of new peptides which may strengthen the interaction between peptide and protonated EPT and provide better encapsulation efficiency. A small library of model peptides, EAR8-II, EAR8-a, ELR8-a and EAR16-II were designed by systematically altering EAK16 with different length, sequence and hydrophobicity, as shown in Figure 3.1 and Table 4.1.

Table 4.1 Library of novel arginine-rich ionic complementary peptides

Peptide name	# of Amino Acid	Sequence (n-c)
EAR8-II	8	n-AEAEARAR-c
EAR8-a	8	n-AAEEAARR-c
ELR8-a	8	n-LLEELLRR-c
EAR16-II	16	n-AEAEARARAEAEARAR-c

Here we chose arginine (R) to replace lysine (K) because of the following reasons. First, the side chain of arginine has higher pKa value than lysine. With a pKa of 12.48, the

guanidinium group is positively charged in acidic, neutral and even more basic environment, which means it can create stabilizing hydrogen bonds even in a slightly basic environment[106]. Hydrogen bonding between the guanidinium group and the pyridine-like nitrogen atoms of EPT could induce electron redistribution and stabilize the protonated EPT, which is the prescribed state we need. Second, the guanidinium group has two amino groups, which allows the formation of hydrogen bonding from two directions. Third, arginine-rich peptides have shown strong cell-penetrating ability through molecular recognition of the guanidinium/phosphate pair. The hydrogen bonding between guanidinium moiety and phosphate group may facilitate arginine rich peptides penetrate the cell membrane efficiently[107]. Overall, these special advantageous properties of arginine over lysine make it possible for arginine rich ionic complementary peptide to be used as an ideal biomaterial to stabilize protonated EPT quickly and encapsulate more drugs. The theoretical model for the mechanism of interaction between arginine rich ionic complementary peptide and protonated EPT was depicted in Figure 4.2.

Since residue Phenylalnine (F) may be too hydrophobic to encapsulate protonated EPT, less hydrophobic residue Leucine (L) was chosen to replace residue Alanine (A) of EAR. Such a slightly change in hydrophobicity may alter the microenvironment surrounded around EPT and lead to different states of EPT molecule. And also, peptide length was changed from 8 amino acids to 16 amino acids to investigate the length effect on peptide assemblies and their complexation with EPT.

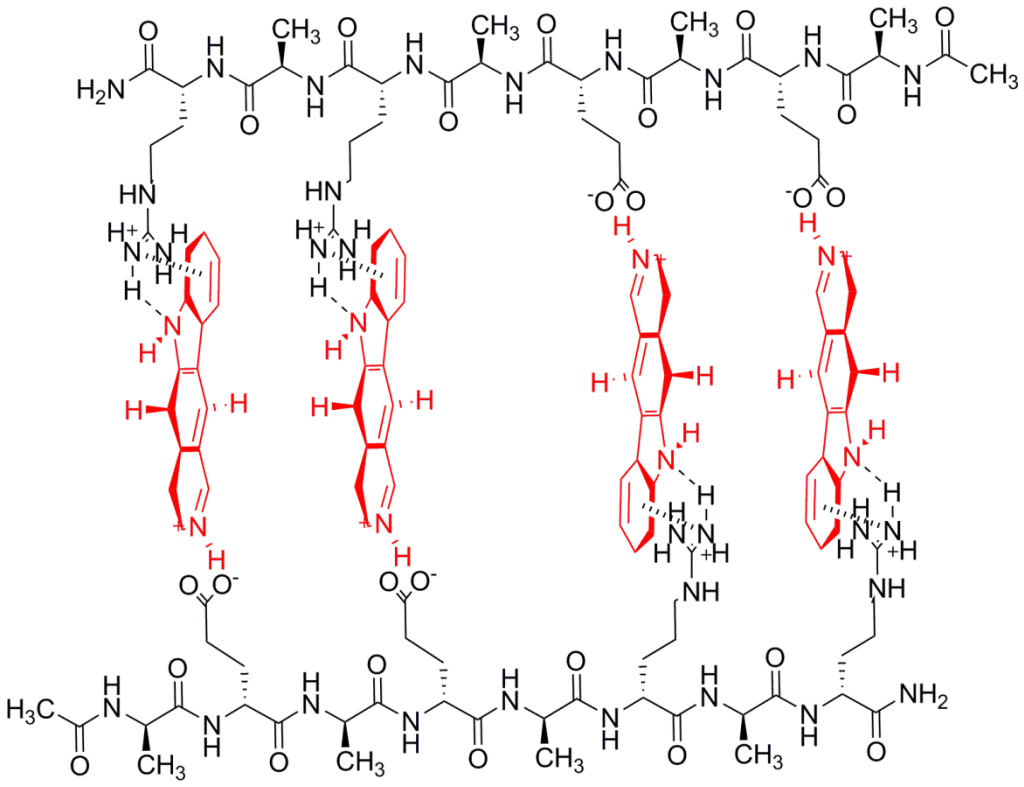

Figure 4.2 Theoretical model for the mechanism of interaction between peptide and protonated EPT.

In the next part, the self-assembly property of the peptides was characterized by Axisymmetric Drop Shape Analysis-Profile (ADSA-P) technique and 1-anilino-8-naphthalene sulfonate (ANS) fluorescence assay. Their potentials in drug delivery application were explored, the fluorescence technique was utilized to characterize the molecular state of EPT in the complex to see if the prescribed protonated EPT can be encapsulated in the peptide self-assembly, and UV technique was used to determine the EPT encapsulation efficiency of peptide-EPT compelxes. Then the effects of length (EAR8-II vs. EAR16-II), sequence (EAR8-II vs. EAR8-a) and hydrophobicity (EAR8-a vs. ELR8-a) on peptide self-assembly and peptide-EPT complexes were studied in details for their secondary

structure, particle size distribution, surface charge, and morphology. The cytotoxicity of the peptide and peptide-EPT complexes was tested *in vitro* against two cancer cell lines: non-small cell lung cancer cell A549 and breast cancer cell MCF-7. The stability of the complexes upon serial dilutions in aqueous solution was further investigated in relation to anticancer activity. Information obtained in this study is aimed at providing appropriate design principles for selecting peptide sequences and length, to construct advanced functional peptide carriers for anticancer drug delivery.

4.2 Self-Assembly Ability of Peptides and Their Potentials to Encapsulate Protonated EPT

The self-assembly ability of peptides were first studied. Critical aggregation concentration (CAC) was measured to evaluate the self-assembly strength by ADSA-P and 1-anilino-8-naphthalene sulfonate (ANS) fluorescence assay. For ELR8-a and EAR16-II, The surface tension of peptides solution decreased with increasing peptide concentration, and then reached to a plateau (Figure 4.3 a, b). This profile could be simply fitted with two straight lines: one for the decline region and the other for the plateau. The intersection of the two lines indicated the CAC of 51.15 μM and 30.40 μM for ELR8-a and EAR16-II, respectively. For EAR8-II and EAR8-a, the surface tension of peptide solutions showed no tendency in relation to the peptide concentration, which means there was no CAC can be obtained. This result was further confirmed by the ANS fluorescence assay as shown in Figure 4.3 c and d, where the ANS fluorescence intensity and peak (at 520 nm) remained unchanged in the range of peptide concentration from 0 to 600 μM, indicating there are no hydrophobic binding sites detected among the test peptide concentrations. It is worth noting

that EAR16-II has a double length (16 amino acids) in the sequence compare to EAR8-II and EAR8-a. It explains the effect of length on the peptide self-assembly ability, the long length can provide more interactions for peptide association[102]. In addition, ELR8-a has more hydrophobic L residue, is believed to have a much stronger hydrophobic interaction than EAR8-a and EAR8-II. This comparison shows that longer length (EAR16-II vs. EAR8-II and EAR8-a) and more hydrophobic residues (ELR8-a vs. EAR-a) in the sequence indeed enhance the peptide self-assembly ability, whereas the effect of sequence (EAR8-II vs. EAR8-a) shows no difference regarding to short peptides. The low CAC may strengthen the association between peptide and hydrophobic drug under extensive dilution in biological systems.

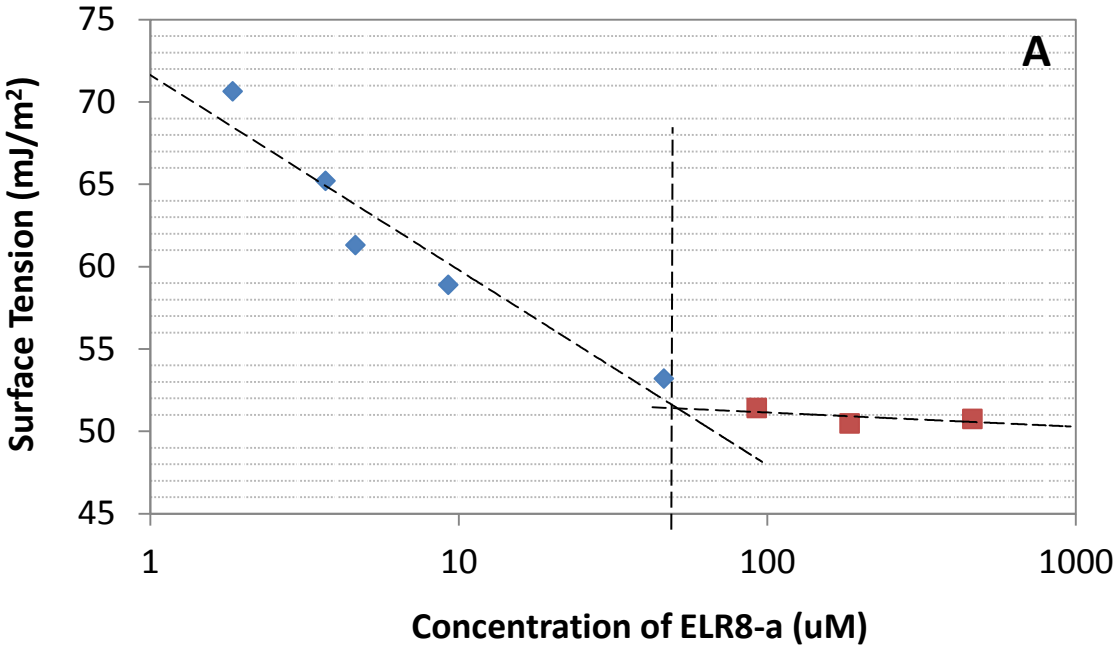
A
75
70
65
60
55
50
45
Surface Tension (mJ/m²)
1
10
100
1000
Concentration of ELR8-a (uM)

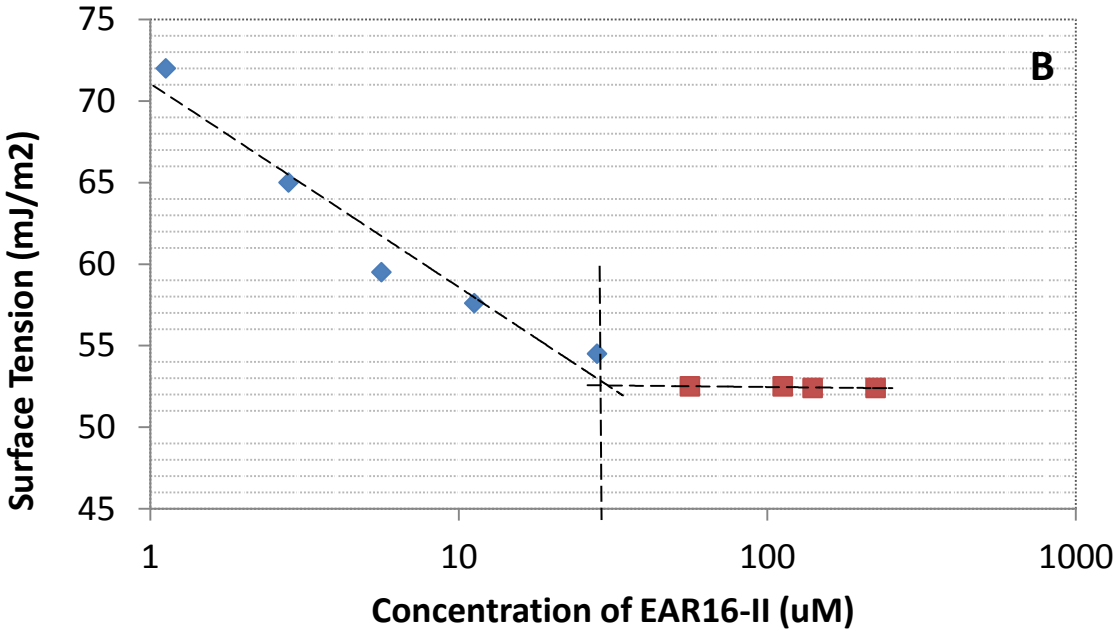
B
75
70
65
60
55
50
45
Surface Tension (mJ/m2)
1
10
100
1000
Concentration of EAR16-II (uM)

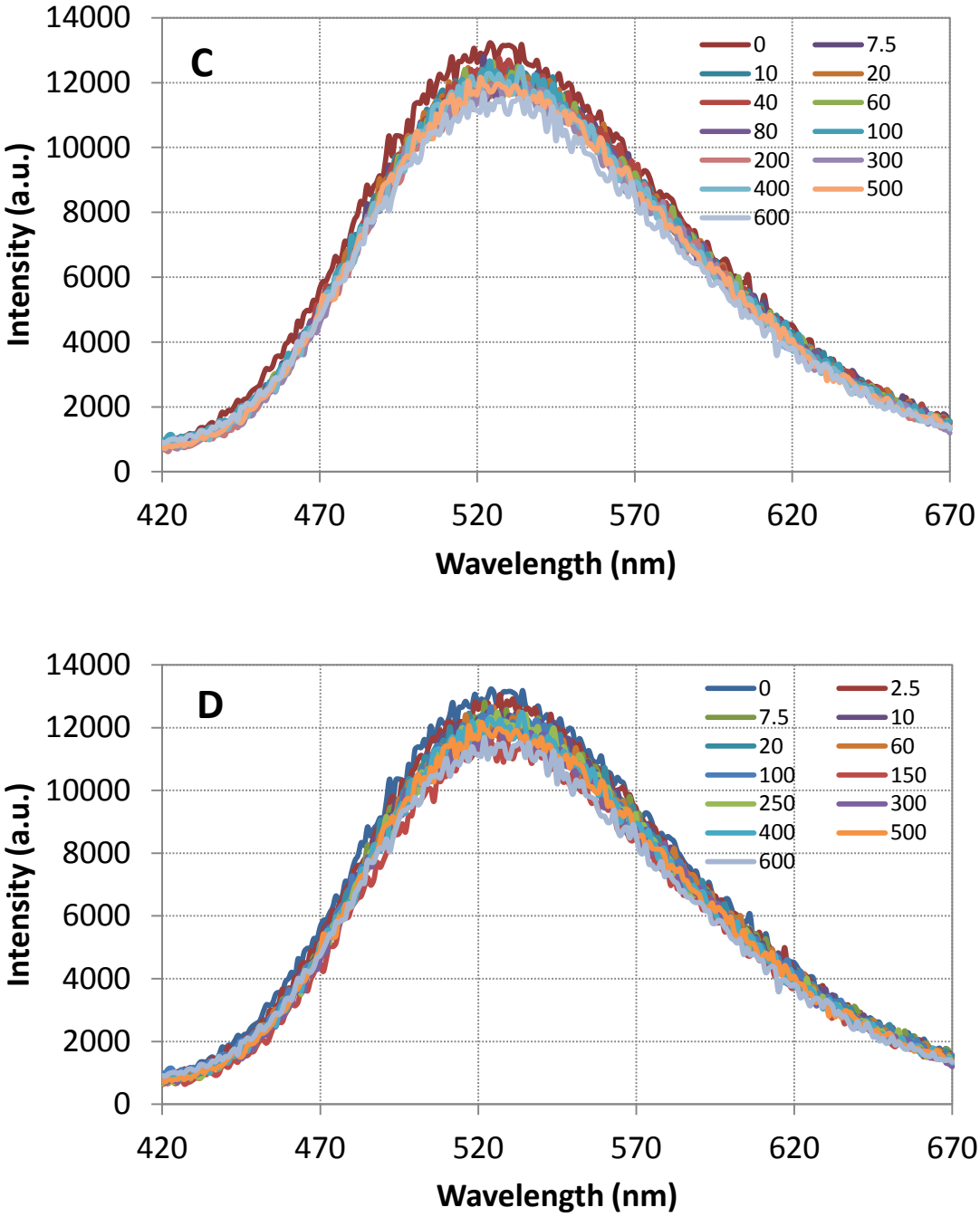

Figure 4.3 The critical aggregation concentration (CAC) of ELR8-a and EAR16-II was determined by a, b) surface tension. c, d) ANS fluorescence binding assay was used to determine the hydrophobicity of EAR8-a and EAR8-II assemblies. The CAC was found to be 51.15 µM

and 30.40 μM for ELR8-a and EAR16-II, respectively. The legend in (c, d) indicates the peptide concentration ranging from 0 to 600 μM.

From our previous studies, the peptide-EPT complex formation in water is peptide concentration-dependent. With a combination of 0.1 mg/mL EPT and 0.5 mg/mL peptide, only EAK16-II can stabilize protonated EPT in the complex[105]. The converted molar ratios between EPT to anionic amino acid E is 1:3, indicating there are more than enough glutamic acids to bind all of the protonated EPT. Here we borrow the 5:1 mass ratio of peptide to EPT to investigate the molecular state of EPT in the complex formation by fluorescence spectrometer. In this case, the molar ratio of EPT to E are 1:2.5, 1:2.3, 1:2.6 for EAR8, ELR8-a and EAR16, respectively. As expected, for all four peptides, the fluorescence spectrum exhibited a characteristic of protonated EPT with a peak at 520 nm after 24 h stirring, as shown in Figure 4.4. The peak at 520 nm initially went up and reached the maximum at 4 times of dilution, this phenomenon might be caused by the inner filter effect (IFE) as indicated in our earlier publication[39]. Then the intensity came down gradually due to the decreased EPT dose upon dilution. Note that even after 4000x dilution, there was no crystalline EPT (468 nm) and neutral EPT (440 nm) were traced. These results proved our theory that the complexes have relatively good stability which can stand upon extensively dilution.

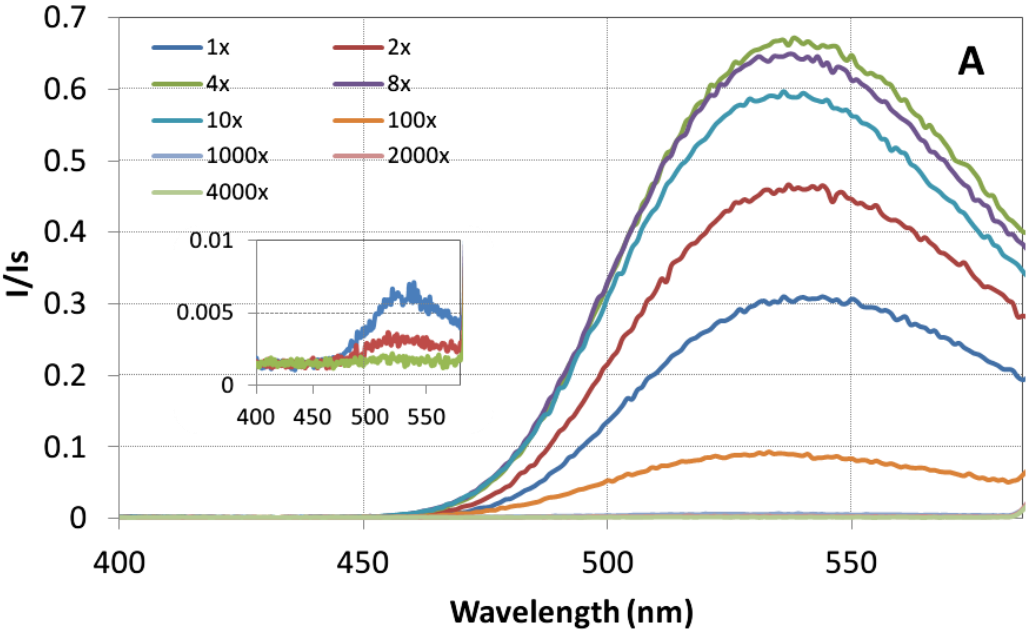
A
1x
2x
4x
8x
10x
100x
1000x
2000x
4000x
I/Is
Wavelength (nm)
0.7
0.6
0.5
0.4
0.3
0.2
0.1
0
400
450
500
550
0.01
0.005

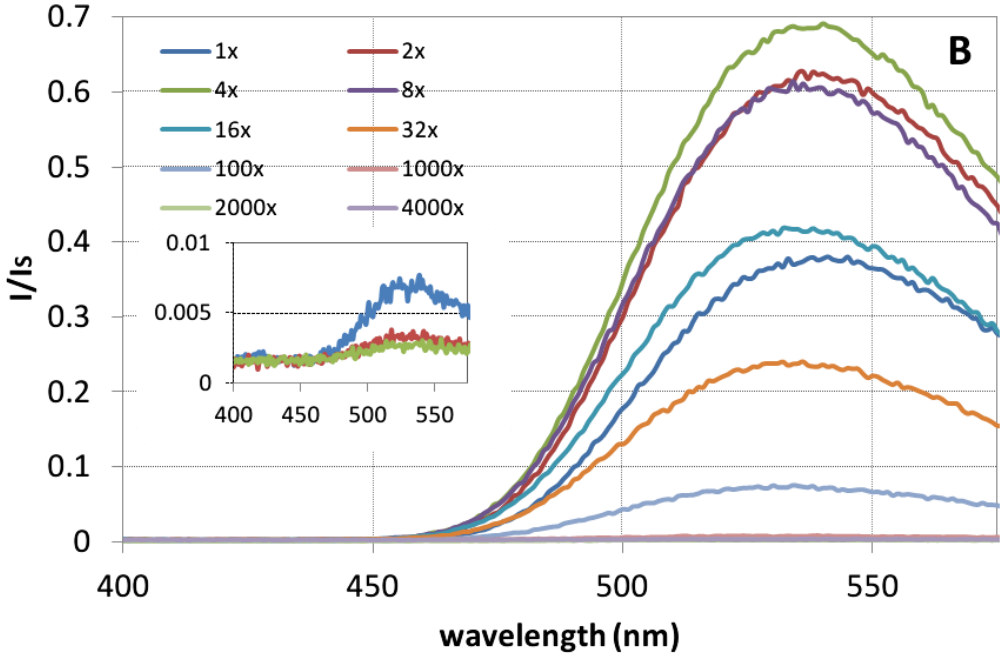
B
1x
2x
4x
8x
16x
32x
100x
1000x
2000x
4000x
I/Is
wavelength (nm)
0.7
0.6
0.5
0.4
0.3
0.2
0.1
0
400
450
500
550
0.01
0.005

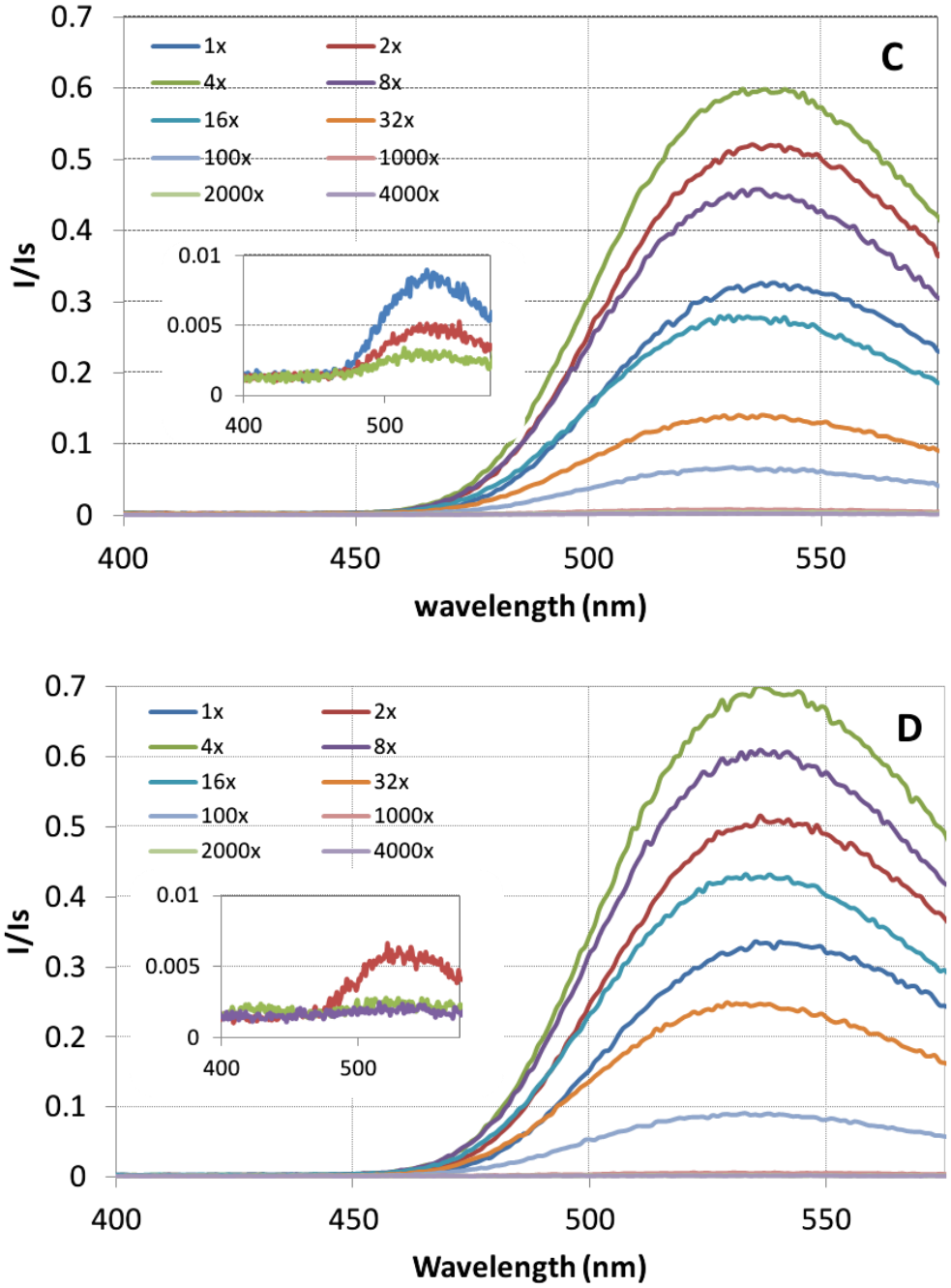

Figure 4.4 The fluorescence spectra of the peptide-ellipticine complexes upon serial dilution for EAR8-II, EAR8-a, ELR8-a and EAR16-II, respectively. The stock solutions were prepared with 0.5 mg/mL peptide and 0.1 mg/mL EPT. Inset indicates the spectra of the complexes upon 1000 to 4000 times dilution.

In addition, even though EAR8-II and EAR-a don't have a specific CAC, fluorescence study showed that these two peptides could interact with protonated EPT and stabilized it to the same extent as ELR8-a and EAR16-II. It may be explained by the molecular binding model proposed in the previous part, as shown in Figure 4.2. More importantly, it is believed that the good dilution stability of the complex will further affect its therapeutic efficiency in biological system.

EPT maximum suspension was determined by UV-vis spectrometer. A standard concentration calibration curve was obtained from the linear fitting of EPT absorption at a wavelength of 295 nm as a function of EPT concentration, as shown in equation (1).

$$y = 216.69x + 0.0008 \quad (1)$$

Where y is the absorbance value and x is the EPT concentration. The calibration curve for the absorbance of EPT was linear over the range of standard concentration EPT at 1×10^{-3}-1×10^{-2} mg/mL with a correlation coefficient of $R^2 = 0.9954$ (Figure 4.5).

With a combination of 0.1 mg/mL EPT and 0.5 mg/mL peptide, all four peptide-EPT complexes show great maximum suspension (~100%), as shown in Table 4.2. It verifies our theory that there is more than enough peptide to bind with protonated EPT in the systems at the 5:1 mass ratio of peptide to EPT.

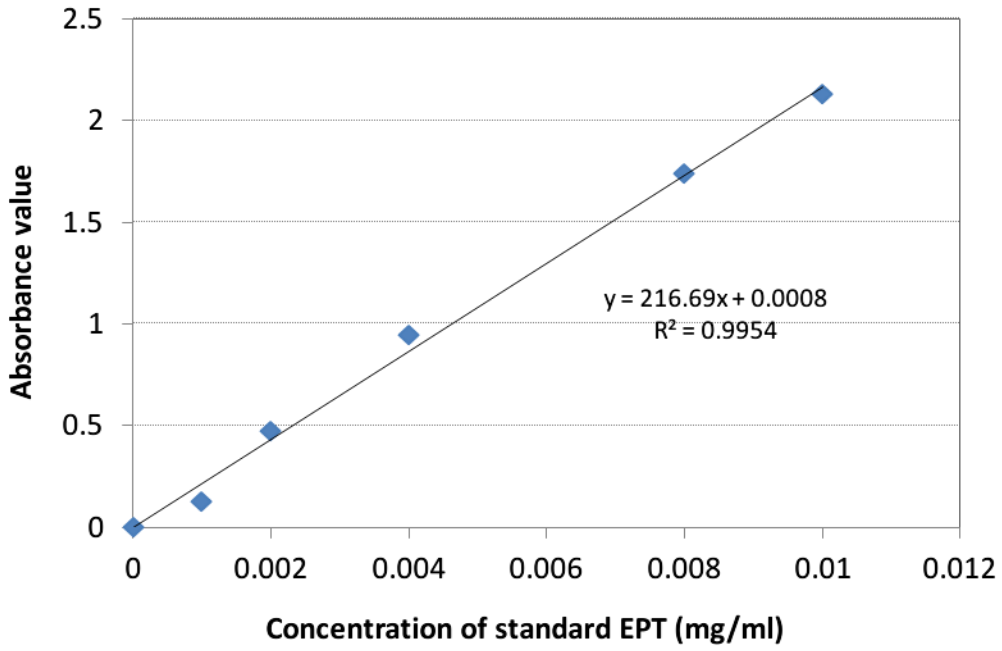

Figure 4.5 Standard curve from the linear fitting of EPT absorption at a wavelength of 295 nm as a function of EPT concentration.

Table 4.2 Characterization of peptide-EPT complexes

Nanoparticle	Mean size (nm)[a]	Polydispersity index	Zeta potential (mV)[a]	Maximum suspension (%)[a]
EAR8-II	336.7±27.5	0.450	7.4±4.9	-
EAR8-a	205.6±16.3	0.487	17.3±5.0	-
ELR8-a	365.2±14.5	0.669	14.5±6.7	-
EAR16-II	199.7±2.69	0.667	43.3±5.0	-
EAR8-II-EPT	212.0±1.89	0.253	51.0±10.4	101.1±0.4
EAR8-a-EPT	222.1±9.53	0.319	48.6±9.6	99.3±0.3
ELR8-a-EPT	116.4±4.59	0.278	43.3±6.2	109.9±0.6
EAR16-II-EPT	174.2±0.24	0.317	59.8±10.4	110.0±1.0

[a] Value reported as mean ± S.D. (n=3)

4.3 Length and Sequence Effect on the Peptide Assemblies and Complex Formation

So far, we have shown that peptide sequence, length and hydrophobicity will affect the peptide self-assembly property and its potential in encapsulating protonated EPT in water. Such effects may further influence the physiochemical properties of complex, such as particles size, surface charge and morphology, which will have effect on the anticancer activity and pathway of cellular uptake for nanoparticles[10, 108].

Secondary structure

The secondary structure of peptides in the absence and presence of EPT were characterized by circular dichroim (CD) spectroscopy. Spectra were collected at 0.5 mg/mL peptide with or without 0.1 mg/mL EPT. As reported in Figure 4.6, the two short peptides, EAR8-II and EAR8-a, presented almost the same CD spectra in pure water characterized by a strong negative band at 197nm and a weak negative band of approximately equal intensity near 222nm, suggesting the presence of a mixture structure of random coil and α-helix. The CD spectra of ELR8-a exhibited similar trend with EAR8-a except a weak positive band near 192nm, it corresponds a mixture structure of random coil and high level of α-helix. In contrast, the CD spectra for EAR16-II, produced a strong positive band at 197nm and negative band around 217nm, indicative of β-sheet formation. The identical nature of the CD profiles clearly indicates that the presence of EPT molecules during self-assembly of peptides do not hinder their original secondary structures.

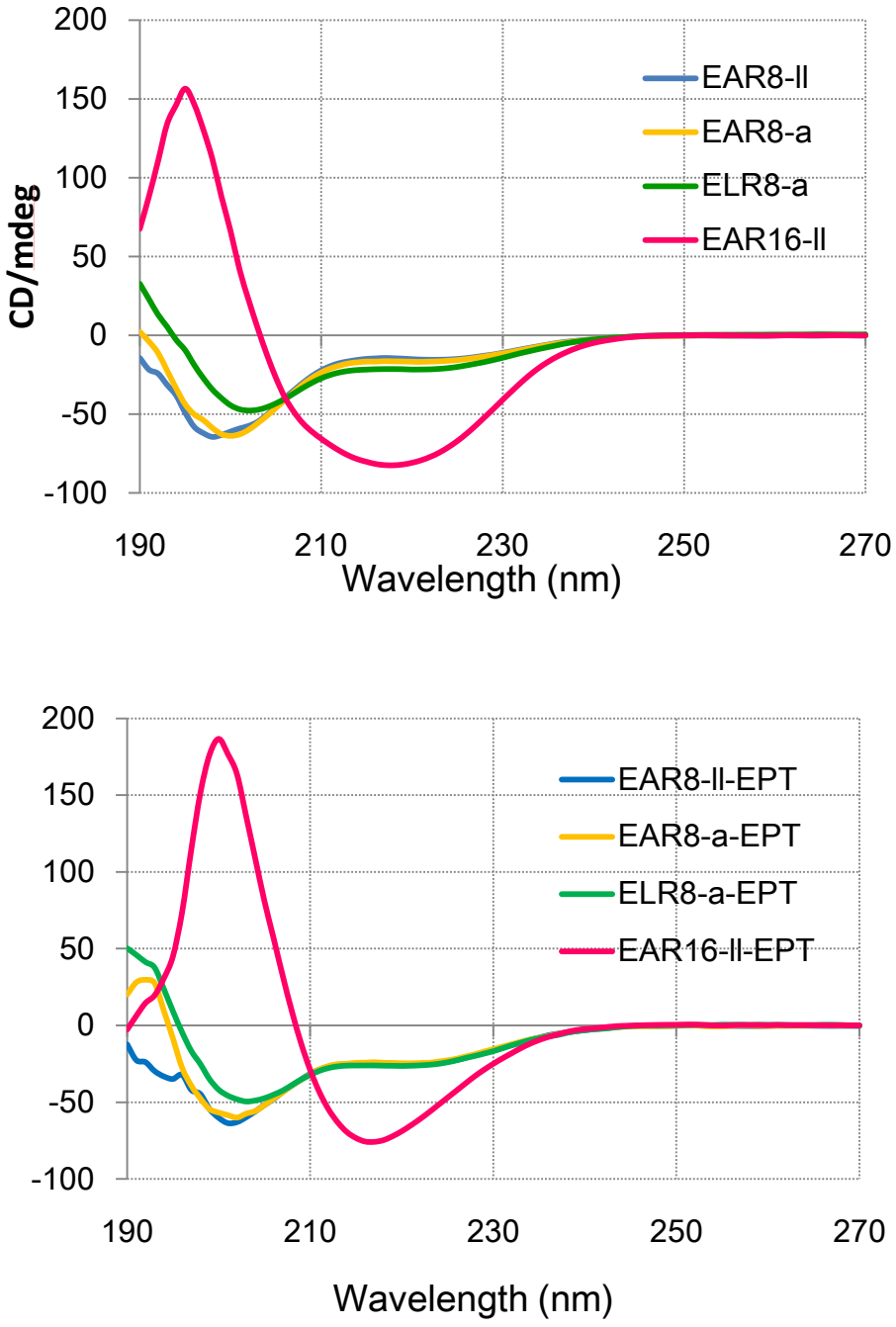

Figure 4.6. CD spectra of 0.5 mg/ml peptide solution (A) and complex of 0.5 mg/ml peptide with 0.1 mg/mL EPT (B). The CD measurement indicated that (A) EAR8-II, EAR8-a and ELR8-a exhibited a mixture structure of random coil and α-helix, whereas EAR16-II forms β-sheet

structure, (B) The identical nature of the CD profiles clearly indicates that the presence of EPT molecules during self-assembly of peptides do not hinder their original secondary structures.

Size ditribution and Surface charge

Ideal nanoparticles encapsulating drug should meet the following requirements: (i) particle size < 200 nm to facilitate passive targeting to solid tumors via the enhanced permeability and retention (EPR) effect[109]; (ii) high positive Zeta-potential to increase interaction with negatively charged cell surface[110]. The size distribution of the peptide assemblies and peptide-EPT complexes were characterized by measuring the hydrodynamic diameter at a peptide concentration of 0.5 mg/mL, EPT concentration of 0.1 mg/mL. It is clearly seen that these four peptide assemblies have a broad size distribution from 1 nm to 10 μm and had several size populations. The peptides alone are very polydispersed and over the detection limit of the instrument (Table 4.2). When the EPT was introduced to the peptide aqueous solution, the size distributions of complexes change significantly as shown in Figure 4.7. An average diameter of ~ 100 to 200 nm was obtained. The significantly change of size distribution indicates peptide assemblies interact with EPT to form a more compact and smaller nanoparticles, which may be ideal for passive targeting to solid tumors via the enhanced permeability and retention effect[12].

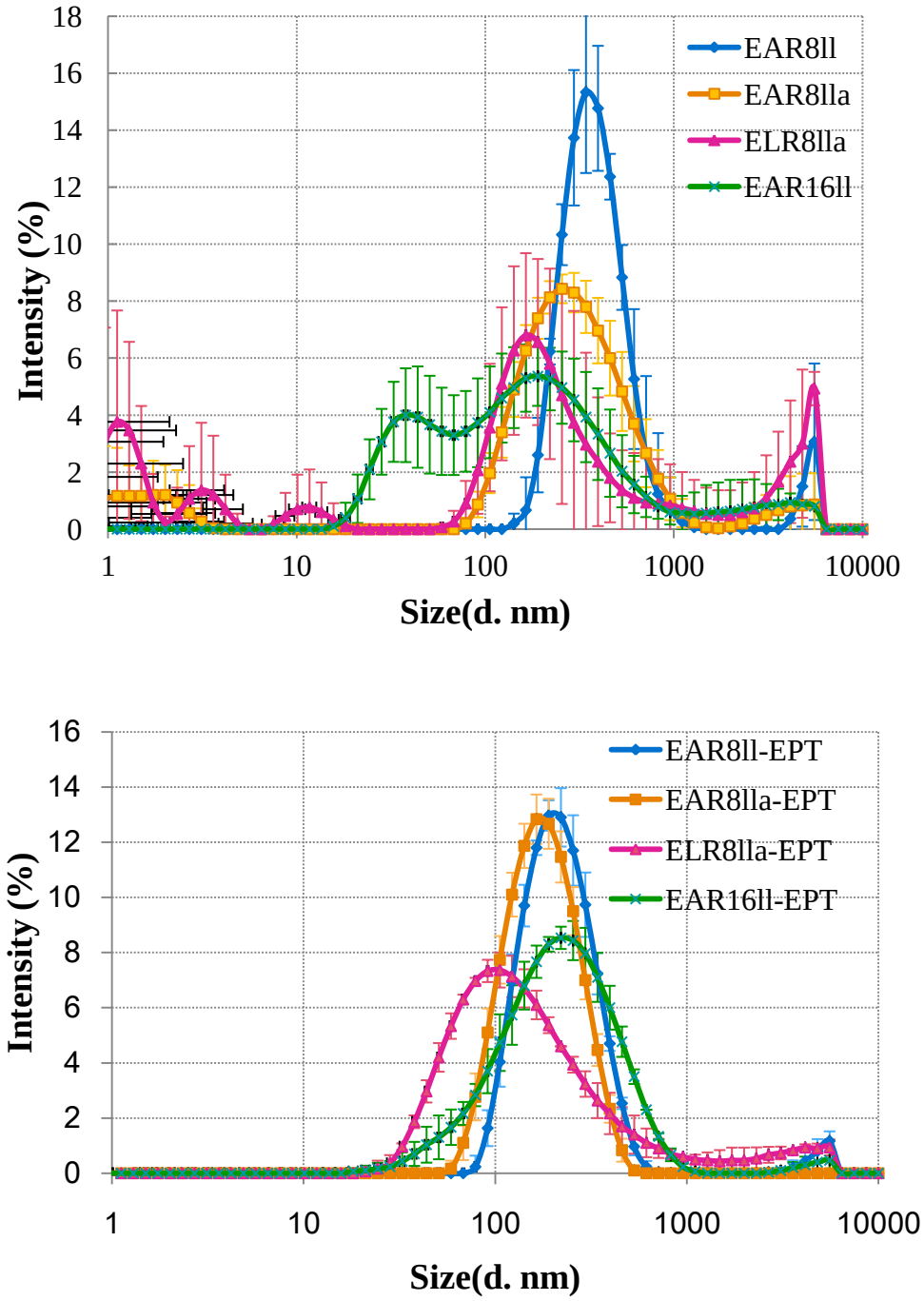

Figure 4.7 Size distributions of peptide self-assemblies and peptide-EPT complexes

Zeta potential, related to both surface charge and the local environment of the particle, might be a critical parameter for cellular interaction. Zeta potential values obtained for three

short peptides are quite similar, with values less than +20 mV as shown in Figure 4.8, which indicates the short peptide assemblies have poor colloidal stability. A value of +43.3 ±4.98 mV was obtained for EAR16, showed better stability than the short peptides. Since EPT is stabilized in protonated form in the peptide-EPT complexes, it is expected to be positively charged. Zeta potential measurements of complexes confirmed our prediction, the values for all peptide-EPT complexes increased to more than +40 mV, which can be considered as an excellent stable system.

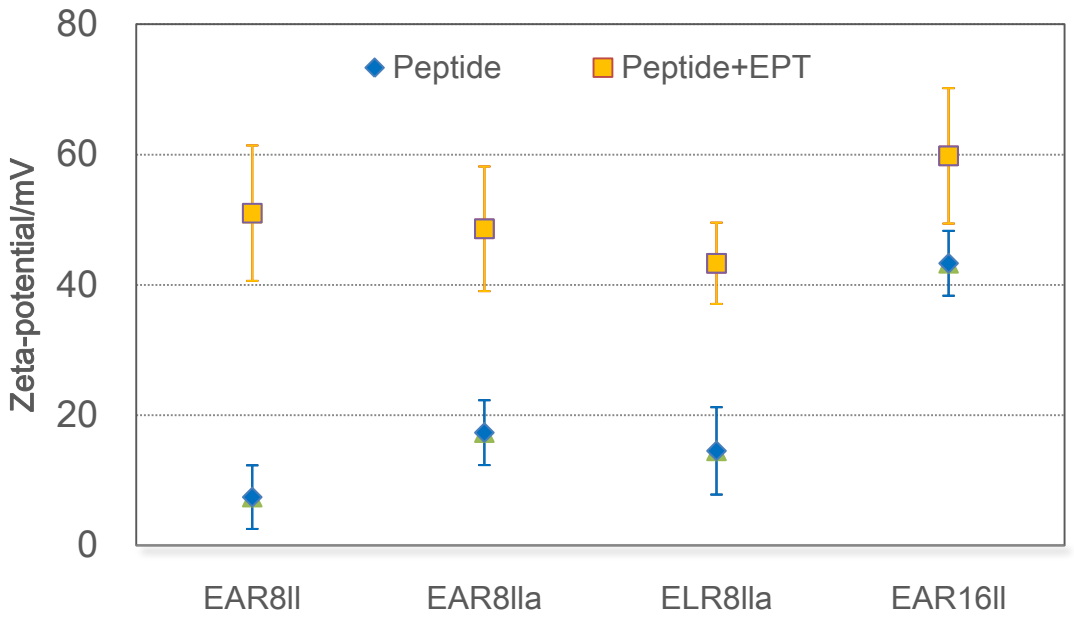

Figure 4.8 Zeta potential of peptide and peptide-EPT complex

Morphology

Atomic Force Microscopy (AFM) and Transmission Electron Microscopy (TEM) were used as complementary methods to study the morphology of peptide assemblies and peptide-EPT complexes. Figure 4.9 shows AFM and TEM images of these peptides and their

complexes with EPT in aqueous solution at a peptide concentration of 0.5 mg/mL and EPT concentration of 0.1 mg/mL. From AFM images, it is clearly seen that both EAR8-II and EAR8-a have a mixture structure of amorphous assemblies and short straight fibers (Figure 4.9 A-i and C-i). The dimentions of these two peptides assemblies are similar, range from 25-40nm (amorphous assemblies) to 100-200 nm (fibril assemblies) with same height of 1 nm. Their complexes with EPT tend to have amorphous assemblies with a radius of 60-90 nm and a height of 10 nm, while three or four globules may aggregate together to form a big amorphous assemblies (Figure 4.9 B-i and D-i). In the case of ELR8-a, similar amorphous assemblies as EAR8-II and EAR8-a are formed in the absence of fibril nanostructures (Figure 4.9 E-i); while the introduction of EPT may bind a few peptides together to form big globules with a radius of 200 nm (Figure 4.9 F-i). For the assemblies of EAR16-II, flat and straight nanofiber structures were observed; larger numbers of crosslinking points were seen in Figure 4.9 G-i, with width distributed from 20 nm to 30 nm and length in micrometers. On the other hand, it was shown that a region of both elongating and thickening fibrillar bundles coexisted with isolated fibrils in the EAR16-EPT complexes system, suggesting that peptide was more than enough to encapsulate EPT molecules.

Transmission electron microscopy was used to confirm the morphology results obtained from AFM imaging. For both EAR8 peptides, fibrillar assemblies disappeared to leave amorphous assemblies alone, which is different from AFM images. In the case of ELR8-EPT complexes, small globular structures with a radius of 50 nm are clearly seen compare with big globules of AFM image.

i ii

A

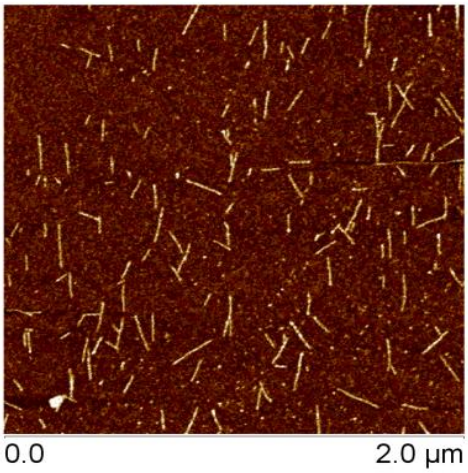

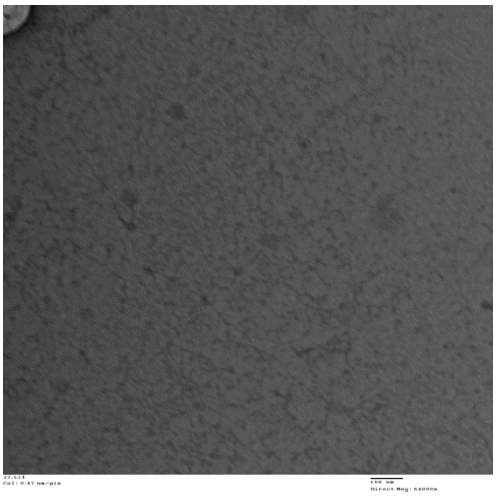

B

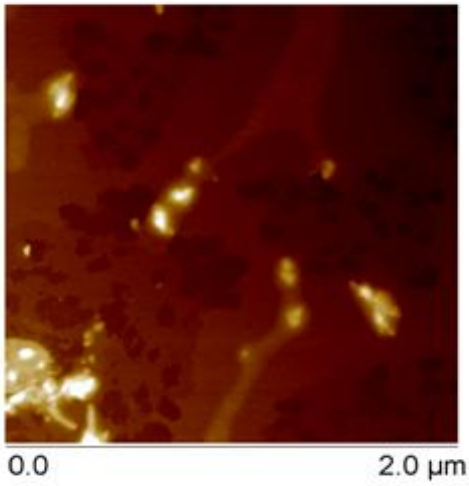

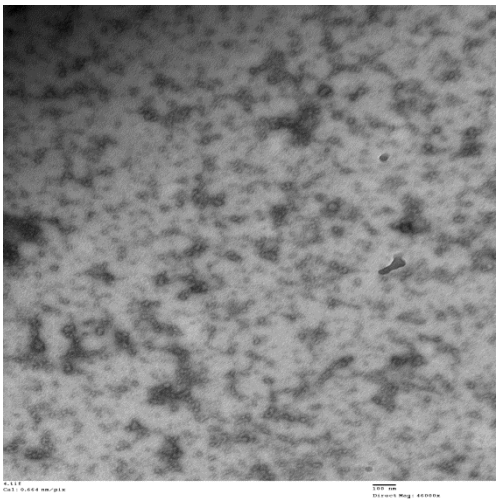

C

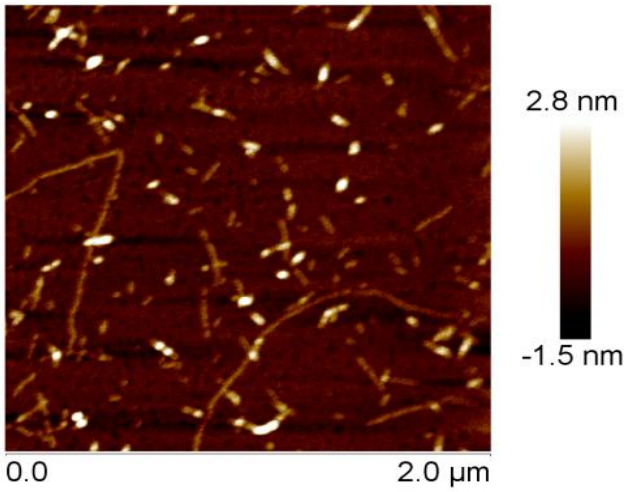

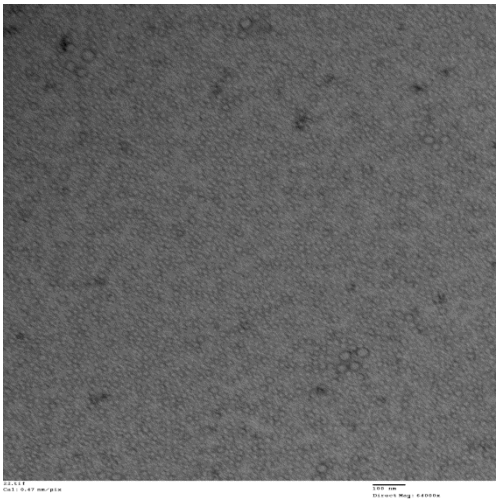

D

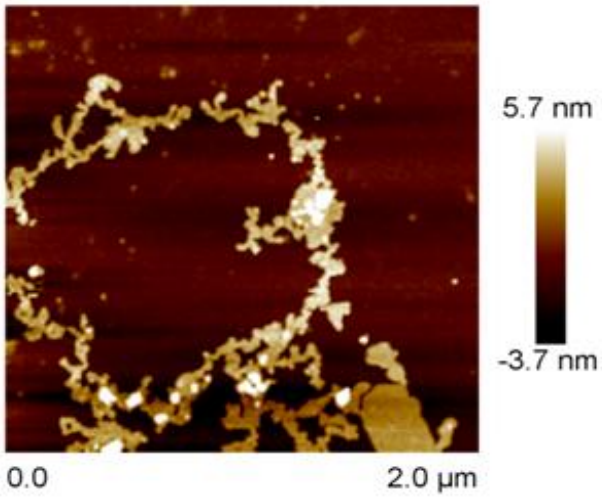

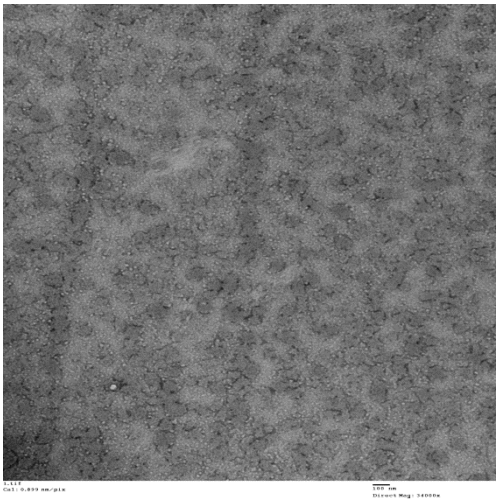

E

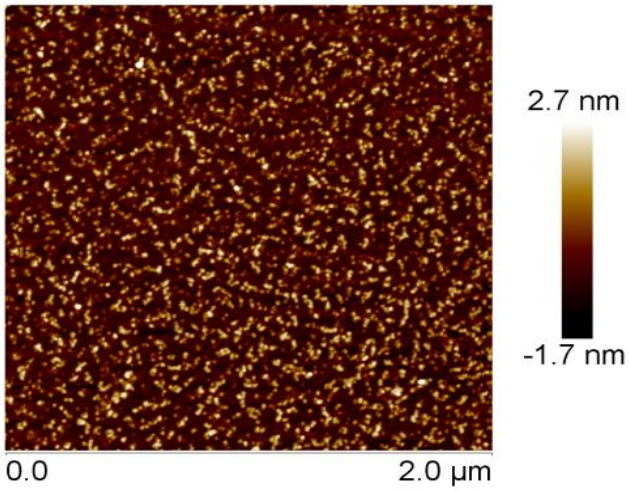

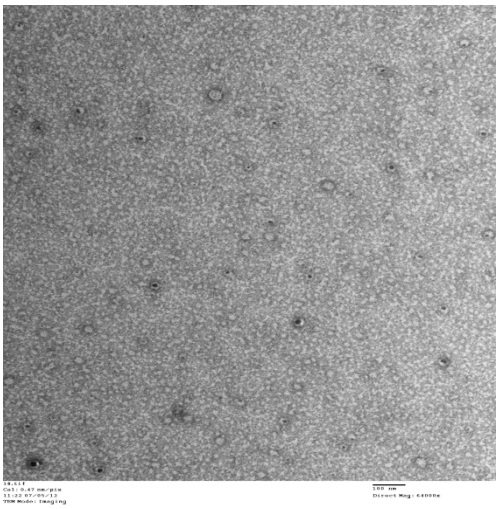

F

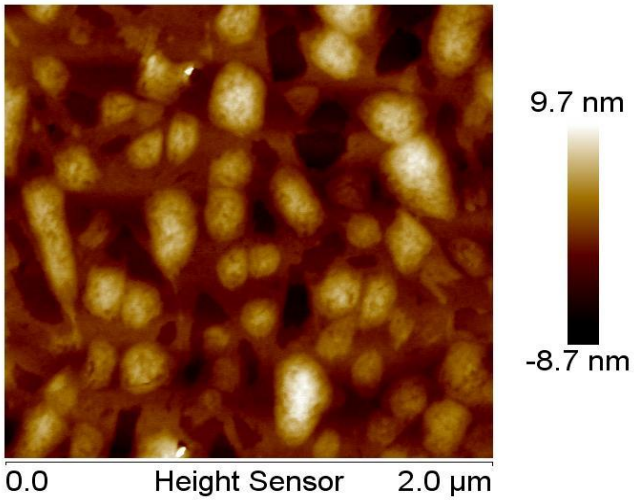

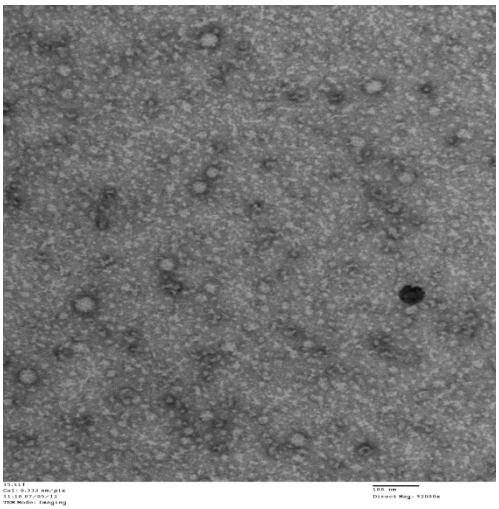

G

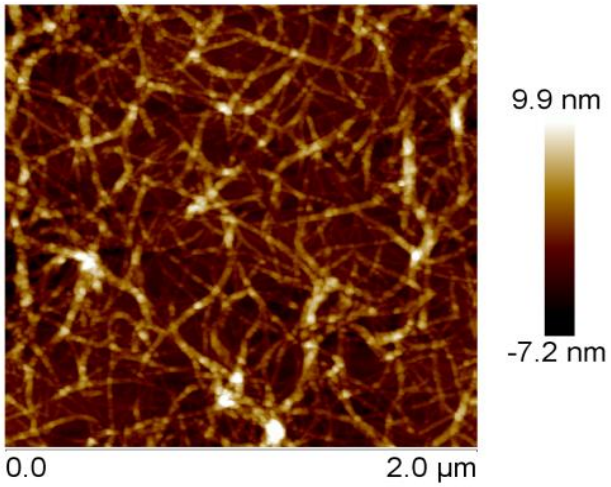

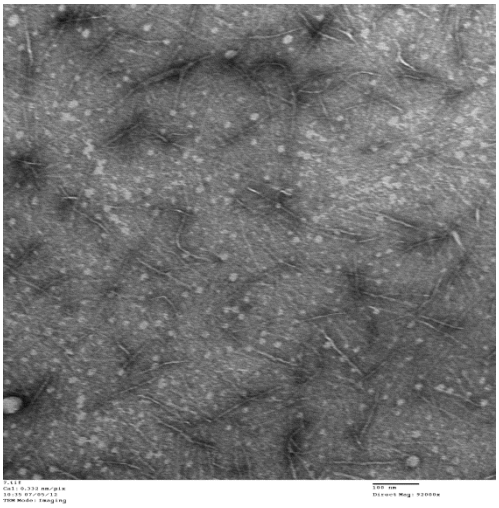

H

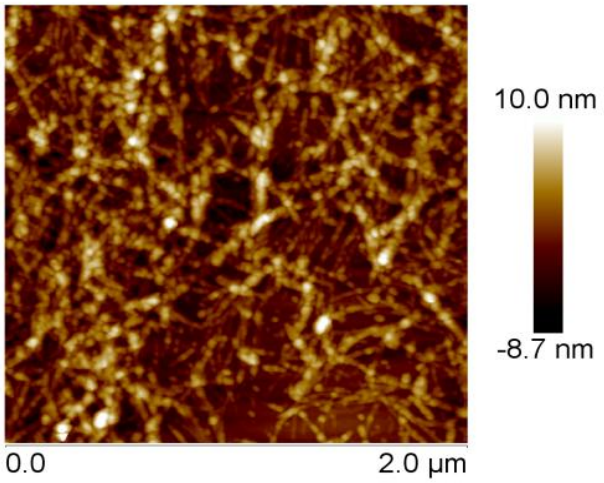

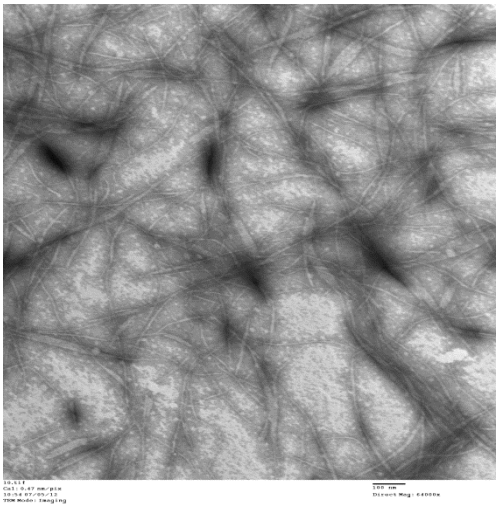

Figure 4.9 AFM and TEM images of EAR8-II (A-i, A-ii), EAR8-II-EPT complexes (B-i, B-ii), EAR8-a (C-i, C-ii), EAR8-a-EPT complexes (D-i, D-ii), ELR8-a (E-i, E-ii), ELR8-a-EPT complexes (F-i, F-ii), EAR16-II (G-i, G-ii), and EAR16-II-EPT complexes (H-i, H-ii). Scan area is 2 µm×2 µm for AFM images. Scale bar is 100 nm for TEM images.

4.4 Cellular Toxicity of Peptide-EPT Complexes and their dilutions

So far, we have shown that these four peptides can solubilize and stabilize protonated EPT in aqueous solution. It has been reported that the protonated EPT is more effective at killing cancer cells than other two states of EPT (neutral and crystalline form). This may due to two reasons: (1) protonated EPT tends to bind with negatively charged cell membranes, and accumulate at the membrane surface; the hydrophobic moiety of EPT further helps it cross the cell membrane[105]. (2) fast release kinetics of protonated EPT from the complexes[21]. To gain more insight concerning the differences in these four peptide-EPT complexes, the cellular toxicity against two cancer cells, MCF-7 and A549, and the stability of the complexes in relation to anticancer activity upon dilution in water were studied. The complexes stability is a crucial factor in determining its applicability in later animal studies and preclinical experiments.

Figure 4.10 shows the cell viability of two cancer cell lines, A549 and MCF-7, upon treatments with control samples and complexes after 24 h. Comparing to the negative control (no treatment), the solvent (water) and four peptides controls had minor toxicity to the cells (90-95% viability), suggesting that the four peptides alone were non-cytotoxic. The drug control (0.1 mg/mL EPT) caused 20-30% more cell death in comparison with the solvent control, whereas all complexes showed great potency in both cancer cells killing than EPT alone in pure water, leading to nearly zero cell viability. This could be a result of peptide stabilizing more protonated EPT in solution.

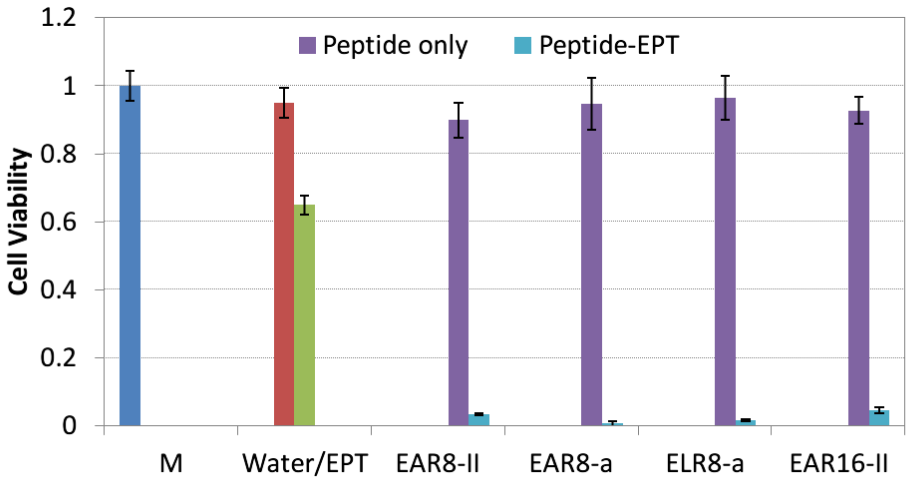

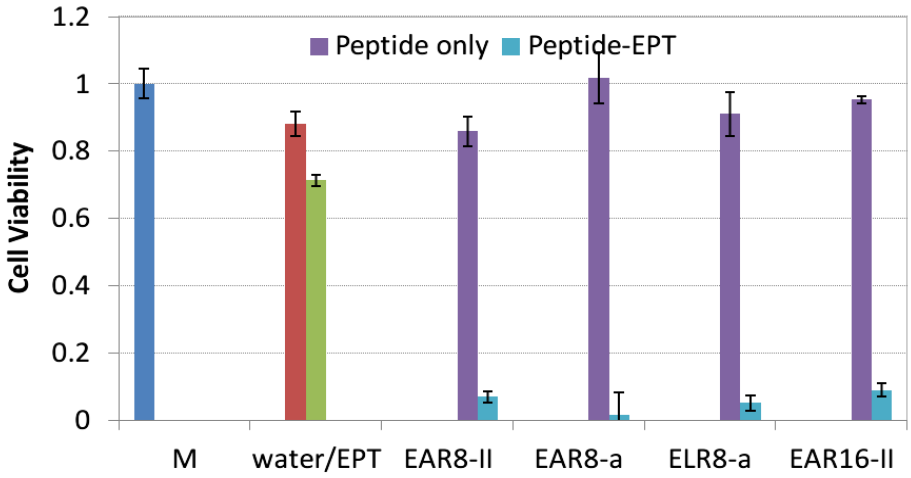

Figure 4.10 Cellular toxicity of the peptides and their complexes with EPT for A549 and MCF-7 cells. The viability of non-treated cells is a (M: cells were treated with culture medium.) For the solvent control, cells were treated with pure water; for the drug control, cells were treated with EPT in pure water with the absence of peptides. Blue bars represent the peptide controls where no ellipticine was added.

Previous fluorescence study has implied that the complexes dilution stability was very good resulting from strong association between EPT and peptide assemblies, we then

proceeded to investigate the dilution stability of peptide-EPT complexes in relation to the cellular toxicity in aqueous solution. Figure 4.11 shows the cellular toxicity of the complexes with 0.5 mg/mL EAR8-II, EAR8-a, ELR8-a and EAR16-II upon serial dilution in water against both cell lines. For A549 cells, the cell viability is very low and less than 2% with these four complexes even at 10 times dilution, gave much stronger cytotoxicity than complex formulated with EAK16 at the same concentration, which was not effective at killing cancer cells after 4 times dilution[105]. After 10 times dilution, cell viability of A549 cells was gradually reduced in a dose-responsive manner. Similar results were observed in MCF-7 cell lines, with the low cell viability after the same treatment (less than 5%) except for in the case of 10 times dilution (20-30%). However, the cell viability increased sharply upon the following serial dilution. These results may due to the decrease concentration of EPT during serial dilution. To further investigate the cytotoxicities of complexes, the IC50 values were estimated from Figure 4.11 and have been listed inTable 2.1. On the basis of the calculated IC50, complexes with EAR8-II, EA8-a and ELR8-a showed similar efficacy at killing both cancer cells with slight differences. In the case of EAR16-EPT complex, the cytotoxicity against MCF-7 is much lower than against A549 by comparing the IC50 values.

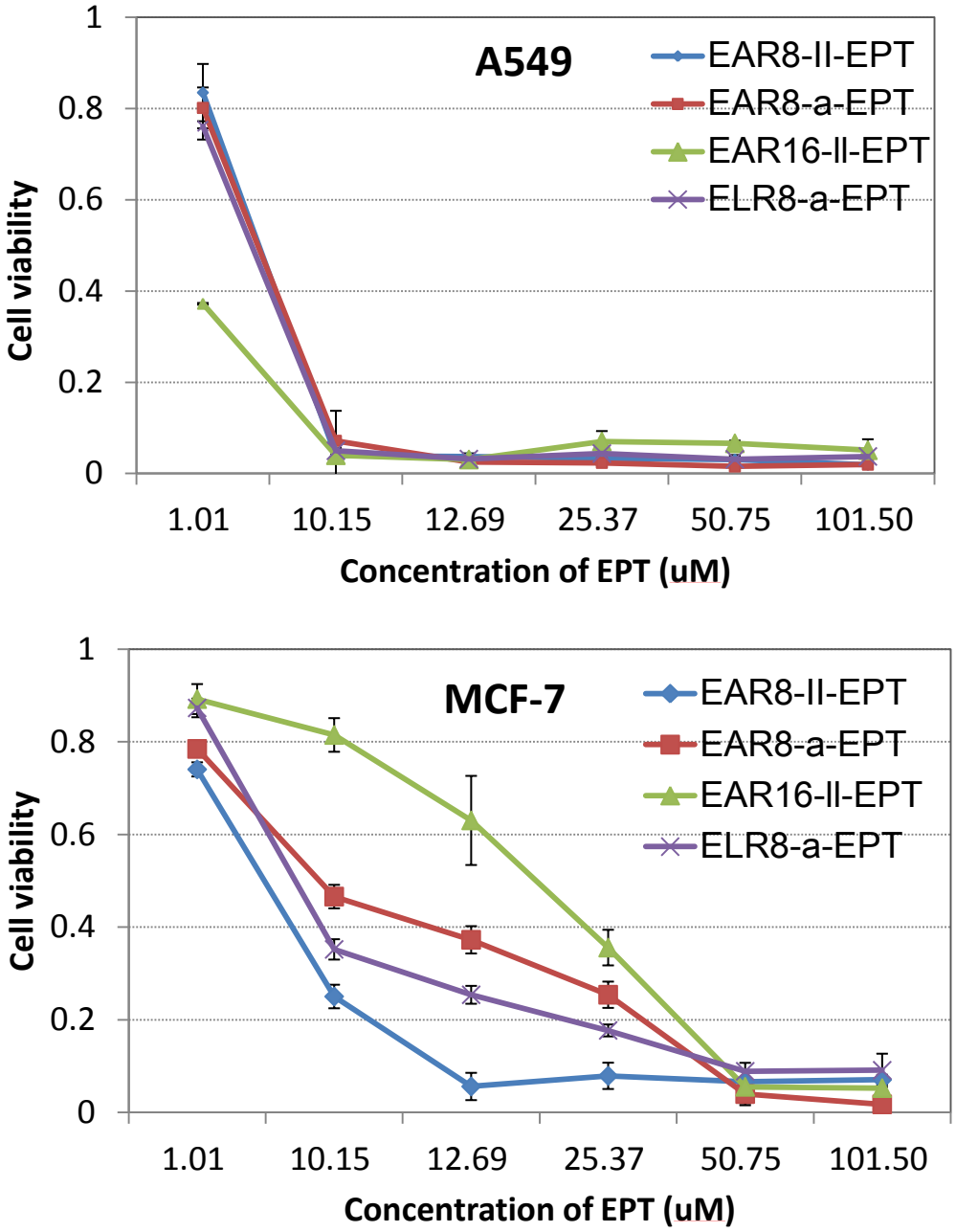

Figure 4.11 Cellular toxicity of the complexes formulated with four peptides at a peptide concentration of 0.5 mg/mL and 0.1 mg/mL EPT and their serial dilutions in water for A549 cells (A) and MCF-7 cells (B).

Table 4.3 Cytotoxic activities of peptide-EPT complexes

Nanoparticles	Cytotoxicity assay (IC50, μM)	
	Lung Cancer (A549)	Breast cancer (MCF-7)
EAR8-II-EPT	4.26±0.62	10.68±1.09
EAR8-a-EPT	3.16±0.35	4.41±0.40
ELR8-a-EPT	5.04±0.98	6.19±1.46
EAR16-II-EPT	0.36±0.12	18.90±0.46

This result seems to contradict to the already known fact that protonated EPT is more effective at killing MCF-7 cells. However, the reason behind this phenomenon is still unclear. Two potential factors are speculated that may cause the huge different therapeutic efficacies of EAR16-EPT for A549 and MCF-7. First, when culturing *in vitro*, MCF-7 cell line is capable of forming small domes while A549 grows as a monolayer. In the case of short peptide-EPT complex, both cancer cells are exposed to the sub-micron amorphous nanoparticles, which increase the opportunity of nanoparticles to attach and penetrate through the membrane surface of cancer cells. However, the dome of MCF-7 may hinder the long fibers of EAR16-EPT to attach to the membrane surface of cancer cells buried inside, causing lower cytotoxicity. By contrast, A549 monolayer exposes every cells outside, which allows the EAR16-EPT fibers to attack each cancer cells, enhanced the cytotoxicity of complex since the long fibers may encapsulate more protonated EPT. Second, it has been reported the membrane surface constitute of A549 and MCF-7 are different. The high

cholesterol content of MCF-7 membrane decreases the membrane fluidity, which may inhibit the uptake of drugs compare with other cancer cells[111].

The cytotoxicity study presented above demonstrates that arginine-rich ionic-complementary peptides, EAR8-II, EAR8-a, ELR8-a and EAR16-II, can stabilize the prescribed protonated EPT in aqueous solution. The combination of 0.5 mg/mL peptide and 0.1 mg/mL EPT exhibits excellent cancer inhibition efficacies and good stability upon dilution. Note that EAR16-EPT complex has a selective targeting to A549 cancer cell, which is important in the next phase studies on the peptide-based delivery of EPT *in vivo*.

Chapter 5
Conclusion and Recommendation

5.1 Conclusion

This thesis explored the capability of arginine-rich ionic complementary peptides as a promising potential carrier for protonated ellipticine delivery. The thesis includes the following four parts: (i) Illustrating basic design principals of arginine-rich ionic complementary peptides; (ii) Studying self-assembly ability of peptides and potential to encapsulate protonated EPT; (iii) Investigating effect of length and sequence on the peptide assemblies and complex formation; (iv) Studying cellular toxicity of peptide-EPT complexes and their dilutions. The original contribution and conclusion for each part are presented in the following.

A small library of model peptides, EAR8-II, EAR8-a, ELR8-a and EAR16-II were designed by systematically altering EAK16-II. Here we chose arginine (R) to replace lysine (K) because of the following reasons. (i) the side chain of arginine has higher pKa value than lysine. (ii) arginine's guanidinium group also could interact with nearby aromatic ring of EPT via π-stacking. (iii) arginine-rich peptides have shown strong cell-penetrating ability without requiring a specific binding site. These special advantageous properties of arginine over lysine make it possible for arginine rich ionic complementary peptide to be used as an ideal biomaterial to stabilize protonated EPT quickly and encapsulate more drugs.

5.1.1 Charge distribution and hydrophobicity effect of peptide

Table 5.1 Charge distribution effect of peptide on physicochemical properties and *in vitro* therapeutic effect of peptide and their complexation with EPT.

	EAR8-II **n- AEAEARAR-c**		**EAR8-a** **n- AAEEAARR-c**	
Surface property	No CAC obtained		No CAC obtained	
EPT state in peptide	Protonated EPT		Protonated EPT	
	EAR8-II	**EAR8-II-EPT**	**EAR8-a**	**EAR8-a-EPT**
Size distribution	High PDI	208.8 nm	High PDI	161.8 nm
Zeta potential	7.40mV	51.00 mV	17.3mV	48.6mV
Secondary structure	α-helix+ random coil		α-helix+ random coil	
Morphology	sGlobules +sFibers	Large globules	sGlobules +sFibers	Large globules
Cytotoxicity capacity	Non-toxic	IC50 (uM): 4.26±0.62 a 10.68±1.09 m	Non-toxic	IC50(uM): 3.16±0.35 a 6.19±1.46 m

Table 5.2 Hydrophobicity effect of peptide on physicochemical properties and *in vitro* therapeutic effect of peptide and their complexation with EPT.

	EAR8-a **n- AAEEAARR-c**		**ELR8-a** **n- LLEELLRR-c**	
Surface property	No CAC obtained		CAC: 51.15 uM	
EPT state in peptide	Protonated EPT		Protonated EPT	
	EAR8-a	**EAR8-a-EPT**	**ELR8-a**	**ELR8-a-EPT**
Size distribution	High PDI	161.8 nm	High PDI	116.4 nm
Zeta potential	17.3mV	48.6mV	14.5mV	43.3mV
Secondary structure	α-helix+ random coil		α-helix+ random coil	
Morphology	sGlobules +sFibers	Large globules	sGlobules	Large globules
Cytotoxicity capacity	Non-toxic	IC50(uM): 3.16±0.35 a 4.41±0.40 m	Non-toxic	IC50(uM): 5.04±0.98 a 6.19±1.46 m

For short peptides, EAR8-II, EAR8-a and ELR8-a, increase in peptide hydrophobicity indeed enhances the peptide self-assembly ability. The surface tension of EAR8-II and EAR8-a peptide solutions shows that there is no relationship between surface tension and the peptide concentration. The ANS fluorescence assay further confirms the results. While ELR8-a, more hydrophobic amino acid leucine increases the hydrophobicity of peptide, a CAC of 51.15 uM is obtained. However, the improved surface property of ELR8-a does not enhance its capability to encapsulate EPT. At a concentration of 0.5:0.1 mg/mL (peptide to EPT), fluorescence spectrum indicates that all three short peptides can solubilize and stabilize EPT in protonated form upon dilution to same extent, which means charge distribution and hydrophobicity effect will not have much effect on their complexations with EPT.

Further studies on physicochemical properties and In vitro therapeutic efficacies of peptide and peptide-EPT complexes indicate that both slight charge distribution and hydrophobicity difference will not affect peptide's complexation with EPT and their anticancer activity. One possible explanation is because the length of 8 amino acids peptide is too short to exhibit such a slight difference in charge distribution and hydrophobicty. Comparison between short length peptides and long length peptide confirms it in the next section. Length effect is more significant than charge distribution and hydrophobicity effects.

5.1.2 Length effect

Length effect of peptide is apparently the most significant effect on peptide assemblies and their complexation with EPT. First of all, longer length of EAR16 can provide more peptide association than short length peptides, resulting in better surface properties with a

CAC value of 30.40 uM. Second, EAR16 forms β-sheet rich nanofibers instead of amorphous nanostructures of short length peptides. Third, the anticancer activity of EAR16-EPT complex against A549 is much stronger than other peptides with a lower IC50 value, which is important in the next phase studies on the peptide-based delivery of EPT *in vivo*.

Table 5.3 Length effect of peptide on physicochemical properties and in vitro therapeutic effect of peptide and their complexation with EPT.

	EAR8-II **n- AEAEARAR-c**		EAR16-II **n- AEAEARARAEAEARAR-c**	
Surface property	No CAC obtained		CAC: 30.40 uM	
EPT state in peptide	Protonated EPT		Protonated EPT	
	EAR8-II	**EAR8-II-EPT**	**EAR16-II**	**EAR16-II-EPT**
Size distribution	High PDI	208.8 nm	High PDI	172.2 nm
Zeta potential	7.40mV	51.00 mV	43.3mV	59.8mV
Secondary structure	α-helix+ random coil		β-sheet	
Morphology	sGlobules	Large globules	Long Fibers	Long Fiber bundles
Cytotoxicity capacity	Non-toxic	IC50 (uM): 4.26±0.62 a 10.68±1.09 m	Non-toxic	IC50(uM): 0.36±0.12 a 18.90±0.46m

Overall, slight charge distribution and hydrophobicity difference of 8 amino acids peptide will not have much effect on peptide assemblies and their complexation with EPT; whereas increase in peptide length could strengthen the interaction between peptide and EPT, which gives the stronger anticancer activity of EAR16-EPT to A549. In addition, replacing lysine in EAK16 with arginine indeed improves peptide's complexation with hydrophobic

anticancer drug. This study provides information for selecting peptide sequence to construct advanced functional peptide-based delivery system.

5.2 Recommendation

Recommended future work to develop arginine-rich ionic complementary peptides as nanocarrier for prescribed protonated EPT delivery can be divided into four groups: (i) determine the aggregation number of peptide self assemblies and its complex with EPT; (ii) further study the mechanism behind EAR16's selectivity targeting to A549; (iii) evaluation of the complexes in 3D cell culture; (iv) design new peptide library based on current peptide sequence. The detailed information is listed in the following:

5.2.1 Determine the aggregation number of peptide assemblies and its complex with EPT

Aggregation number is an important parameter to characterize the nanostructure of peptide assemblies and its complex with EPT. One method to obtain aggregation number is performing static light scattering technique. Based on the aggregation number results and AFM morphology images, we may have a clear idea of the nanostructure of peptide assemblies.

$$\text{Aggregation number} = \frac{\text{Molecular weight of peptide aggregation}}{\text{Molecular weight of peptide monomer}}$$

5.2.2 Further study the mechanism behind EAR16's selectivity targeting to A549

It has been found that the cellular uptake of a free drug may depend on membrane properties, in particular on cholesterol content which has been shown to have a high impact

on membrane stiffness and fluidity. Petra et al. have shown that the uptake of doxorubicin is enhanced if membrane fluidity is increased upon cholesterol depletion. The same protocol can be applied to our complexes to evaluate the impact of cholesterol content of cell membrane.

5.2.3 Evaluation of the complexes in 3D cell culture

In a further step towards clinical application, 2-dimensional cell culture may be replaced by 3-dimensional cell culture, whose physiology, morphology and nutrient supply is closer to the *in vivo* situation in tumors. Two major advantages of 3D cell culture technique are (i) increasing the accuracy of predicting complex in vivo drug interactions; (ii) decreasing the time and cost of drug development. Thus, the use of 3D culture techniques is an alternative approach to translate into better modeling of drug behavior on cancer cells.

5.2.4 Design new peptide library based on current peptide sequence

New peptides are designed based on our current research results. These peptides may possess higher encapsulation efficiency of drug and better stability.

Peptide	# of Amino Acids	Sequence (n-c)	Charge distribution
EAR16-a	16	n-AAEEAARRAAEEAARR-c	--++--++
ELR16-a	16	n-LLEELLRRLLEELLRR-c	--++--++
ELR16-II	16	n-LELELRLRLELELRLR-c	--++--++

Bibliography

1. Boyle, P.; Levin, B.; International Agency for Research on Cancer.; World Health Organization., World cancer report 2008.

2. Canadian Cancer Statistics 2012.

3. Ambrose, M. A. E. J., The Surface Properties of Cancer Cells: A Review. Cancer Res. 1962, 22, 525-548.

4. Gibbs, W. W., Untangling the roots of cancer. Sci Am 2003, 289 (1), 56-65.

5. Anand, P.; Kunnumakara, A. B.; Sundaram, C.; Harikumar, K. B.; Tharakan, S. T.; Lai, O. S.; Sung, B. Y.; Aggarwal, B. B., Cancer is a Preventable Disease that Requires Major Lifestyle Changes. Pharm. Res. 2008, 25 (9), 2097-2116.

6. Bonadonna, G.; Brusamolino, E.; Valagussa, P.; Rossi, A.; Brugnatelli, L.; Brambilla, C.; Delena, M.; Tancini, G.; Bajetta, E.; Musumeci, R.; Veronesi, U., Combination Chemotherapy as an Adjuvant Treatment in Operable Breast-Cancer. New Engl J Med 1976, 294 (8), 405-410.

7. Baskar, R.; Lee, K. A.; Yeo, R.; Yeoh, K. W., Cancer and Radiation Therapy: Current Advances and Future Directions. Int J Med Sci 2012, 9 (3), 193-199.

8. Park, J. H.; von Maltzahn, G.; Xu, M. J.; Fogal, V.; Kotamraju, V. R.; Ruoslahti, E.; Bhatia, S. N.; Sailor, M. J., Cooperative nanomaterial system to sensitize, target, and treat tumors. Proc. Natl. Acad. Sci. U. S. A. 2010, 107 (3), 981-986.

9. Li, J. W. H.; Vederas, J. C., Drug Discovery and Natural Products: End of an Era or an Endless Frontier? Science 2009, 325 (5937), 161-165.

10. Davis, M. E.; Chen, Z.; Shin, D. M., Nanoparticle therapeutics: an emerging treatment modality for cancer. Nat Rev Drug Discov 2008, 7 (9), 771-782.

11. Bawarski, W. E.; Chidlowsky, E.; Bharali, D. J.; Mousa, S. A., Emerging nanopharmaceuticals. Nanomed.-Nanotechnol. Biol. Med. 2008, 4 (4), 273-282.

12. Singh, R.; Lillard, J. W., Nanoparticle-based targeted drug delivery. Exp Mol Pathol 2009, 86 (3), 215-223.

13. Wang, A. Z.; Langer, R.; Farokhzad, O. C., Nanoparticle Delivery of Cancer Drugs. Annu Rev Med 2012, 63, 185-198.

14. Malam, Y.; Loizidou, M.; Seifalian, A. M., Liposomes and nanoparticles: nanosized vehicles for drug delivery in cancer. Trends Pharmacol. Sci. 2009, 30 (11), 592-599.

15. Torchilin, V. P., Recent advances with liposomes as pharmaceutical carriers. Nat Rev Drug Discov 2005, 4 (2), 145-160.

16. Prakash, S.; Malhotra, M.; Shao, W.; Tomaro-Duchesneau, C.; Abbasi, S., Polymeric nanohybrids and functionalized carbon nanotubes as drug delivery carriers for cancer therapy. Adv Drug Deliver Rev 2011, 63 (14-15), 1340-1351.

17. Liu, J. B.; Xiao, Y. H.; Allen, C., Polymer-drug compatibility: A guide to the development of delivery systems for the anticancer agent, Ellipticine. J. Pharm. Sci. 2004, 93 (1), 132-143.

18. Calderon, M.; Welker, P.; Licha, K.; Fichtner, I.; Graeser, R.; Haag, R.; Kratz, F., Development of efficient acid cleavable multifunctional prodrugs derived from dendritic polyglycerol with a poly(ethylene glycol) shell. J. Control. Release 2011, 151 (3), 295-301.

19. Myc, A.; Majoros, I. J.; Thomas, T. P.; Baker, J. R., Dendrimer-based targeted delivery of an apoptotic sensor in cancer cells. Biomacromolecules 2007, 8 (1), 13-18.

20.Liu, X. X.; Liu, C.; Laurini, E.; Posocco, P.; Pricl, S.; Qu, F. Q.; Rocchi, P.; Peng, L., Efficient Delivery of Sticky siRNA and Potent Gene Silencing in a Prostate Cancer Model Using a Generation 5 Triethanolamine-Core PAMAM Dendrimer. Mol. Pharm. 2012, 9 (3), 470-481.

21. Fung, S. Y.; Yang, H.; Bhola, P. T.; Sadatmousavi, P.; Muzar, E.; Liu, M.; Chen, P., Self-Assembling Peptide as a Potential Carrier for Hydrophobic Anticancer Drug Ellipticine: Complexation, Release and In Vitro Delivery. Adv Funct Mater 2009, 19 (1), 74-83.

22. Hong, Y. S.; Legge, R. L.; Zhang, S.; Chen, P., Effect of amino acid sequence and pH on nanofiber formation of self-assembling peptides EAK16-II and EAK16-IV. Biomacromolecules 2003, 4 (5), 1433-1442.

23. Zhang, S. G., Emerging biological materials through molecular self-assembly. Biotechnol Adv 2002, 20 (5-6), 321-339.

24. Goeden-Wood, N. L.; Keasling, J. D.; Muller, S. J., Self-assembly of a designed protein polymer into beta-sheet fibrils and responsive gels. Macromolecules 2003, 36 (8), 2932-2938.

25. Yang, H.; Fung, S.-Y.; Pritzker, M.; Chen, P., Ionic-Complementary Peptide Matrix for Enzyme Immobilization and Biomolecular Sensing. Langmuir 2009, 25 (14), 7773-7777.

26. Zou, D.; Tie, Z.; Lu, C.; Qin, M.; Lu, X.; Wang, M.; Wang, W.; Chen, P., Effects of hydrophobicity and anions on self-assembly of the peptide EMK16-II. Biopolymers 2009, NA-NA.

27. Doles, T.; Bozic, S.; Gradisar, H.; Jerala, R., Functional self-assembling polypeptide bionanomaterials. Biochem Soc T 2012, 40, 629-634.

28. Balciunas, E. M.; Martinez, F. A. C.; Todorov, S. D.; Franco, B. D. G. D. M.; Converti, A.; Oliveira, R. P. D., Novel biotechnological applications of bacteriocins: A review. Food Control 2013, 32 (1), 134-142.

29. Rodina, E. V., Nanomaterials based on peptides. Polym Sci Ser C+ 2012, 54 (1), 88-95.

30. Zhang, S. G.; Lockshin, C.; Cook, R.; Rich, A., Unusually Stable Beta-Sheet Formation in an Ionic Self-Complementary Oligopeptide. Biopolymers 1994, 34 (5), 663-672.

31. Michel, S.; Tillequin, F.; Koch, M.; Assi, L. A., Ellipticine, Major Alkaloid from Bark of Strychnos-Dinklagei. J. Nat. Prod. 1980, 43 (2), 294-295.

32. Sureau, F.; Moreau, F.; Millot, J. M.; Manfait, M.; Allard, B.; Aubard, J.; Schwaller, M. A., Microspectrofluorometry of the Protonation State of Ellipticine, an Antitumor Alkaloid, in Single Cells. Biophys. J. 1993, 65 (5), 1767-1774.

33. Grossman, C.; Cacoub, P.; Guillevin, L.; Royer, I., A Fatality during Ellipticine Therapy. Ann Med Interne 1985, 136 (6), 519-519.

34. Masood, F.; Chen, P.; Yasin, T.; Fatima, N.; Hasan, F.; Hameed, A., Encapsulation of Ellipticine in poly-(3-hydroxybutyrate-co-3-hydroxyvalerate) based nanoparticles and its in vitro application. Mat Sci Eng C-Mater 2013, 33 (3), 1054-1060.

35. Cavalcanti, L. P.; Torriani, I. L., Thermotropic phase behavior of DPPC liposome systems in the presence of the anti-cancer agent 'Ellipticine'. Eur. Biophys. J. Biophys. Lett. 2006, 36 (1), 67-71.

36.Bawa, R.; Fung, S. Y.; Shiozaki, A.; Yang, H.; Zheng, G.; Keshavjee, S.; Liu, M. Y., Self-assembling peptide-based nanoparticles enhance cellular delivery of the hydrophobic anticancer drug ellipticine through caveolae-dependent endocytosis. Nanomed.-Nanotechnol. Biol. Med. 2012, 8 (5), 647-654.

37. Yoo, H. S.; Park, T. G., Folate receptor targeted biodegradable polymeric doxorubicin micelles. J. Control. Release 2004, 96 (2), 273-283.

38. Lai, P. S.; Lou, P. J.; Peng, C. L.; Pai, C. L.; Yen, W. N.; Huang, M. Y.; Young, T. H.; Shieh, M. J., Doxorubicin delivery by polyamidoamine dendrimer conjugation and photochemical internalization for cancer therapy. J. Control. Release 2007, 122 (1), 39-46.

39. Lu, S.; Wang, H.; Sheng, Y. B.; Liu, M. Y.; Chen, P., Molecular binding of self-assembling peptide EAK16-II with anticancer agent EPT and its implication in cancer cell inhibition. J. Control. Release 2012, 160 (1), 33-40.

40. Oerlemans, C.; Bult, W.; Bos, M.; Storm, G.; Nijsen, J. F. W.; Hennink, W. E., Polymeric Micelles in Anticancer Therapy: Targeting, Imaging and Triggered Release. Pharm. Res. 2010, 27 (12), 2569-2589.

41. Thurston, D. E., Chemistry and Pharmacology of Anticancer Drugs. CRC Press: 2006.

42. Ashworth, A.; Lord, C. J.; Reis, J. S., Genetic Interactions in Cancer Progression and Treatment. Cell 2011, 145 (1), 30-38.

43. Mroz, P.; Hashmi, J. T.; Huang, Y. Y.; Lang, N.; Hamblin, M. R., Stimulation of anti-tumor immunity by photodynamic therapy. Expert Rev Clin Immu 2011, 7 (1), 75-91.

44. Vanneman, M.; Dranoff, G., Combining immunotherapy and targeted therapies in cancer treatment. Nat Rev Cancer 2012, 12 (4), 237-251.

45. Kinzler, K. W. V., Bert, The genetic basis of human cancer. New York: McGraw-Hill, Medical Pub. Division.: New York, 2002; p 5.

46. Damm, K., Erba - Tumor-Suppressor Turned Oncogene. Faseb J 1993, 7 (10), 904-909.

47. Bartek, J.; Lukas, J.; Bartkova, J., Perspective: Defects in cell cycle control and cancer. J Pathol 1999, 187 (1), 95-99.

48. Lodish H, B. A., Zipursky SL, et al., Molecular Cell Biology:Section 24.2, Proto-Oncogenes and Tumor-Suppressor Genes. W. H. Freeman: New York, 2000.

49. Hale, A. J.; Smith, C. A.; Sutherland, L. C.; Stoneman, V. E. A.; Longthorne, V. L.; Culhane, A. C.; Williams, G. T., Apoptosis: Molecular regulation of cell death. Eur J Biochem 1996, 236 (1), 1-26.

50. Bakken, K.; Fournier, A.; Lund, E.; Waaseth, M.; Dumeaux, V.; Clavel-Chapelon, F.; Fabre, A.; Hemon, B.; Rinaldi, S.; Chajes, V.; Slimani, N.; Allen, N. E.; Reeves, G. K.; Bingham, S.; Khaw, K. T.; Olsen, A.; Tjonneland, A.; Rodriguez, L.; Sanchez, M. J.; Etxezarreta, P. A.; Ardanaz, E.; Tormo, M. J.; Peeters, P. H.; van Gils, C. H.; Steffen, A.; Schulz, M.; Chang-Claude, J.; Kaaks, R.; Tumino, R.; Gallo, V.; Norat, T.; Riboli, E.; Panico, S.; Masala, G.; Gonzalez, C. A.; Berrino, F., Menopausal hormone therapy and breast cancer risk: impact of different treatments. The European Prospective Investigation into Cancer and Nutrition. Int. J. Cancer 2011, 128 (1), 144-156.

51. Cea-Soriano, L.; Blenk, T.; Wallander, M. A.; Rodriguez, L. A. G., Hormonal therapies and meningioma: Is there a link? Cancer Epidemiol 2012, 36 (2), 198-205.

52. Jordan, V. C., Tamoxifen or raloxifene for breast cancer chemoprevention: A tale of two choices-point. Cancer Epidem Biomar 2007, 16 (11), 2207-2209.

53. Leung, F. P.; Tsang, S. Y.; Wong, C. M.; Yung, L. M.; Chan, Y. C.; Leung, H. S.; Yao, X. Q.; Huang, Y., Raloxifene, tamoxifen and vascular tone. Clin Exp Pharmacol P 2007, 34 (8), 809-813.

54. Brannon-Peppas, L.; Blanchette, J. O., Nanoparticle and targeted systems for cancer therapy. Adv Drug Deliver Rev 2012, 64, 206-212.

55. Folkman, J.; Merler, E.; Abernath.C; Williams, G., Isolation of a Tumor Factor Responsible for Neovascularization. J Clin Invest 1970, 49 (6), A30-&.

56. Di Lorenzo, G.; Autorino, R.; Sternberg, C. N., Metastatic Renal Cell Carcinoma: Recent Advances in the Targeted Therapy Era. Eur Urol 2009, 56 (6), 959-971.

57. Hoerr, I.; Obst, R.; Rammensee, H. G.; Jung, G., In vivo application of RNA leads to induction of specific cytotoxic T lymphocytes and antibodies. Eur J Immunol 2000, 30 (1), 1-7.

58. Emens, L. A., Chemotherapy and tumor immunity: an unexpected collaboration. Front Biosci-Landmrk 2008, 13, 249-257.

59. Brewer, E.; Coleman, J.; Lowman, A., Emerging Technologies of Polymeric Nanoparticles in Cancer Drug Delivery. J Nanomater 2011.

60.Berna, M.; Dalzoppo, D.; Pasut, G.; Manunta, M.; Izzo, L.; Jones, A. T.; Duncan, R.; Veronese, F. M., Novel monodisperse PEG-dendrons as new tools for targeted drug delivery: Synthesis, characterization and cellular uptake. Biomacromolecules 2006, 7 (1), 146-153.

61. Gu, F.; Zhang, L.; Teply, B. A.; Mann, N.; Wang, A.; Radovic-Moreno, A. F.; Langer, R.; Farokhzad, O. C., Precise engineering of targeted nanoparticles by using self-assembled biointegrated block copolymers. Proc. Natl. Acad. Sci. U. S. A. 2008, 105 (7), 2586-2591.

62. Talekar, M.; Kendall, J.; Denny, W.; Garg, S., Targeting of nanoparticles in cancer: drug delivery and diagnostics. Anti-Cancer Drugs 2011, 22 (10), 949-962.

63. Alkhatib, M. H.; Albishi, H. M.; Mahassni, S. H., Impact of Nanoparticles on Cancer Therapy. Trop J Pharm Res 2012, 11 (6), 1001-1011.

64. Ferrari, M., Nanovector therapeutics. Curr Opin Chem Biol 2005, 9 (4), 343-346.

65. Gregoria.G; Ryman, B. E., Liposomes as Carriers of Enzymes or Drugs - New Approach to Treatment of Storage Diseases. Biochem. J. 1971, 124 (5), P58-&.

66. Klibanov, A. L.; Maruyama, K.; Torchilin, V. P.; Huang, L., Amphipathic Polyethyleneglycols Effectively Prolong the Circulation Time of Liposomes. FEBS Lett. 1990, 268 (1), 235-237.

67. Fassas, A.; Anagnostopoulos, A., The use of liposomal daunorubicin (DaunoXome) in acute myeloid leukemia. Leukemia Lymphoma 2005, 46 (6), 795-802.

68. Ghosh, P.; Han, G.; De, M.; Kim, C. K.; Rotello, V. M., Gold nanoparticles in delivery applications. Adv Drug Deliver Rev 2008, 60 (11), 1307-1315.

69. des Rieux, A.; Fievez, V.; Garinot, M.; Schneider, Y. J.; Preat, V., Nanoparticles as potential oral delivery systems of proteins and vaccines: A mechanistic approach. J. Control. Release 2006, 116 (1), 1-27.

70. Liechty, W. B.; Peppas, N. A., Expert opinion: Responsive polymer nanoparticles in cancer therapy. Eur. J. Pharm. Biopharm. 2012, 80 (2), 241-246.

71. Lavasanifar, A.; Samuel, J.; Kwon, G. S., Poly(ethylene oxide)-block-poly(L-amino acid) micelles for drug delivery. Adv Drug Deliver Rev 2002, 54 (2), 169-190.

72. Matsumura, Y., Poly (amino acid) micelle nanocarriers in preclinical and clinical studies. Adv Drug Deliver Rev 2008, 60 (8), 899-914.

73. Fauzee, N. J. S.; Dong, Z.; Wang, Y. L., Taxanes: Promising Anti-Cancer Drugs. Asian Pac J Cancer P 2011, 12 (4), 837-851.

74. Batrakova, E. V.; Dorodnych, T. Y.; Klinskii, E. Y.; Kliushnenkova, E. N.; Shemchukova, O. B.; Goncharova, O. N.; Arjakov, S. A.; Alakhov, V. Y.; Kabanov, A. V., Anthracycline antibiotics non-covalently incorporated into the block copolymer micelles: In vivo evaluation of anti-cancer activity. Brit J Cancer 1996, 74 (10), 1545-1552.

75. Uchino, H.; Matsumura, Y.; Negishi, T.; Koizumi, F.; Hayashi, T.; Honda, T.; Nishiyama, N.; Kataoka, K.; Naito, S.; Kakizoe, T., Cisplatin-incorporating polymeric micelles (NC-6004) can reduce nephrotoxicity and neurotoxicity of cisplatin in rats. Brit J Cancer 2005, 93 (6), 678-687.

76. Kim, T. Y.; Kim, D. W.; Chung, J. Y.; Shin, S. G.; Kim, S. C.; Heo, D. S.; Kim, N. K.; Bang, Y. J., Phase I and pharmacokinetic study of Genexol-PM, a cremophor-free, polymeric micelle-formulated paclitaxel, in patients with advanced malignancies. Clin. Cancer Res. 2004, 10 (11), 3708-3716.

77. Ringsdorf, H., Structure and Properties of Pharmacologically Active Polymers. J Polym Sci Pol Sym 1975, (51), 135-153.

78. Hu, X. L.; Jing, X. B., Biodegradable amphiphilic polymer-drug conjugate micelles. Expert Opin Drug Del 2009, 6 (10), 1079-1090.

79. Li, C.; Wallace, S., Polymer-drug conjugates: Recent development in clinical oncology. Adv Drug Deliver Rev 2008, 60 (8), 886-898.

80. Kang, S. I.; Na, K.; Bae, Y. H., Physicochemical characteristics and doxorubicin-release behaviors of pH/temperature-sensitive polymeric nanoparticles. Colloid Surface A 2003, 231 (1-3), 103-112.

81. Malik, N.; Evagorou, E. G.; Duncan, R., Dendrimer-platinate: a novel approach to cancer chemotherapy. Anti-Cancer Drugs 1999, 10 (8), 767-776.

82. Taratula, O.; Garbuzenko, O.; Savla, R.; Wang, Y. A.; He, H. X.; Minko, T., Multifunctional Nanomedicine Platform for Cancer Specific Delivery of siRNA by Superparamagnetic Iron Oxide Nanoparticles-Dendrimer Complexes. Curr Drug Deliv 2011, 8 (1), 59-69.

83. Madani, S. Y.; Naderi, N.; Dissanayake, O.; Tan, A.; Seifalian, A. M., A new era of cancer treatment: carbon nanotubes as drug delivery tools. Int J Nanomed 2011, 6, 2963-2979.

84. Lim, Y. B.; Kim, T.; Lee, J. W.; Kim, S. M.; Kim, H. J.; Kim, K.; Park, J. S., Self-assembled ternary complex of cationic dendrimer, cucurbituril, and DNA: Noncovalent strategy in developing a gene delivery carrier. Bioconjugate Chem 2002, 13 (6), 1181-1185.

85. Xu, S. J.; Luo, Y.; Graeser, R.; Warnecke, A.; Kratz, F.; Hauff, P.; Licha, K.; Haag, R., Development of pH-responsive core-shell nanocarriers for delivery of therapeutic and diagnostic agents. Bioorg. Med. Chem. Lett. 2009, 19 (3), 1030-1034.

86. Majoros, I. J.; Myc, A.; Thomas, T.; Mehta, C. B.; Baker, J. R., PAMAM dendrimer-based multifunctional conjugate for cancer therapy: Synthesis, characterization, and functionality. Biomacromolecules 2006, 7 (2), 572-579.

87. Mullen, D. G.; Fang, M.; Desai, A.; Baker, J. R.; Orr, B. G.; Holl, M. M. B., A Quantitative Assessment of Nanoparticle-Ligand Distributions: Implications for Targeted Drug and Imaging Delivery in Dendrimer Conjugates. Acs Nano 2010, 4 (2), 657-670.

88. Fung, S. Y.; Yang, H.; Sadatmousavi, P.; Sheng, Y.; Mamo, T.; Nazarian, R.; Chen, P., Amino Acid Pairing for De Novo Design of Self-Assembling Peptides and Their Drug Delivery Potential. Adv Funct Mater 2011, 21 (13), 2456-2464.

89. Ryan, D. M.; Nilsson, B. L., Self-assembled amino acids and dipeptides as noncovalent hydrogels for tissue engineering. Polym Chem-Uk 2012, 3 (1), 18-33.

90. Wang, T.; Zhong, X. Z.; Wang, S. T.; Lv, F.; Zhao, X. J., Molecular Mechanisms of RADA16-1 Peptide on Fast Stop Bleeding in Rat Models. Int. J. Mol. Sci. 2012, 13 (11), 15279-15290.

91. Zhang, S. G.; Holmes, T.; Lockshin, C.; Rich, A., Spontaneous Assembly of a Self-Complementary Oligopeptide to Form a Stable Macroscopic Membrane. Proc. Natl. Acad. Sci. U. S. A. 1993, 90 (8), 3334-3338.

92. Keyes-Baig, C.; Duhamel, J.; Fung, S. Y.; Bezaire, J.; Chen, P., Self-assembling peptide as a potential carrier of hydrophobic compounds. J. Am. Chem. Soc. 2004, 126 (24), 7522-7532.

93. Chen, P., Self-assembly of ionic-complementary peptides: a physicochemical viewpoint. Colloid Surface A 2005, 261 (1-3), 3-24.

94. Zhang, S. G.; Holmes, T. C.; Dipersio, C. M.; Hynes, R. O.; Su, X.; Rich, A., Self-Complementary Oligopeptide Matrices Support Mammalian-Cell Attachment. Biomaterials 1995, 16 (18), 1385-1393.

95. Sieminski, A. L.; Was, A. S.; Kim, G.; Gong, H.; Kamm, R. D., The stiffness of three-dimensional ionic self-assembling peptide gels affects the extent of capillary-like network formation. Cell Biochem. Biophys. 2007, 49 (2), 73-83.

96. Fung, S. Y.; Keyes, C.; Duhamel, J.; Chen, P., Concentration effect on the aggregation of a self-assembling oligopeptide. Biophys. J. 2003, 85 (1), 537-548.

97.Ghosh, A.; Haverick, M.; Stump, K.; Yang, X. Y.; Tweedle, M. F.; Goldberger, J. E., Fine-Tuning the pH Trigger of Self-Assembly. J. Am. Chem. Soc. 2012, 134 (8), 3647-3650.

98. Zhang, S.; Fung, S. Y.; Yang, H.; Chen, P., Sequence Effect of Self-Assembling Peptides on the Complexation and In Vitro Delivery of the Hydrophobic Anticancer Drug Ellipticine. PLoS One 2008, 3 (4), e1956.

99. Wu, Y.; Sadatmousavi, P.; Wang, R.; Lu, S.; Yuan, Y. F.; Chen, P., Self-assembling peptide-based nanoparticles enhance anticancer effect of ellipticine in vitro and in vivo. Int J Nanomed 2012, 7, 3221-3233.

100. Poljakova, J.; Eckschlager, T.; Hrabeta, J.; Hrebackova, J.; Smutny, S.; Frei, E.; Martinek, V.; Kizek, R.; Stiborova, M., The mechanism of cytotoxicity and DNA adduct formation by the anticancer drug ellipticine in human neuroblastoma cells. Biochem. Pharmacol. 2009, 77 (9), 1466-1479.

101. Fung, S. Y.; Duhamel, J.; Chen, P., Solvent effect on the photophysical properties of the anticancer agent ellipticine. J. Phys. Chem. A 2006, 110 (40), 11446-11454.

102. Hong, Y.; Lau, L. S.; Legge, R. L.; Chen, P., Critical Self-Assembly Concentration of an Ionic-Complementary Peptide Eak16-I. The Journal of Adhesion 2004, 80 (10-11), 913-931.

103. Kundu, B.; Guptasarma, P., Use of a hydrophobic dye to indirectly probe the structural organization and conformational plasticity of molecules in amorphous aggregates of carbonic anhydrase. Biochem Biophys Res Commun 2002, 293 (1), 572-7.

104. Sedlacek, O.; Hruby, M.; Studenovsky, M.; Kucka, J.; Vetvicka, D.; Kovar, L.; Rihova, B.; Ulbrich, K., Ellipticine-Aimed Polymer-Conjugated Auger Electron Emitter: Multistage Organelle Targeting Approach. Bioconjugate Chem 2011, 22 (6), 1194-1201.

105. Fung, S. Y.; Yang, H.; Chen, P., Sequence Effect of Self-Assembling Peptides on the Complexation and In Vitro Delivery of the Hydrophobic Anticancer Drug Ellipticine. Plos One 2008, 3 (4).

106. Shimoni, L.; Glusker, J. P., Hydrogen-Bonding Motifs of Protein Side-Chains - Descriptions of Binding of Arginine and Amide Groups. Protein Sci 1995, 4 (1), 65-74.

107. Onda, M.; Yoshihara, K.; Koyano, H.; Ariga, K.; Kunitake, T., Molecular recognition of nucleotides by the guanidinium unit at the surface of aqueous micelles and bilayers. A comparison of microscopic and macroscopic interfaces. J. Am. Chem. Soc. 1996, 118 (36), 8524-8530.

108. Cho, Y. W.; Park, S. A.; Han, T. H.; Son, D. H.; Park, J. S.; Oh, S. J.; Moon, D. H.; Cho, K. J.; Ahn, C. H.; Byun, Y.; Kim, I. S.; Kwon, I. C.; Kim, S. Y., In vivo tumor targeting and radionuclide imaging with self-assembled nanoparticles: Mechanisms, key factors, and their implications. Biomaterials 2007, 28 (6), 1236-1247.

109. Greish, K., Enhanced permeability and retention of macromolecular drugs in solid tumors: A royal gate for targeted anticancer nanomedicines. J Drug Target 2007, 15 (7-8), 457-464.

110. Zahr, A. S.; Davis, C. A.; Pishko, M. V., Macrophage uptake of core-shell nanoparticles surface modified with poly(ethylene glycol). Langmuir 2006, 22 (19), 8178-8185.

111. Weber, P.; Wagner, M.; Schneckenburger, H., Cholesterol Dependent Uptake and Interaction of Doxorubicin in MCF-7 Breast Cancer Cells. Int. J. Mol. Sci. 2013, 14 (4), 8358-8366.